The Evolution of Coeval Stellar Hierarchical Triple Systems

Master research report

July 2012

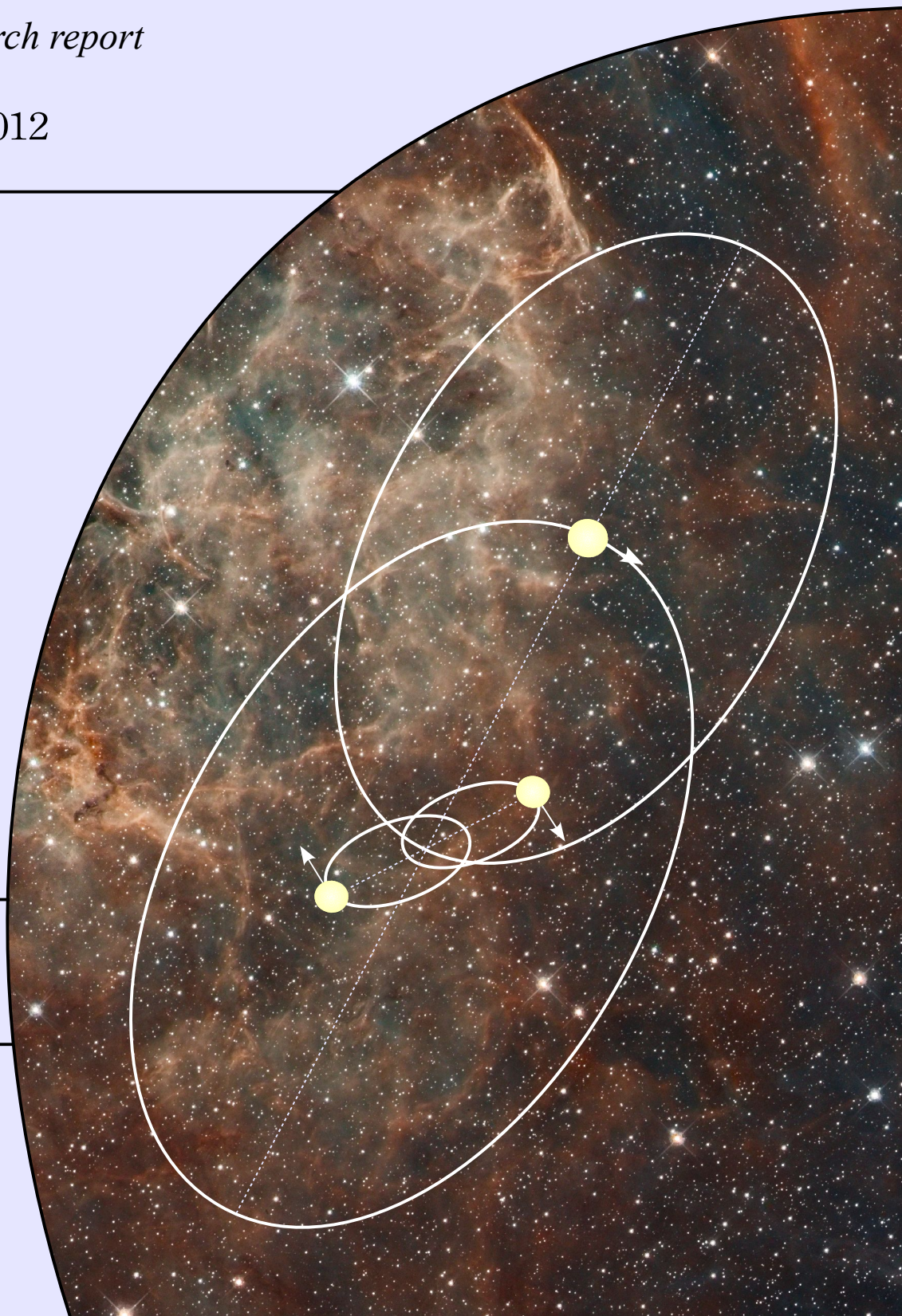

Adrian Hamers
Utrecht University

Supervisors:
O.R. Pols
G. Nelemans
Radboud University
Nijmegen

Abstract We study the evolution of coeval stellar hierarchical triple systems with intermediate mass (initial primary mass $1.0 < m_1/M_\odot < 6.5$) and relatively wide inner binary systems ($a_1[1-e_1^2] > 12\,\mathrm{AU}$, where a_1 and e_1 are the initial inner orbit semi-major axis and eccentricity respectively). For these triple systems, the inner binary stars do not interact in the absence of the third star (tertiary). Special attention is paid to the channels in which the tertiary affects the inner binary system through high-amplitude eccentricity cycles or dynamical instability of the triple system such that potentially a compact object merger is triggered in the inner binary system. To model hierarchical triple systems, we have developed a new algorithm which couples an existing rapid binary population synthesis code with a newly written module that computes the secular gravitational three-body dynamics. With this algorithm, we perform a population synthesis study of triples and we present the main channels. We find that in $\sim 9\%$ of systems of the computed sample, Kozai cycles with tidal friction (KCTF) are responsible for significantly shrinking the inner binary orbit to $a_1 < 12\,\mathrm{AU}$, possibly leading to common-envelope (CE) evolution and/or an inner binary merger. In $\sim 5\%$ of all systems the eccentricity driven by Kozai cycles is high enough for an orbital collision (eccentric merger) and $\sim 10\%$ of the triple systems become dynamically unstable. In the latter possibility, previous N-body simulations show that in $\sim 10\%$ of such cases the destabilization eventually leads to a collision. The latter two channels of eccentric mergers and dynamical instability are unique channels in the evolution of hierarchical triple systems and the associated type of mergers are otherwise expected to occur only in dense stellar systems. Several channels found in the population synthesis study involve mergers of CO WDs and therefore potentially lead to type Ia supernovae (SNe Ia). We estimate the expected rate of SNe Ia and compare the delay time distribution to a binary population synthesis study and observations. We find that the expected triple-induced SNe Ia rate is one to three orders of magnitude lower than the binary population synthesis rate. The former represents a lower limit, however, due to fact that only initially wide-orbit inner binary systems are considered in this work. Further study is needed in which triple systems are included with initially tighter inner orbits.

Contents

Chapter 1

Introduction

From the naked eye, the night sky appears to contain mostly isolated stars. However, detailed measurements, either by astrometry, spectroscopy or photometry, show that many stars are binaries and that the multiplicity of a non-negligible fraction of all stellar systems is even higher, i.e. they consist of three or more stars. For solar-like stars in the *Hipparcos* catalogue, for example, the observed fractions of single, double, triple and higher-order systems are approximately 54%, 34%, 9% and 3% respectively (Raghavan et al., 2010). Moreover, stellar multiplicity is believed to increase with stellar mass (e.g. Zinnecker 2008); for example, for massive B stars the triple fraction is believed to be as high as 50% (Remage Evans, 2011). The fact that systems with multiplicity higher than two are observed with such large frequency implies that these systems are dynamically stable on long timescales. Despite their relatively high frequency and stability, many aspects of their evolution remain elusive and unstudied.

The evolution of single stars is reasonably well understood, although uncertainties remain such as convective overshooting and mass loss in massive stars. By bringing another star into the picture, the evolution of binary systems is made much more complicated than that of single stars. Yet it appears that such complication is needed to explain a multitude of phenomena which cannot be explained in terms of single stellar evolution, e.g. stars with peculiar properties such as carbon-enhanced metal poor stars or more violent phenomena such as cataclysmic variables and transient X-ray sources. By extension, the evolution of triple systems is even more complicated. For example, to describe the initial state of a triple system which is dynamically stable one needs at least ten parameters, compared to one parameter for single stars (the mass) and four for binaries (primary mass, mass ratio, orbital period and eccentricity)[1]. In this thesis we shall attempt to take on the daunting task of describing the evolution of such dynamically stable triple systems. In particular, we will focus on those dynamically stable triples which are coeval, i.e. in which the three stars formed at the same time. The most important aspect will be the interplay between gravitational dynamics and stellar evolution.

Most multiple systems, including triple systems, are endowed with a hierarchical structure, which implies that the system is composed of nested binary pairs, each of which is characterized by the masses of the components, the orbital period and the eccentricity. Such systems with hierarchical structure are almost invariably dynamically stable on long time scales, i.e. over times scales much longer than the orbital periods of any binary pair. Non-hierarchical multiple systems[2] exist but are rare, as such systems are not dynamically stable and are thus likely to be disrupted on dynamical timescales. In particular hierarchical triple systems are well-described in terms of two perturbed Keplerian orbits, the "inner binary" and the "outer binary" orbits. The outer binary orbit consists of a single star (the tertiary) and the inner binary, which is to be interpreted as a point mass at the position of the center of mass of the inner binary system with a mass equal to the total inner binary mass. See Fig. 1.1 for a schematic depiction of a hierarchical triple system. We will use the following nomenclature throughout this thesis. The inner binary component masses are denoted by m_1 and m_2 and the mass of the tertiary is denoted by m_3. The orbital periods, semi-major axes, eccentricities, arguments of periastron and longitudes of the ascending nodes are denoted by P_j, a_j, e_j, g_j and h_j respectively for the inner ($j = 1$) and outer ($j = 2$) orbits. The mutual inclination angle between the inner and outer binary orbits, $i_{\rm tot}$, is defined as the angle between the orbital angular momentum vectors of the inner and outer binary orbits. With these coordinates, a hierarchical triple system is minimally described in terms of the ten parameters m_1, m_2, m_3, a_1, a_2, e_1, e_2, g_1, g_2 and $i_{\rm tot}$. The longitudes of the ascending notes h_j and orbital phases f_j are not included in this list as the secular (i.e. long-term) evolution is not dependent on these quantities (see Chapter 2).

[1] The metallicity is also an important parameter for any stellar system, but in this thesis we shall restrict exclusively to the standard quasi-solar metallicity $Z = 0.02$.

[2] By these we mean to exclude groups of a large number of stars such as (the cores of) globular clusters.

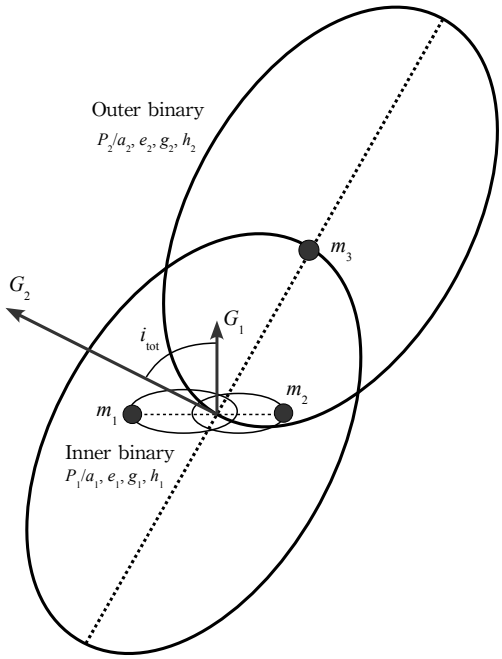

Figure 1.1: Schematic depiction of a hierarchical triple system. Jacobi coordinates are used to describe both inner and outer binary orbits. The orbital angular momenta of both orbits are denoted by G_1 and G_2. Note that typically $a_2 \gg a_1$ (and thus $G_2 \gg G_1$), which is not the case in this depiction.

Unquestionably the most notable feature of the secular gravitational dynamics of hierarchical triple systems is the periodic exchange of orbital angular momentum between the inner and outer binary orbits if the initial mutual inclination angle $i_{\rm tot}$ is sufficiently large, i.e. $39.2^\circ \lesssim i_{\rm tot} \lesssim 140.8^\circ$ (Kozai, 1962; Lidov, 1962). This exchange results in the perturbation of the shapes of the inner and outer binary orbits while the orbital energies and thus a_1 and a_2 are conserved to very high accuracy (see e.g. Mardling & Aarseth 2001, their Fig. 11). Consequently the inner (and outer) orbit eccentricities and mutual inclination angle $i_{\rm tot}$ vary periodically in cycles known as Kozai cycles. During these cycles, the quantity $\sqrt{1-e_1^2}\cos(i_{\rm tot})$ remains (approximately) constant, implying that inner orbit eccentricity maxima are associated with maxima in $\cos(i_{\rm tot})$. In addition, the arguments of periastron g_j and longitudes of ascending nodes h_j change during these cycles. During the Kozai cycles, the inner orbit eccentricity may reach high values on a timescale which is on the order of $(P_2/P_1)\,P_2$. The magnitude of the associated maximum inner orbit eccentricity, $e_{1,\rm max}$, is mainly determined by the mutual inclination angle $i_{\rm tot}$ and the ratio of semi-major axes a_2/a_1. Typical values of this ratio for which Kozai cycles are important are $10 \lesssim a_2/a_1 \lesssim 10^3$, where the rough lower limit corresponds to triples which are close to being dynamically unstable. The rough upper limit corresponds to triples in which in most physical situations, the mechanism of orbital angular momentum exchange in Kozai cycles is suppressed by other processes in the inner binary orbit, in particular those related to general relativistic effects, tidal distortion and stellar rotation. This phenomenon will be investigated in detail in Sect. 2.3. In the regime around the lower limit ($a_2/a_1 \sim 10$), $e_{1,\rm max}$ may reach extremely high values at times when the mutual orientation between both binary orbits changes from prograde ($0 < i_{\rm tot} < 90^\circ$; i.e. the components in the inner and outer orbits rotate in the same sense) to retrograde ($90 < i_{\rm tot} < 180^\circ$; i.e. the components in the inner and outer orbits rotate in the opposite sense) and vice versa. The latter process is known as the eccentric Kozai mechanism (e.g. Naoz et al. 2011), during which very high inner orbit eccentricities can be reached – e.g. Shappee & Thompson (2012) find values as high as $1 - e_1 = 10^{-6}$. Such high eccentricities can trigger various interesting processes such as strong tidal friction, strong gravitational wave emission and even direct orbital collisions.

Extremely high eccentricities in the inner binary system are quite rare, however. Much more common is that the eccentricity cycles reach amplitudes of order $e_1 \sim 1 - 10^{-1}$ to $e_1 \sim 1 - 10^{-3}$, sufficient to induce significant tidal effects in the inner binary system in many cases. These tidal effects are strongly dependent on the distance between the inner binary components relative to their radii and may thus become important even in relatively wide orbits if the inner orbit eccentricity is high enough. This is because the binary periastron distance $r_p = a_1(1-e_1)$ decreases with increasing eccentricity. During the process of tidal friction, the total inner binary angular momentum remains constant while orbital and spin energies are exchanged until circularization, synchronization and coplanarity are achieved (Hut, 1980). The coupling between tidal friction and Kozai eccentricity cycles introduces a complex behavior in which the eccentricity cycles are gradually damped while keeping the eccentricity at a fairly high value, until complete circularization and orbital shrinkage occurs. This process of Kozai cycles with tidal friction (KCTF)

has been studied in a simplified fashion by Mazeh & Shaham (1979) and in more detail by Eggleton & Kisseleva-Eggleton (2001). A population synthesis study incorporating KCTF in triples with solar-like main sequence (MS) stars has been performed by Fabrycky & Tremaine (2007), who showed that KCTF can explain the observed peak in the period distribution in close MS binaries around 3 days. These close MS binaries are indeed found to be very likely orbited by a third star (Tokovinin et al., 2006).

The same process does not automatically apply to more massive ($m \gtrsim 1.25\,M_{\odot}$) stars, however, because these stars possess radiative envelopes, in contrast to their less massive counterparts for which the envelope is convective. Consequently tidal friction is much less effective because convective regions precipitate dissipation of tidal energy much more than radiative regions do (e.g. Zahn 1977). Therefore KCTF is not expected to play a major role during the MS evolution of these more massive triples. As they evolve beyond the MS, however, they develop deep convective envelopes during the red giant branch (RGB) and asymptotic giant branch (AGB) phases. During those phases, not only the structure of the star changes in favor of potentially much stronger tidal effects, but also the radii increase substantially. Therefore KCTF can be an important process in the later phases in the evolution of higher mass triples.

The aim of this thesis is to study quantitatively the process of KCTF and other processes which are induced by Kozai cycles in the evolution of coeval stellar triples. We will in particular be interested in channels leading to mergers of carbon-oxygen (CO) white dwarfs (WDs). Such mergers are considered one of the main candidate progenitors of type Ia supernovae (SNe Ia), which are important in many aspects of physics and astrophysics. Most notably they play a central role as distance indicators in cosmology (Riess et al., 1998; Perlmutter et al., 1999). We will focus on triple systems in which the inner binary is initially relatively wide such that in the absence of the tertiary, the inner binary stars would not interact during their evolution and end as relatively wide CO WD binaries. Because of this application to CO WD systems, we choose an initial inner orbit primary mass range of $1.0 < m_1/M_{\odot} < 6.5$. Furthermore, we select the initial inner orbit semi-major axes such that $a_1\left(1-e_1^2\right) > 12\,\mathrm{AU}$, where the factor $\left(1-e_1^2\right)$ ensures that in the absence of the tertiary, tidal friction in the inner orbit would not decrease a_1 below 12 AU – the lower value of a_1 of 12 AU satisfies the requirement of non-interactivity without a tertiary. We will show that the secular gravitational influence of the tertiary introduces various channels in which two CO WDs merge in the inner binary system. Channels leading to CO WD mergers are important in binary population synthesis studies (e.g. Nelemans et al. 2001; Ruiter et al. 2009; Claeys et al. 2012), which are generally faced with the problem that the predicted SNe Ia rate is too low compared to the observed rate (see Maoz & Mannucci 2012 and Wang & Han 2012 for recent reviews). Any (new) channel leading to a CO WD merger not considered previously is therefore a welcome one. We will also compare the expected SNe Ia rate in our study with those predicted in a binary population synthesis study and observed rates.

The notion that a tertiary in a wide orbit around a binary system could introduce novel channels leading to SNe Ia is not a new one. For example, in Iben & Tutukov (1999) several channels are discussed in which the tertiary plays an important role at the moment when the triple system becomes dynamically unstable due to mass transfer and/or wind mass loss in the inner binary system, the latter two processes which increase the inner orbital period. More general scenarios (i.e. not necessarily leading to a SN Ia) involving dynamically unstable triple systems are explored quantitatively with N-body techniques in Perets & Kratter (2012). In these studies, the dynamical instability plays a key role in the scenarios. Since many dynamically stable triple systems are observed, however, it is also relevant to consider the effect that the tertiary has in dynamically stable systems in which Kozai cycles can play an important role. For example, Thompson (2011) suggests that high eccentricities induced by the tertiary in close CO WD binaries can significantly reduce the merger time due to gravitational wave emission. In the latter study the evolution of the triple system prior to the formation of the CO WD binary is not taken into account, however. It is important to consider such prior evolution because in the standard binary evolution scenarios a common-envelope (CE) evolution phase is needed to produce the close CO WD binary. During this CE phase the inner orbital period P_1 decreases substantially. Thus even if the ratio of the outer to the inner orbital period P_2/P_1 prior to CE is relatively small, it is increased significantly after the CE, thus quenching any subsequent Kozai cycles as these are typically suppressed for close inner binary systems unless P_2/P_1 is relatively small. In this thesis we will investigate quantitatively whether this effect of the CE is important.

A (limited) quantitative study of these intermediate (and higher) mass triple systems has recently been performed by Shappee & Thompson (2012) using N-body integrations to demonstrate the existence of the eccentric Kozai mechanism, which can be induced by mass loss in triple systems with low P_2/P_1. However, Shappee & Thompson (2012) did not fully include the statistics of triples and we therefore aim to perform a population synthesis study where such statistics are taken into account. To achieve this goal we have developed a new algorithm, which we will refer to as `triple_c`, which couples an existing binary population synthesis code (`binary_c`) with a new code that takes into account the secular gravitational dynamics of hierarchical triple systems. The main feature of this algorithm is that it is very fast, such that it is feasible to perform a population synthesis study of a sizable sample of triples.

The outline of this thesis is as follows. In Chapter 2 we discuss the theoretical background of hierarchical triple systems. This background forms the basis of the `triple_c` algorithm which is described in Chapter 3. As a demonstration of this algorithm, we give a few relevant examples of the evolution of coeval stellar triples as computed with this new algorithm in Chapter 4. Subsequently, the results of a population synthesis study performed with `triple_c` are described in Chapter 5, where we also compute the expected SNe Ia rates. We discuss some of the assumptions made and uncertainties in this work and compare our findings to other studies in Chapter 6. We conclude in Chapter 7.

Chapter 2

Theory

Unlike the two-body problem for which the orbits are either parabolic, hyperbolic or elliptic, no closed-form analytic solutions exist to the three-body problem, as first shown by Henri Poincaré in the mid 1890s. This is not surprising because in the case in which the distances between the three bodies (for now treated as point particles) are comparable to each other, the behavior can be chaotic, i.e. highly sensitive to the initial conditions. Time integrations show that in this case one body is likely ejected from the system and escapes to infinity, while the two remaining bodies form a stable binary system. If, on the other hand, one of the three particles is relatively distant from the other two, the three-body system can remain dynamically stable on long timescales and it is referred to as a hierarchical triple system. In the latter case, the system is well-described in terms of two perturbed elliptical orbits, those of the inner and outer binary orbits. One method of investigating this perturbation quantitatively is by formulating the Hamiltonian of the three-body system and deriving the secular equations of motion. This is done in Sect. 2.1. Subsequently in Sect. 2.2 an analytic solution to a simplified case is given to illustrate how basic Kozai cycles arise. Furthermore additional physical effects are included which modify the behavior of Kozai cycles in Sect. 2.3. Note that most of the results discussed in this chapter have been derived before in the literature. In many cases, however, many details are omitted. In the present thesis, effort has been made to present a consistent and complete theoretical framework for the secular description of hierarchical triple systems, starting from basic physical principles such as Hamiltonian mechanics.

2.1 Hamiltonian formalism

2.1.1 The three-body Hamiltonian

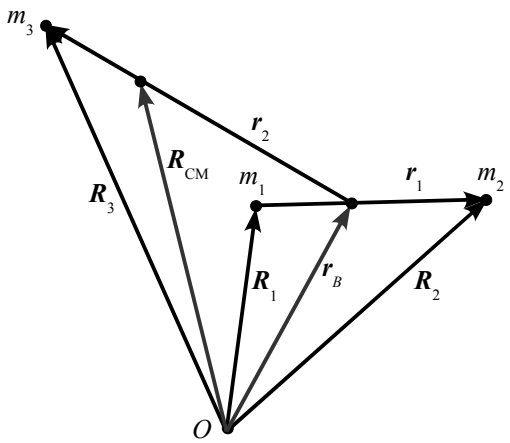

Figure 2.1: Graphical depiction of the definitions of various position vectors required for the formulation of the three-body Hamiltonian.

The (classical) Hamiltonian $\mathcal{H}$ is defined as $\mathcal{H} = T + V$ where T is the total kinetic energy and V the potential energy. Consider a system of three point masses with position vectors $\mathbf{R}_1$, $\mathbf{R}_2$ and $\mathbf{R}_3$. Following conventions commonly used (e.g. Ford

et al. 2000) define the position vector $\mathbf{r}_1 = \mathbf{R}_2 - \mathbf{R}_1$ pointing from mass 1 towards mass 2, the center of mass of point masses m_1 and m_2, $\mathbf{r}_B = (\mathbf{R}_1 m_1 + \mathbf{R}_2 m_2)/(m_1 + m_2)$ and the vector of the third point mass m_3 relative to $\mathbf{r}_B$, $\mathbf{r}_2 = \mathbf{R}_3 - \mathbf{r}_B$ (see Fig. 2.1). By simple manipulation of these definitions, one finds the following two useful relations:

$$\mathbf{r}_B = \frac{1}{m_1 + m_2}\left[m_1\mathbf{R}_1 + m_2\mathbf{R}_2\right] = \frac{1}{m_1 + m_2}\left[m_1\mathbf{R}_1 + m_2\left(\mathbf{r}_1 + \mathbf{R}_1\right)\right] = \mathbf{R}_1 + \frac{m_2}{m_1 + m_2}\mathbf{r}_1 \tag{2.1}$$

$$= \frac{1}{m_1 + m_2}\left[m_1\left(\mathbf{R}_2 - \mathbf{r}_1\right) + m_2\mathbf{R}_2\right] = \mathbf{R}_2 - \frac{m_1}{m_1 + m_2}\mathbf{r}_1. \tag{2.2}$$

Hence, using the definition of $\mathbf{r}_2$ and Eqs. 2.1 and 2.2, the distances between masses 3 and 1 and masses 3 and 2 respectively are given by the lengths of the difference vectors

$$\mathbf{R}_3 - \mathbf{R}_1 = \mathbf{r}_2 + \mathbf{r}_B - \mathbf{R}_1 = \mathbf{r}_2 + \frac{m_2}{m_1 + m_2}\mathbf{r}_1; \tag{2.3}$$

$$\mathbf{R}_3 - \mathbf{R}_2 = \mathbf{r}_2 + \mathbf{r}_B - \mathbf{R}_2 = \mathbf{r}_2 - \frac{m_1}{m_1 + m_2}\mathbf{r}_1. \tag{2.4}$$

The gravitational potential of the three-body system V may thus be readily computed, taking into account all pairs of point masses:

$$\begin{aligned} V &= -\frac{1}{2}\sum_{\substack{i,j=1\\ i\neq j}}^{3}\frac{G_N m_i m_j}{\left\|\mathbf{R}_i - \mathbf{R}_j\right\|} = -\frac{G_N m_2 m_1}{\|\mathbf{R}_2 - \mathbf{R}_1\|} - \frac{G_N m_3 m_1}{\|\mathbf{R}_3 - \mathbf{R}_1\|} - \frac{G_N m_3 m_2}{\|\mathbf{R}_3 - \mathbf{R}_2\|} \\ &= -\frac{G_N m_2 m_1}{r_1} - \frac{G_N m_3 m_1}{\left\|\mathbf{r}_2 + \frac{m_2}{m_1+m_2}\mathbf{r}_1\right\|} - \frac{G_N m_3 m_2}{\left\|\mathbf{r}_2 - \frac{m_1}{m_1+m_2}\mathbf{r}_1\right\|}, \end{aligned} \tag{2.5}$$

where G_N is the gravitational constant and $r_1 \equiv \|\mathbf{r}_1\|$ (similar notation applies to all other vectors). It will prove advantageous to expand the last two terms in Eq. (2.5) in terms of r_1/r_2 by means of the generating function of the Legendre polynomials. Consider two arbitrary position vectors $\mathbf{r}$ and $\mathbf{r}'$, let γ be the angle between $\mathbf{r}$ and $\mathbf{r}'$ such that $\hat{\mathbf{r}} \cdot \hat{\mathbf{r}}' = \cos(\gamma)$ and let α be a real constant. Then:

$$\begin{aligned} \frac{1}{\|\mathbf{r} - \alpha\mathbf{r}'\|} &= \left[(\mathbf{r} - \alpha\mathbf{r}')^2\right]^{-1/2} = \left[r^2 - 2\alpha\,\mathbf{r}\cdot\mathbf{r}' + \alpha^2 r'^2\right]^{-1/2} = \frac{1}{r}\left[1 - 2\alpha\left(\frac{r'}{r}\right)\cos(\gamma) + \alpha^2\left(\frac{r'}{r}\right)^2\right]^{-1/2} \\ &= \frac{1}{r}\sum_{n=0}^{\infty}\alpha^n\left(\frac{r'}{r}\right)^n \widetilde{P}_n(\cos(\gamma)), \end{aligned} \tag{2.6}$$

where $\widetilde{P}_n$ is the n^{th} Legendre polynomial (the tilde is to avoid any confusion with the inner and outer orbital periods P_j). Applying Eq. 2.6 with $\mathbf{r} = \mathbf{r}_2$ and $\mathbf{r}' = \mathbf{r}_1$ twice to the last two terms in Eq. 2.5 with $\alpha = -m_2/(m_1 + m_2)$ and $\alpha = m_1/(m_1 + m_2)$ respectively, one obtains:

$$\begin{aligned} V &= -\frac{G_N m_2 m_1}{r_1} - \frac{G_N m_3 m_1}{r_2}\sum_{n=0}^{\infty}\left(\frac{-m_2}{m_1 + m_2}\right)^n\left(\frac{r_1}{r_2}\right)^n \widetilde{P}_n(\cos(\Phi)) - \frac{G_N m_3 m_2}{r_2}\sum_{n=0}^{\infty}\left(\frac{m_1}{m_1 + m_2}\right)^n\left(\frac{r_1}{r_2}\right)^n \widetilde{P}_n(\cos(\Phi)) \\ &= -\frac{G_N m_2 m_1}{r_1} - \frac{G_N m_3 m_2 m_1}{r_2}\sum_{n=0}^{\infty}\frac{-(-m_2)^{n-1}}{(m_1 + m_2)^n}\left(\frac{r_1}{r_2}\right)^n \widetilde{P}_n(\cos(\Phi)) - \frac{G_N m_3 m_2 m_1}{r_2}\sum_{n=0}^{\infty}\frac{m_1^{n-1}}{(m_1 + m_2)^n}\left(\frac{r_1}{r_2}\right)^n \widetilde{P}_n(\cos(\Phi)) \\ &= -\frac{G_N m_2 m_1}{r_1} - \frac{G_N}{r_2}\sum_{n=0}^{\infty}\left[m_1 m_2 m_3\frac{m_1^{n-1} - (-m_2)^{n-1}}{(m_1 + m_2)^n}\right]\left(\frac{r_1}{r_2}\right)^n \widetilde{P}_n(\cos(\Phi)), \end{aligned} \tag{2.7}$$

where Φ is the angle between $\mathbf{r}_1$ and $\mathbf{r}_2$. Using the fact that $\widetilde{P}_0(x) = 1\ \forall\ x \in \mathbb{R}$ and noting that the term $n = 1$ in the last line of Eq. 2.7 vanishes, the potential energy can be written as:

$$\begin{aligned} V &= -\frac{G_N m_2 m_1}{r_1} - \frac{G_N}{r_2}m_1 m_2 m_3\left(\frac{1}{m_1} + \frac{1}{m_2}\right) - \frac{G_N}{r_2}\sum_{n=2}^{\infty}\left[m_1 m_2 m_3\frac{m_1^{n-1} - (-m_2)^{n-1}}{(m_1 + m_2)^n}\right]\left(\frac{r_1}{r_2}\right)^n \widetilde{P}_n(\cos(\Phi)) \\ &= -\frac{G_N m_2 m_1}{r_1} - \frac{G_N m_3(m_1 + m_2)}{r_2} - \frac{G_N}{r_2}\sum_{n=2}^{\infty} M_n\left(\frac{r_1}{r_2}\right)^n \widetilde{P}_n(\cos(\Phi)), \end{aligned} \tag{2.8}$$

where we have defined a mass parameter $M_n \equiv m_1 m_2 m_3 \left(m_1^{n-1} - (-m_2)^{n-1}\right)/(m_1+m_2)^n$.

Next we compute the kinetic energy T, which is defined as:

$$T = \frac{1}{2}\sum_{i=1}^{3} m_i \dot{\mathbf{R}}_i^2 = \frac{1}{2}m_1\dot{\mathbf{R}}_1^2 + \frac{1}{2}m_2\dot{\mathbf{R}}_2^2 + \frac{1}{2}m_3\dot{\mathbf{R}}_3^2. \tag{2.9}$$

The aim is to write T in terms of the relative velocities $\dot{\mathbf{r}}_1$ and $\dot{\mathbf{r}}_2$ as measured in a frame comoving with the center of mass, i.e. in a frame in which the time derivative of the centre of mass

$$\mathbf{R}_{\rm CM} = \frac{1}{m_1+m_2+m_3}\left(m_1\mathbf{R}_1 + m_2\mathbf{R}_2 + m_3\mathbf{R}_3\right), \tag{2.10}$$

vanishes: $\dot{\mathbf{R}}_{\rm CM} = \mathbf{0}$. Such a frame clearly exists if there are no external forces acting on the three-body system. To this aim we first write $\dot{\mathbf{R}}_1$ and $\dot{\mathbf{R}}_2$ in Eq. 2.9 in terms of $\dot{\mathbf{r}}_1$ and $\dot{\mathbf{r}}_B$ using Eqs. 2.1 and 2.2, giving:

$$\begin{aligned} T &= \frac{1}{2}m_1\left(\dot{\mathbf{r}}_B - \frac{m_2}{m_1+m_2}\dot{\mathbf{r}}_1\right)^2 + \frac{1}{2}m_2\left(\dot{\mathbf{r}}_B + \frac{m_1}{m_1+m_2}\dot{\mathbf{r}}_1\right)^2 + \frac{1}{2}m_3\dot{\mathbf{R}}_3^2 = \frac{1}{2}(m_1+m_2)\,\dot{\mathbf{r}}_B^2 - \frac{m_1m_2}{m_1+m_2}\dot{\mathbf{r}}_B\cdot\dot{\mathbf{r}}_1 \\ &\quad + \frac{m_1m_2}{m_1+m_2}\dot{\mathbf{r}}_B\cdot\dot{\mathbf{r}}_1 + \frac{1}{2}\frac{m_1m_2^2}{(m_1+m_2)^2}\dot{\mathbf{r}}_1^2 + \frac{1}{2}\frac{m_2m_1^2}{(m_1+m_2)^2}\dot{\mathbf{r}}_1^2 + \frac{1}{2}m_3\dot{\mathbf{R}}_3^2 \\ &= \frac{1}{2}\frac{m_1m_2}{m_1+m_2}\dot{\mathbf{r}}_1^2 + \frac{1}{2}(m_1+m_2)\,\dot{\mathbf{r}}_B^2 + \frac{1}{2}m_3\dot{\mathbf{R}}_3^2. \end{aligned} \tag{2.11}$$

To express $\mathbf{r}_B$ and $\mathbf{R}_3$ in terms of $\mathbf{R}_{\rm CM}$ and $\mathbf{r}_2$, first note that, by virtue of Eqs. 2.1 and 2.2:

$$\begin{aligned} \mathbf{R}_{\rm CM} &= \frac{1}{M}\left(m_1\mathbf{R}_1 + m_2\mathbf{R}_2 + m_3\mathbf{R}_3\right) = \frac{1}{M}\left(m_1\mathbf{r}_B - \frac{m_1m_2}{m_1+m_2}\mathbf{r}_1 + m_2\mathbf{r}_B + \frac{m_1m_2}{m_1+m_2}\mathbf{r}_1 + m_3\mathbf{R}_3\right) \\ &= \frac{1}{M}\left((m_1+m_2)\,\mathbf{r}_B + m_3\mathbf{R}_3\right), \end{aligned} \tag{2.12}$$

where $M \equiv m_1+m_2+m_3$. Thus one has the following two equations,

$$\begin{cases} \mathbf{r}_2 &= \mathbf{R}_3 - \mathbf{r}_B; \\ M\mathbf{R}_{\rm CM} &= (m_1+m_2)\,\mathbf{r}_B + m_3\mathbf{R}_3, \end{cases} \tag{2.13}$$

which can be solved for $\mathbf{R}_3$ and $\mathbf{r}_B$ in terms of $\mathbf{R}_{\rm CM}$ and $\mathbf{r}_2$. Multiplying the first equation in Eq. 2.13 by (m_1+m_2) and adding the result to the second equation yields:

$$\mathbf{R}_3 = \mathbf{R}_{\rm CM} + \frac{m_1+m_2}{M}\mathbf{r}_2, \tag{2.14}$$

while multiplying the first equation in Eq. 2.13 by m_3 and subtracting from the result the second equation yields:

$$\mathbf{r}_B = \mathbf{R}_{\rm CM} - \frac{m_3}{M}\mathbf{r}_2 \tag{2.15}$$

(note that Eqs. 2.14 and 2.15 are natural extensions of Eqs. 2.1 and 2.2, which apply to the inner binary system, to the outer binary system). Differentiating Eqs. 2.14 and 2.15 with respect to time, substituting the results into Eq. 2.11 and using that $\dot{\mathbf{R}}_{\rm CM} = \mathbf{0}$ then gives:

$$\begin{aligned} T &= \frac{1}{2}\frac{m_1m_2}{m_1+m_2}\dot{\mathbf{r}}_1^2 + \frac{1}{2}(m_1+m_2)\frac{m_3^2}{M^2}\dot{\mathbf{r}}_2^2 + \frac{1}{2}m_3\frac{(m_1+m_2)^2}{M^2}\dot{\mathbf{r}}_2^2 = \frac{1}{2}\frac{m_1m_2}{m_1+m_2}\dot{\mathbf{r}}_1^2 + \frac{1}{2}\frac{m_3(m_1+m_2)}{M}\underbrace{\left(\frac{m_3}{M} + \frac{m_1+m_2}{M}\right)}_{=1}\dot{\mathbf{r}}_2^2 \\ &= \frac{1}{2}\frac{m_1m_2}{m_1+m_2}\dot{\mathbf{r}}_1^2 + \frac{1}{2}\frac{m_3(m_1+m_2)}{M}\dot{\mathbf{r}}_2^2. \end{aligned} \tag{2.16}$$

In other words, the total kinetic energy, as measured in any frame comoving with the frame of the centre of mass, consists of the relative kinetic energies of the inner and outer binary orbits.

The Hamiltonian is thus given by (cf. Eqs. 2.8 and 2.16):

$$\mathcal{H} = T + V = \left(\frac{1}{2}\frac{m_1 m_2}{m_1 + m_2}\dot{\mathbf{r}}_1^2 - \frac{G_N m_1 m_2}{r_1}\right) + \left(\frac{1}{2}\frac{(m_1 + m_2)m_3}{m_1 + m_2 + m_3}\dot{\mathbf{r}}_2^2 - \frac{G_N (m_1 + m_2)m_3}{r_2}\right) - \frac{G_N}{r_2}\sum_{n=2}^{\infty} M_n \left(\frac{r_1}{r_2}\right)^n \widetilde{P}_n(\cos(\Phi)). \tag{2.17}$$

The two terms in large brackets in Eq. 2.17 can be interpreted as the Hamiltonians of two isolated binary systems. The inner binary system consists of point masses m_1 and m_2, while the outer binary system consists of point masses with masses (m_1+m_2) and m_3. The last term in Eq. 2.17 represents a coupling term and is a source of perturbations to the Keplerian orbits of these binary systems. Since the total energy in a binary system comprised of point masses m_1 and m_2 can be written as $\mathcal{H}_{\rm bin} = -Gm_1m_2/(2a)$, where a is the semi-major axis, it is natural to introduce in a similar fashion the semi-major axes a_1 and a_2 of the inner and outer binary systems respectively, such that the Hamiltonian of the three-body system can be written rather suggestively as:

$$\mathcal{H} = -\frac{G_N m_1 m_2}{2a_1} - \frac{G_N (m_1 + m_2)m_3}{2a_2} - \frac{G_N}{r_2}\sum_{n=2}^{\infty} M_n \left(\frac{r_1}{r_2}\right)^n \widetilde{P}_n(\cos(\Phi)). \tag{2.18}$$

If $r_2 \gg r_1$ during both binary orbits, the coupling term in Eq. 2.18 is relatively small and both binary orbits remain almost unaffected by the perturbing term, i.e. the orbits continue to be Keplerian orbits, although their shape and orientation may change over timescales which are (much) longer than the orbital periods. In this situation the triple system is hierarchical. Because in such systems $a_2 \gg a_1$ (or at least $a_2 > a_1$), it is convenient to write the coupling term in terms of the quantity $\alpha \equiv a_1/a_2$ as follows:

$$\mathcal{H} = -\frac{G_N m_1 m_2}{2a_1} - \frac{G_N (m_1 + m_2)m_3}{2a_2} - \frac{G_N}{a_2}\sum_{n=2}^{\infty} \alpha^n M_n \left(\frac{r_1}{a_1}\right)^n \left(\frac{a_2}{r_2}\right)^{n+1} \widetilde{P}_n(\cos(\Phi)). \tag{2.19}$$

Note that in the literature, the total energy expressed by Eq. 2.19 is usually multiplied by -1 such that for bound systems $\mathcal{H} > 0$ (e.g. Harrington 1968). In Sect. 2.1.2 we express Eq. 2.19 in terms of Euler angles commonly used in celestial mechanics and we perform an averaging procedure, effectively eliminating any short-term effects. The resulting Hamiltonian is then referred to as the secular Hamiltonian.

2.1.2 Secularization of the Hamiltonian

Numerical N-body calculations show that in hierarchical triple systems (i.e. dynamically stable three-body systems), the semi-major axes of the inner and outer orbits, a_1 and a_2, remain secularly constant to very good approximation (see. e.g. Mardling & Aarseth 2001 and Naoz et al. 2011). The two separate binary energy terms in Eq. 2.19 are therefore also secularly constant, i.e. in hierarchical triple systems, energy is not exchanged between the inner and outer orbits. It will turn out, however, that angular momentum is exchanged between both orbits, of course in such a way to conserve the total angular momentum of the three-body system.

It is necessary to introduce some coordinates and coordinate systems before averaging the Hamiltonian. We shall refer to the invariable plane as the plane perpendicular to the z component of the total angular momentum vector $\mathbf{G}_{\rm tot}$. Due to the fact that this component is conserved, this plane is indeed fixed in space at all times. The invariant coordinate system (X, Y, Z) is then defined as the coordinate system in which the X and Y axes lie within the invariable plane and the Z axis is perpendicular to this plane. The relative orbits of both binary systems are well-described in terms of elliptical orbits at least for the duration of one orbital period. The quantities r_1/a_1 and r_2/a_2 in Eq. 2.19 are then functions only of the phase angles (i.e. mean, true or eccentric anomalies) and eccentricities of their respective orbits. The relative orbits each lie within a plane which forms the (x_j, y_j) plane (with $j = 1$ and $j = 2$ for the inner and outer binary orbits respectively) of the orbital coordinate systems, with the x_j axes pointing to the periapses. The z_j axes are perpendicular to these (x_j, y_j) planes. The transformations between the orbital coordinate systems (x_j, y_j, z_j) and the invariant coordinate system (X, Y, Z) are described in terms of 6 rotations (3 per orbit), each involving an Euler angle. These Euler angles are (g_j, i_j, h_j), i.e. arguments of periastron, inclination angles and longitudes of the ascending nodes[1]. We refer to Appendix A.1.1 for the precise definitions of these angles and further derivation for an expression

[1] In celestial mechanics, the argument of periastron is also frequently denoted by ω and the longitude of the ascending node by Ω.

for the quantity $\cos(\Phi)$, which appears in the perturbing term in Eq. 2.19. Recall that Φ is the angle between $\mathbf{r}_1$ and $\mathbf{r}_2$. In terms of the true anomalies f_j of orbit j, $\cos(\Phi)$ is given by:

$$\begin{aligned}\cos(\Phi) = \cos(g_2 + f_2)\left[\cos(g_1 + f_1)\cos(\Delta h) - \cos(i_1)\sin(g_1 + f_1)\sin(\Delta h)\right] + \sin(g_2 + f_2)\left[\cos(i_2)\cos(g_1 + f_1)\sin(\Delta h)\right.\\ \left. + \sin(g_1 + f_1)\left\{\cos(i_1)\cos(i_2)\cos(\Delta h) + \sin(i_1)\sin(i_2)\right\}\right],\end{aligned} \tag{2.20}$$

where $\Delta h \equiv h_1 - h_2$. Furthermore, as shown in Appendix A.1.2, the choice of coordinate system (which is linked to conservation of total angular momentum) implies a constraint on Δh, namely $\Delta h = \pi$. As shown by Naoz et al. (2011), caution is advised as to when to apply this constraint because it suggests that $\cos(\Phi)$, and hence the Hamiltonian, is independent on h_j, which would lead to the conclusion that the associated z components of the canonical momenta $H_j = G_j \cos(i_j)$ are conserved, where G_j is the magnitude the angular momentum of orbit j. We will return to this issue in Sect. 2.1.3.

The secularization procedure amounts to averaging Eq. 2.19 over the mean anomalies l_1 and l_2 of both inner and outer orbits, which for orbit j we denote as:

$$\langle ... \rangle_j = \frac{1}{2\pi}\int_0^{2\pi} ... \, \mathrm{d}l_j, \tag{2.21}$$

where the dots denote the quantity to be averaged. Note that it is incorrect to average over the true or eccentric anomalies because these quantities are not linear in time, whereas the mean anomaly is (for any binary orbit, the mean anomaly l is generally given by $l = 2\pi(t-T)/P$ where t is the time, T is the time of periastron passage and P is the orbital period). To simplify the integration, however, it may be more convenient to transform the integration over mean anomaly to an integration over true or eccentric anomaly. In principle the calculations can be done for any arbitrary order of $\alpha = a_1/a_2$ in Eq. 2.19, but for many hierarchical triple systems, already the lowest order-term $\propto \alpha^2$ (referred to as the quadrupole order term) is quite adequate. For a smaller but non-negligible fraction of systems, also the next order term $\propto \alpha^3$ (the octupole order term) is required for an adequate description. It has not been investigated whether the next order term $\propto \alpha^4$ introduces any substantial new behavior, although according to Naoz et al. (2011) this is likely not the case. More importantly, in the regime in which terms $\propto \alpha^4$ would be expected to be important (i.e. large α), hierarchical triple systems are not expected to be dynamically stable anyway.

In this section we include the quadrupole and octupole perturbing terms of the three-body Hamiltonian, which we denote as $R_{\rm quad}$ and $R_{\rm oct}$. Eq. 2.19 is thus rewritten as:

$$\mathcal{H} = -\frac{G_N m_1 m_2}{2a_1} - \frac{G_N (m_1+m_2) m_3}{2a_2} - R_{\rm quad} - R_{\rm oct} - \frac{G_N}{a_2}\sum_{n=4}^{\infty} \alpha^n M_n \left(\frac{r_1}{a_1}\right)^n \left(\frac{a_2}{r_2}\right)^{n+1} \widetilde{P}_n(\cos(\Phi)), \tag{2.22}$$

where

$$\begin{aligned}R_{\rm quad} &= \frac{G_N}{a_2}\left(\frac{a_1}{a_2}\right)^2 M_2 \left(\frac{r_1}{a_1}\right)^2 \left(\frac{a_2}{r_2}\right)^3 \widetilde{P}_2(\cos(\Phi)) = \frac{G_N m_1 m_2 m_3}{(m_1+m_2)\,a_2}\left(\frac{a_1}{a_2}\right)^2 \left(\frac{r_1}{a_1}\right)^2 \left(\frac{a_2}{r_2}\right)^3 \widetilde{P}_2(\cos(\Phi))\\ &= 16\, C_{\rm quad} \left(\frac{r_1}{a_1}\right)^2 \left(\frac{a_2}{r_2}\right)^3 \left(1-e_2^2\right)^{3/2} \widetilde{P}_2(\cos(\Phi)),\end{aligned} \tag{2.23}$$

with the quantity (with dimensions of energy) $C_{\rm quad}$:

$$C_{\rm quad} \equiv \frac{1}{16}\frac{G_N m_1 m_2 m_3}{(m_1+m_2)\,a_2}\left(\frac{a_1}{a_2}\right)^2 \left(1-e_2^2\right)^{-3/2} \tag{2.24}$$

and

$$\begin{aligned}R_{\rm oct} &= \frac{G_N}{a_2}\left(\frac{a_1}{a_2}\right)^3 M_3 \left(\frac{r_1}{a_1}\right)^3 \left(\frac{a_2}{r_2}\right)^4 \widetilde{P}_3(\cos(\Phi)) = \frac{G_N}{a_2}\left(\frac{a_1}{a_2}\right)^3 \left(\frac{r_1}{a_1}\right)^3 \left(\frac{a_2}{r_2}\right)^4 \frac{m_1 m_2 m_3}{(m_1+m_2)^3}\left(m_1^2 - m_2^2\right)\widetilde{P}_3(\cos(\Phi))\\ &= \frac{G_N}{a_2}\left(\frac{a_1}{a_2}\right)^3 \left(\frac{r_1}{a_1}\right)^3 \left(\frac{a_2}{r_2}\right)^4 \frac{m_1 m_2 m_3}{(m_1+m_2)^2}(m_1 - m_2)\,\widetilde{P}_3(\cos(\Phi))\\ &= -\frac{16}{15}\,4\,C_{\rm oct}\left(1-e_2^2\right)^{5/2}\left(\frac{r_1}{a_1}\right)^3 \left(\frac{a_2}{r_2}\right)^4 \widetilde{P}_3(\cos(\Phi)),\end{aligned} \tag{2.25}$$

with the quantity (again, with dimensions of energy) $C_{\rm oct}$:

$$C_{\rm oct} \equiv -\frac{15}{16}\frac{G_N}{4}\frac{m_1 m_2 m_3}{(m_1+m_2)^2}(m_1 - m_2)\left(\frac{a_1}{a_2}\right)^3 \frac{1}{a_2}\left(1-e_2^2\right)^{-5/2}. \tag{2.26}$$

Note that the factors in Eqs. 2.24 and 2.26 are introduced to ensure that the final expressions for the secularly averaged perturbing terms to both quadrupole and octupole orders are without an overall multiplicative factor. After some straightforward calculations, which are described in Appendix A.1.3, the secularly averaged perturbing terms are found to be:

$$\langle\langle R_{\rm quad}\rangle_2\rangle_1 = C_{\rm quad}\left[6\left(Z_a^2+Z_c^2\right)\left(1+4e_1^2\right)+6\left(Z_b^2+Z_d^2\right)\left(1-e_1^2\right)-4\left(2+3e_1^2\right)\right]; \tag{2.27}$$

$$\langle\langle R_{\rm oct}\rangle_2\rangle_1 = C_{\rm oct}e_1e_2\left[Z_a\left\{5\left(3+4e_1^2\right)\left(Z_a^2+Z_c^2\right)-4\left(3e_1^2+4\right)\right\}+5\left(1-e_1^2\right)\left(3Z_aZ_b^2+Z_aZ_d^2+2Z_bZ_cZ_d\right)\right]. \tag{2.28}$$

Here the quantities Z_a, Z_b, Z_c and Z_d are functions of g_1, g_2, i_1, i_2 and $\Delta h \equiv h_1 - h_2$ and we have defined them as follows:

$$\begin{cases} Z_a &\equiv D_a\cos(g_1)\cos(g_2) - D_b\sin(g_1)\cos(g_2) + D_c\cos(g_1)\sin(g_2) + D_d\sin(g_1)\sin(g_2); \\ Z_b &\equiv -D_a\sin(g_1)\cos(g_2) - D_b\cos(g_1)\cos(g_2) - D_c\sin(g_1)\sin(g_2) + D_d\cos(g_1)\sin(g_2); \\ Z_c &\equiv -D_a\cos(g_1)\sin(g_2) + D_b\sin(g_1)\sin(g_2) + D_c\cos(g_1)\cos(g_2) + D_d\sin(g_1)\cos(g_2); \\ Z_d &\equiv D_a\sin(g_1)\sin(g_2) + D_b\cos(g_1)\sin(g_2) - D_c\sin(g_1)\cos(g_2) + D_d\cos(g_1)\cos(g_2); \end{cases}$$

$$\begin{cases} D_a &\equiv \cos(\Delta h); \\ D_b &\equiv \cos(i_1)\sin(\Delta h); \\ D_c &\equiv \cos(i_2)\sin(\Delta h); \\ D_d &\equiv \cos(i_1)\cos(i_2)\cos(\Delta h) + \sin(i_1)\sin(i_2). \end{cases} \tag{2.29}$$

Note that the Z-functions satisfy the following two relations:

$$\begin{cases} Z_a^2 + Z_c^2 &= \left(D_a\cos(g_1) - D_b\sin(g_1)\right)^2 + \left(D_c\cos(g_1) + D_d\sin(g_1)\right)^2; \\ Z_b^2 + Z_d^2 &\equiv \left(D_a\sin(g_1) + D_b\cos(g_1)\right)^2 + \left(D_c\sin(g_1) - D_d\cos(g_1)\right)^2, \end{cases} \tag{2.30}$$

which implies that the secularly averaged Hamiltonian to quadrupole order is independent of g_2, which in turn implies that e_2 is constant in this approximation (cf. Sect. 2.1.3). Making the substitution $\Delta h = \pi$ into Eqs. 2.27 and 2.28 (which is strictly incorrect for deriving the equations of motion), one finds the following simplified expressions (see Appendix A.1.3 for details):

$$\langle\langle R_{\rm quad}\rangle_2\rangle_1|_{\Delta h=\pi} = C_{\rm quad}\left[\left(2+3e_1^2\right)\left(3\cos^2(i_{\rm tot})-1\right)+15e_1^2\sin^2(i_{\rm tot})\cos(2g_1)\right]; \tag{2.31}$$

$$\langle\langle R_{\rm oct}\rangle_2\rangle_1|_{\Delta h=\pi} = C_{\rm oct}e_1e_2\left[A\cos(\phi)+10\cos(i_{\rm tot})\sin^2(i_{\rm tot})\left(1-e_1^2\right)\sin(g_1)\sin(g_2)\right], \tag{2.32}$$

where $i_{\rm tot} = i_1 + i_2$ and:

$$\cos(\phi) = Z_a|_{\Delta h=\pi}; \quad A = 4 + 3e_1^2 - \frac{5}{2}\sin^2(i_{\rm tot})B; \qquad B = 2 + 5e_1^2 - 7e_1^2\cos(2g_1). \tag{2.33}$$

Eqs. 2.31 and 2.32 are identical to the expressions in Ford et al. (2000). In Sect. 2.1.3 the equations of motion are derived that follow from Eqs. 2.27 and 2.28.

2.1.3 The equations of motion

Following common convention (Harrington, 1968; Ford et al., 2000) we employ canonical coordinates known as Delaunay's elements, which are the mean anomalies l_j, arguments of periastron g_j and longitudes of the ascending nodes h_j of both binary orbits. These coordinates are found as follows (Valtonen & Karttunen, 2006). Starting from the Hamiltonian of the two-body problem expressed in terms of spherical coordinates (r, θ, ϕ) one performs a canonical coordinate transformation such that the pure binary terms in the Hamiltonian (i.e. the first two terms in Eq. 2.19), expressed in these new coordinates, vanish identically. The reason to perform such a transformation is that the equations of motion in the pure binary case are trivial in such a coordinate system, i.e. all coordinates are simply constant. The explicit equation giving such a transformation is the Hamilton-Jacobi equation (Valtonen & Karttunen 2006, Chapter 4.10). The result is that the new canonical coordinates in which the Hamiltonian of the binary system vanishes are minus the time of periastron passage, $-\tau$, the longitude of the ascending node h and the argument of periastron g (Valtonen & Karttunen 2006, Chapter 4.11). Now another canonical transformation is made such that the first coordinate is the mean anomaly rather than minus the time of periastron passage. The conjugate momenta of these coordinates, denoted by L_j, G_j and H_j for orbit j, are then given by (Valtonen & Karttunen 2006, Chapter 4.12):

$$\begin{cases} L_1 &= m_1m_2\sqrt{\dfrac{G_Na_1}{m_1+m_2}}; \\ L_2 &= (m_1+m_2)m_3\sqrt{\dfrac{G_Na_2}{m_1+m_2+m_3}}; \\ G_j &= L_j\sqrt{1-e_j^2}; \quad H_j = G_j\cos(i_j), \end{cases} \tag{2.34}$$

The Hamiltonian equations of motion are then given by:

$$\begin{cases} \dot{L}_j &= \dfrac{\partial \mathcal{H}}{\partial l_j}; \quad \dot{l}_j = -\dfrac{\partial \mathcal{H}}{\partial L_j}; \\ \dot{G}_j &= \dfrac{\partial \mathcal{H}}{\partial g_j}; \quad \dot{g}_j = -\dfrac{\partial \mathcal{H}}{\partial G_j}; \\ \dot{H}_j &= \dfrac{\partial \mathcal{H}}{\partial h_j}; \quad \dot{h}_j = -\dfrac{\partial \mathcal{H}}{\partial H_j}. \end{cases} \tag{2.35}$$

As a consequence of the secularization procedure, $\mathcal{H}$ is no longer dependent on l_j, hence L_j and thus a_j are constant. Furthermore, if one substitutes the constraint $\Delta h = \pi$ into the Hamiltonian, one finds that it is independent of h_j and thus that the H_j are constant. This is formally incorrect because the derivation of Hamilton's equations of motion relies on the possibility of making arbitrary variations of the system's trajectory and these arbitrary variations are restricted by the dynamical constraint $\Delta h = \pi$. The correct approach is thus to apply the constraint *after* deriving the equations of motion (Naoz et al., 2011). The inclination angles i_1 and i_2 are not part of the canonical coordinates $(l_1, l_2, g_1, g_2, h_1, h_2)$; they are readily found from the fact that the total angular momentum $\mathbf{G}_{\rm tot} \equiv \mathbf{G}_1 + \mathbf{G}_2$ is conserved. Squaring this definition gives $\mathbf{G}_{\rm tot}^2 = \mathbf{G}_1^2 + \mathbf{G}_2^2 + 2\mathbf{G}_1 \cdot \mathbf{G}_2 = G_1^2 + G_2^2 + 2G_1G_2\cos(i_{\rm tot})$, where $i_{\rm tot} = i_1 + i_2$ is the mutual inclination angle between $\mathbf{G}_1$ and $\mathbf{G}_2$. Separate equations for the time derivatives of i_1 and i_2 follow from the cosine rule in the triangle spanned by $\mathbf{G}_1$, $\mathbf{G}_2$ and $\mathbf{G}_{\rm tot}$:

$$\cos(i_1) = \frac{G_{\rm tot}^2 + G_1^2 - G_2^2}{2G_{\rm tot}G_1}; \quad \cos(i_2) = \frac{G_{\rm tot}^2 + G_2^2 - G_1^2}{2G_{\rm tot}G_2}. \tag{2.36}$$

Eq. 2.36 describes the evolution of i_1 and i_2 as a consequence of a change in G_1 and G_2. To find first-order differential equations for the secular evolution of the orbital quantities e_j and g_j we apply 2.35 to the secularly averaged perturbing terms Eqs. 2.27 and 2.28 and substitute $\Delta h = \pi$. The details are included in Appendix A.1.4. The resulting equations are:

$$\begin{aligned}
\dot{g}_1 &= 6\,C_{\rm quad}\left\{\frac{1}{G_1}\left[4\cos^2(i_{\rm tot}) + (5\cos(2g_1) - 1)\left(1 - e_1^2 - \cos^2(i_{\rm tot})\right)\right] + \frac{\cos(i_{\rm tot})}{G_2}\left[2 + e_1^2(3 - 5\cos(2g_1))\right]\right\} \\
&\quad - C_{\rm oct}e_2\left\{e_1\left(\frac{1}{G_2} + \frac{\cos(i_{\rm tot})}{G_1}\right)\left[\sin(g_1)\sin(g_2)\left[A + 10\left(3\cos^2(i_{\rm tot}) - 1\right)\left(1 - e_1^2\right)\right] - 5B\cos(i_{\rm tot})\cos(\phi)\right]\right. \\
&\quad \left. - \frac{1 - e_1^2}{e_1G_1}\left[\cos(\phi)\left(3A - 10\cos^2(i_{\rm tot}) + 2\right) + 10\cos(i_{\rm tot})\sin^2(i_{\rm tot})\left(1 - 3e_1^2\right)\sin(g_1)\sin(g_2)\right]\right\}; \qquad (2.37) \\
\dot{g}_2 &= 3\,C_{\rm quad}\left\{\frac{2\cos(i_{\rm tot})}{G_1}\left[2 + e_1^2(3 - 5\cos(2g_1))\right] + \frac{1}{G_2}\left[4 + 6e_1^2 + \left(5\cos^2(i_{\rm tot}) - 3\right)\left(2 + e_1^2(3 - 5\cos(2g_1))\right)\right]\right\} \\
&\quad + C_{\rm oct}e_1\left\{\sin(g_1)\sin(g_2)\left[\frac{4e_2^2 + 1}{e_2G_2}10\cos(i_{\rm tot})\sin^2(i_{\rm tot})\left(1 - e_1^2\right) - e_2\left(\frac{1}{G_1} + \frac{\cos(i_{\rm tot})}{G_2}\right)\left(A + 10\left(3\cos^2(i_{\rm tot}) - 1\right)\right.\right.\right. \\
&\quad \left.\left.\left. \times\left(1 - e_1^2\right)\right)\right] + \cos(\phi)\left[5B\cos(i_{\rm tot})\,e_2\left(\frac{1}{G_1} + \frac{\cos(i_{\rm tot})}{G_2}\right) + \frac{4e_2^2 + 1}{e_2G_2}A\right]\right\}; \qquad (2.38) \\
\dot{e}_1 &= C_{\rm quad}\frac{1 - e_1^2}{G_1}\,30\,e_1\sin^2(i_{\rm tot})\sin(2g_1) + C_{\rm oct}e_2\frac{1 - e_1^2}{G_1}\left\{35\cos(\phi)\sin^2(i_{\rm tot})e_1^2\sin(2g_1) - 10\cos(i_{\rm tot})\sin^2(i_{\rm tot})\right. \\
&\quad \left. \times\cos(g_1)\sin(g_2)\left(1 - e_1^2\right) - A\left(\sin(g_1)\cos(g_2) - \cos(i_{\rm tot})\cos(g_1)\sin(g_2)\right)\right\}; \qquad (2.39) \\
\dot{e}_2 &= -C_{\rm oct}e_1\frac{1 - e_2^2}{G_2}\left\{10\cos(i_{\rm tot})\sin^2(i_{\rm tot})\left(1 - e_1^2\right)\sin(g_1)\cos(g_2) + A\left(\cos(g_1)\sin(g_2) - \cos(i_{\rm tot})\sin(g_1)\cos(g_2)\right)\right\}. \qquad (2.40)
\end{aligned}$$

In general, it is necessary to employ numerical integration techniques to solve these highly non-linear first order coupled differential equations. For a limiting case in the quadrupole order approximation, analytic solutions exist and are discussed below in Sect. 2.2.

2.2 Analytic solutions in the test particle quadrupole order limit

In order to gain some analytical insight into the nature and properties of Kozai cycles, we investigate solutions which exist for the quadrupole order with the additional constraint that $G_2 \gg G_1$, i.e. that the outer orbital angular momentum completely dominates the inner orbital angular momentum. Since in most cases the masses are comparable, this implies $a_2 \gg a_1$. This limit is also

known as the test particle quadrupole order limit (Naoz et al., 2011) and is the limit originally explored by Kozai (1962). Many of the results given here were first derived by Kinoshita & Nakai (1999).

Consider the three-body system at the initial state, denoted with a subscript 0 and at some later time. Due to conservation of total angular momentum the following relation holds:

$$G_{1,0}^2 + G_{2,0}^2 + 2G_{1,0}G_{2,0}\theta_0 = G_1^2 + G_2^2 + 2G_1G_2\theta, \tag{2.41}$$

where $\theta \equiv \cos(i_{\rm tot})$. In the quadrupole approximation, e_2 is constant (cf. Appendix A.1.4), thus with Eq. 2.34 this becomes:

$$\begin{aligned}
&L_1^2\left(1-e_{1,0}^2\right) + L_2^2\left(1-e_{2,0}^2\right) + 2L_1L_2\sqrt{1-e_{1,0}^2}\sqrt{1-e_{2,0}^2}\,\theta_0 = L_1^2\left(1-e_1^2\right) + L_2^2\left(1-e_{2,0}^2\right) + 2L_1L_2\sqrt{1-e_1^2}\sqrt{1-e_{2,0}^2}\,\theta \\
&\iff \frac{L_1}{L_2}\left(1-e_{1,0}^2\right) + 2\sqrt{1-e_{1,0}^2}\sqrt{1-e_{2,0}^2}\,\theta_0 = \frac{L_1}{L_2}\left(1-e_1^2\right) + 2\sqrt{1-e_1^2}\sqrt{1-e_{2,0}^2}\,\theta \\
&\iff \theta = \frac{1}{2\sqrt{1-e_1^2}\sqrt{1-e_{2,0}^2}}\left[2\sqrt{1-e_{1,0}^2}\sqrt{1-e_{2,0}^2}\,\theta_0 + \frac{L_1}{L_2}\left(e_1^2 - e_{1,0}^2\right)\right]
\end{aligned} \tag{2.42}$$

$$\xrightarrow{L_2 \gg L_1} \frac{\sqrt{1-e_{1,0}^2}}{\sqrt{1-e_1^2}}\,\theta_0 \equiv \sqrt{\frac{x_0}{x}}\theta_0, \tag{2.43}$$

where for convenience we defined $x \equiv 1 - e_1^2$ and $x_0 \equiv 1 - e_{1,0}^2$. Eq. 2.43 implies that $\sqrt{1-e_1^2}\cos(i_{\rm tot})$ is constant in the limit $L_2 \gg L_1$. This is a well-known property of the Kozai resonance: during eccentricity maxima, $\cos(i_{\rm tot})$ is at its maximum value and vice versa. Another conserved quantity besides total angular momentum is total energy and hence the Hamiltonian. Since a_j (and m_i) are constant, Eq. 2.19 implies (after secularization) that Eq. 2.31 is conserved to quadrupole order. Thus:

$$\begin{aligned}
C_{\rm quad} r_0 &\equiv C_{\rm quad}\left[\left(2+3e_{1,0}^2\right)\left(3\theta_0^2-1\right) + 15e_{1,0}^2\left(1-\theta_0^2\right)\cos(2g_{1,0})\right] \\
&= C_{\rm quad}\left[\left(2+3e_1^2\right)\left(3\theta^2-1\right) + 15e_1^2\left(1-\theta^2\right)\cos(2g_1)\right].
\end{aligned} \tag{2.44}$$

In Eq. 2.44, θ can be eliminated in favor of e_1 with Eq. 2.43 and the resulting equation can be solved for $\cos(2g_1)$ in terms of e_1 and initial parameters. With this expression for $\cos(2g_1)$ and Eq. 2.43, the quadrupole order term of $\dot{e}_1$, given by Eq. 2.39, can be expressed solely in terms of e_1, or, equivalently, a differential equation is found for $\dot{x}$ in terms of x and constants. The result is (see Appendix A.1.5 for details):

$$\frac{{\rm d}x}{{\rm d}t} = -\frac{24\sqrt{6}}{\tau}\sqrt{(x-x_A)(x-x_B)(x-x_C)}, \tag{2.45}$$

where τ is a characteristic time scale of the problem,

$$\tau = \frac{8}{\pi}\left(\frac{P_2}{P_1}\right)P_2\frac{m_1+m_2+m_3}{m_3}\left(1-e_2^2\right)^{3/2} \tag{2.46}$$

(with $e_2 = e_{2,0}$) and the quantities x_A, x_B and x_C are functions of x_0, θ_0 and $g_{1,0}$ and are given by:

$$\begin{aligned}
&\begin{cases} x_A &= x_0 + \frac{5}{2}(1-x_0)\left(1-\theta_0^2\right)\sin^2(g_{1,0}); \\ x_B &= \frac{1}{2}b - \frac{1}{2}\sqrt{b^2-4c}; \\ x_C &= \frac{1}{2}b + \frac{1}{2}\sqrt{b^2-4c}; \end{cases} \\
&\begin{cases} b &= x_0 + \frac{5}{3}\left[\theta_0^2 + (1-x_0)\left(1-\theta_0^2\right)\cos^2(g_{1,0})\right]; \\ c &= \frac{5}{3}\theta_0^2 x_0. \end{cases}
\end{aligned} \tag{2.47}$$

These quantities satisfy $x_A - x_B > 0$ and $x_C - x_B > 0$. As shown in Appendix A.1.5, the solution of Eq. 2.45 is given in terms of a Jacobi elliptic function:

$$x(t) = x_A + (x_B - x_A)\,{\rm cn}^2\left(12\sqrt{6}\,\frac{t}{\tau}\sqrt{x_C - x_B} - \tilde{t}_0\,\middle|\,k\right), \tag{2.48}$$

where ${\rm cn}(t|k)$ is a Jacobi elliptic function (Gradshteyn & Ryzhik 2007, 8.154) with modulus:

$$k^2 = \frac{x_A - x_B}{x_C - x_B} \tag{2.49}$$

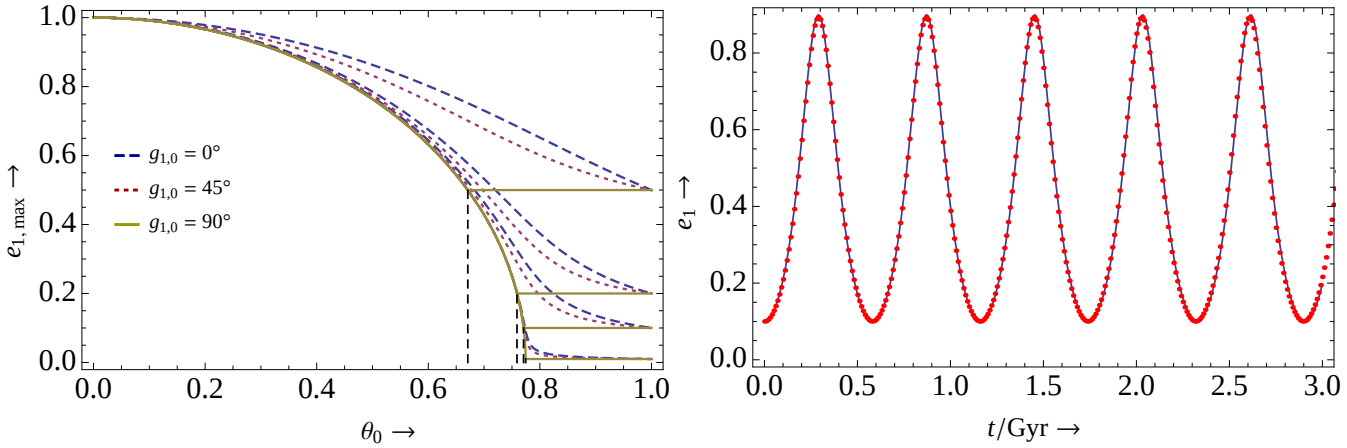

Figure 2.2: Left panel: maximum inner orbit inclination, $e_{1,\max}$, as function of $\theta_0 \equiv \cos(i_{\mathrm{tot},0})$, where $i_{\mathrm{tot},0}$ is the initial mutual inclination angle, for $g_{1,0} = 0$ (dashed), $g_{1,0} = 45°$ (dotted) and $g_{1,0} = 90°$ (solid). Four different values of $e_{1,0}$ are shown: 0.01, 0.1, 0.2 and 0.5 (from bottom to top). The vertical dashed lines show the values of $\theta_0 = \left[\frac{3}{5}\left(1 - e_{1,0}^2\right)\right]^{1/2}$ corresponding to each set of curves with different $e_{1,0}$. Right panel: inner orbit eccentricity as function of time according to the solution Eq. 2.48 for the example system discussed in the text. Also included are points from numerical integrations of Eqs. 2.37, 2.38, 2.39 and 2.40.

and $\tilde{t}_0$ is defined via:

$$\tilde{t}_0 = -\mathrm{arccn}\left(\sqrt{\frac{x_0 - x_A}{x_B - x_A}}\right). \tag{2.50}$$

The function $\mathrm{cn}(t|k)$ is $4K$-periodic, where K is the complete elliptic integral of the first kind,

$$K = \int_0^{\pi/2} \frac{\mathrm{d}\theta}{\sqrt{1 - k^2 \sin^2(\theta)}}. \tag{2.51}$$

Furthermore, $\mathrm{cn}(t|k)$ is symmetric around $t = 2K$, hence $\mathrm{cn}^2(t|k)$ is $2K$-periodic. This implies that a full cycle of x, and hence e_1, is completed after a "Kozai period" P_K, where P_K is given by:

$$12\sqrt{6}\frac{P_K}{\tau}\sqrt{x_C - x_B} = 2K \Rightarrow P_K = \frac{\tau K}{6\sqrt{6}}\frac{1}{\sqrt{x_C - x_B}} = \frac{4K}{3\pi\sqrt{6}}\frac{1}{\sqrt{x_C - x_B}}\left(\frac{P_2}{P_1}\right)P_2\frac{m_1 + m_2 + m_3}{m_3}\left(1 - e_2^2\right)^{3/2}. \tag{2.52}$$

The factor $4K/\left(3\pi\sqrt{6}\sqrt{x_C - x_B}\right)$ in Eq. 2.52 is typically of order unity, as are the mass and outer orbit eccentricity factors; the most important quantity that determines P_K is therefore $(P_2/P_1)\,P_2$. Since $(P_2/P_1) \gg 5$ for most observed hierarchical triple systems (Tokovinin et al., 2006) this implies that typically $P_K \gg P_2$, thus Kozai cycles can play an important role on timescales which are much longer than the dynamical timescales. Kozai timescales of Myr are common and even timescales of Gyr are possible (for an example see Sect. 4.2), which are comparable to stellar evolutionary timescales. During the Kozai cycle, x varies between x_B and x_A, implying that the minimum and maximum values of e_1 are given by $e_{1,\min} = \sqrt{1 - x_A}$ and $e_{1,\max} = \sqrt{1 - x_B}$. Fig. 2.2 (left) shows $e_{1,\max}$ as a function of $\theta_0 \equiv \cos(i_{\mathrm{tot},0})$, where $i_{\mathrm{tot},0}$ is the initial mutual inclination angle, for several values of $e_{1,0}$ and $g_{1,0}$. In the case that $g_{1,0} = 90°$, if $\theta_0^2 > \frac{3}{5}\left(1 - e_{1,0}^2\right)$ then $e_{1,\max} = e_{1,0}$. However, this does not mean that there are no Kozai cycles (see below). In the other two cases shown in Fig. 2.2 (left), $g_{1,0} = 0°$ and $g_{1,0} = 45°$, $e_{1,\max} > e_{1,0}$ for all values of $\theta_0 < 1$. Regardless of the value of $g_{1,0}$ the maximum eccentricity can become very high as θ_0 approaches 0. In particular, if $e_{1,0} = 0$ and $\theta_0^2 < \frac{3}{5}$ then it follows from $e_{1,\max} = \sqrt{1 - x_B}$ and Eq. 2.47 that $e_{1,\max} = \left(1 - \frac{5}{3}\theta_0^2\right)^{1/2}$ independent of the value of $g_{1,0}$, which is consistent with Fabrycky & Tremaine (2007). Note that $e_{1,\max} \rightarrow 1$ as $\theta_0 \rightarrow 0$. This may seem unrealistic, but it is important to remember that this derivation is only strictly valid in the limit $a_1/a_2 \rightarrow 0$. The latter limit implies that $a_2 \rightarrow \infty$ (for finite $a_1 > 0$), which in turn implies an infinitely long Kozai period (cf. Eq. 2.52) – this is clearly not possible in realistic situations. For any realistic systems, the second term $\propto L_1/L_2 \propto \sqrt{a_1/a_2}$ in Eq. 2.42 is not negligible, in which case the above expression for $e_{1,\max}$ is no longer valid. In Sect. 2.3.3 we will take into account this second term in Eq. 2.42, however.

To better understand the different behavior of $e_{1,\max}$ as function of θ_0 for different $g_{1,0}$, Fig. 2.3 shows the $(\cos(g_1), e_1)$ space for $e_{1,0} = 0.5$. The curves are obtained from Eq. 2.44 with θ given by Eq. 2.43. Solid curves correspond to $g_{1,0} = 0°$ and dashed curves to $g_{1,0} = 90°$. From top to bottom, both sets of curves correspond to $i_{\mathrm{tot},0} = 70°$, $i_{\mathrm{tot},0} = 46°$, $i_{\mathrm{tot},0} = 40°$ and $i_{\mathrm{tot},0} = 39°$ (the dashed curve with $-1 \leq \cos(g_1) \leq 1$ corresponds to $i_{\mathrm{tot},0} = 39°$). If $g_{1,0} = 0°$ then $\cos(g_{1,0}) = 1$ and g_1 increases monotonically ($-1 \leq \cos(g_1) \leq 1$), which qualitative behaviour is independent of θ_0. In this case g_1 is said to circulate. Whenever $g_{1,0} = 0°$, $e_{1,\max} > e_{1,0}$ as also shown by Fig. 2.2 (left). If $g_{1,0} = 90°$ then the behaviour is more complicated and strongly dependent on θ_0.

If $\theta_0^2 > \frac{3}{5}$ (cf. the curve corresponding to $i_{\rm tot,0} = 39°$ in Fig. 2.3) then g_1 circulates, although the fact that the cycle starts with $\cos(g_{1,0}) = 0$ implies that $e_{1,0} = e_{1,\rm max}$. As θ_0 decreases and passes the point where $\theta_0^2 = \frac{3}{5}$ (cf. the dashed curve corresponding to $i_{\rm tot,0} = 40°$ in Fig. 2.3), g_1 no longer circulates but oscillates between two fixed values ($-0.4 \lesssim \cos(g_1) \lesssim 0.4$ in Fig. 2.3). In the latter case g_1 is said to librate. As demonstrated by Fig. 2.3, still $e_{1,\rm max} = e_{1,0}$ at this point. As θ_0 decreases further, the size of the "libration island" decreases (cf. the curve corresponding to $i_{\rm tot,0} = 46°$ in Fig. 2.3), until at some critical value of θ_0 this island is reduced to a single point in the $(\cos(g_1), e_1)$ space at $(\cos(g_1), e_1) = (0, e_{1,0})$. This critical value of θ_0 can be obtained by setting $\dot{g}_{1,\rm quad} = 0$ with $(\cos(g_1), e_1) = (0, e_{1,0})$, where $\dot{g}_{1,\rm quad}$ is given by the quadrupole order part of Eq. 2.37, neglecting the term $\propto G_2^{-1}$ as appropriate for the limit in which the solutions of this section are valid. Thus we find that the critical value is given by $\theta_0 = \left[\frac{3}{5}\left(1 - e_{1,0}^2\right)\right]^{1/2}$. For $e_{1,0} = 0.5$, this expression yields a critical mutual inclination angle of $i_{\rm tot,0} \approx 47.9°$. If θ_0 is less than the critical value then $e_{1,\rm min} = e_{1,0}$ and $e_{1,\rm max} > e_{1,0}$, i.e. the "libration island" has "flipped" from the region $e_1 \leq e_{1,0}$ to $e_1 \geq e_{1,0}$ (note that for $g_{1,0} = 0°$, always $e_1 \geq e_{1,0}$). This explains why in the case that $g_{1,0} = 90°$, $e_{1,\rm max} > e_{1,0}$ only if $\theta_0 < \left[\frac{3}{5}\left(1 - e_{1,0}^2\right)\right]^{1/2}$. In the latter case, if $\theta_0 > \left[\frac{3}{5}\left(1 - e_{1,0}^2\right)\right]^{1/2}$ then still there are Kozai cycles from the point of view that e_1, g_1 and θ still exhibit periodic behaviour. However, the maximum eccentricity does not exceed the initial eccentricity.

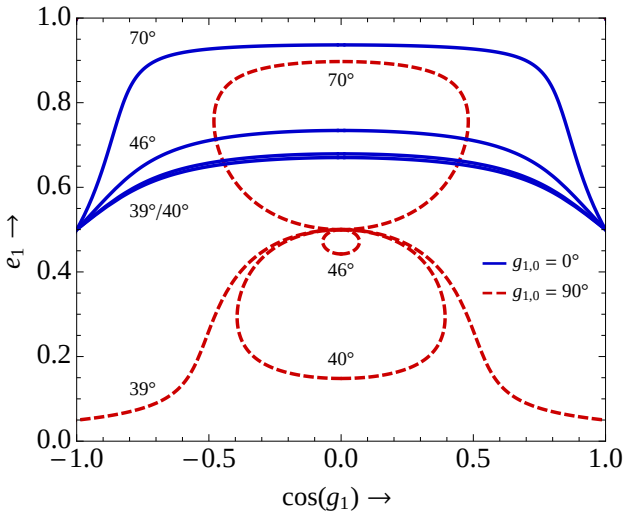

Figure 2.3: The $(\cos(g_1), e_1)$ space for $e_{1,0} = 0.5$. The curves are obtained from Eq. 2.44 with θ given by Eq. 2.43. Solid curves correspond to $g_{1,0} = 0°$ and dashed curves to $g_{1,0} = 90°$. From top to bottom (also indicated by the numbers) both sets of curves correspond to $i_{\rm tot,0} = 70°$, $i_{\rm tot,0} = 46°$, $i_{\rm tot,0} = 40°$ and $i_{\rm tot,0} = 39°$ (the dashed curve with $-1 \leq \cos(g_1) \leq 1$ corresponds to $i_{\rm tot,0} = 39°$).

As an illustration of Eq. 2.48, Fig. 2.2 (right) shows a few Kozai cycles for an equal-mass three-body system with $m_1 = m_2 = m_3 = 1\,M_\odot$, $a_1 = 1$ AU, $a_2 = 10^3$ AU, $e_{1,0} = 0.1$, $e_{2,0} = 0.5$, $i_{\rm tot,0} = 70°$ and $g_{1,0} = 0°$ (in the quadrupole limit, the dynamics are independent of g_2). In addition to this analytical solution, calculations from numerical integrations of the three-body dynamics to quadrupole order (not neglecting the L_1/L_2 term in Eq. 2.42) have been shown with red points. These numerical integrations are performed in a standalone c-code which implements the CVODE ordinary differential equation integrator software package (Cohen & Hindmarsh, 1996). This code will be discussed in Sect. 3.2. Eq. 2.52 gives $P_K = 0.58$ Gyr for this system, which is in excellent agreement with Fig. 2.48, as is the value $e_{1,\rm max} \approx 0.90$ given by Eq. 2.47.

For this particular system, octupole order terms are completely unimportant (we have verified this by means of numerical integration with the same code as above) because the ratio $a_2/a_1 = 10^3$ is very large. This implies that $C_{\rm oct}$ is small compared to $C_{\rm quad}$, (cf. Eqs. 2.24 and 2.26; see also Sect. 2.3.3 and in particular Eq. 2.56). An effect which is important, however, and is not included in the above discussion is apsidal motion in the inner binary system due to general relativity. This additional source of apsidal motion acts to detune the Kozai resonance between e_1 and g_1. For the example system, this effect completely dominates three-body dynamic apsidal motion, thus Kozai cycles are completely damped[2] (see Fig. 2.4). This and other additional sources of apsidal motion are discussed further in Sect. 2.3.

2.3 Additional sources of apsidal motion

The secular three-body dynamics (STD) cause apsidal motion in both inner and outer binary orbits, cf. Eqs. 2.37 and 2.38. Various physical processes may be responsible for additional apsidal motion. In terms of celestial mechanics, they are the result of forces which do not obey the Newtonian gravity law (i.e. the force being inversely proportional to the square of the distance). A common property of the additional apsidal motion terms is that they do not change sign over time and thus act to detune the resonances between e_j, g_j and $i_{\rm tot}$ which are present during Kozai cycles. Consequently the latter may be reduced in amplitude or even be completely suppressed. Here the main additional sources which are of interest in stellar systems are discussed. In addition, a semi-analytic method is introduced to calculate the maximum eccentricity reached during Kozai cycles.

[2] A different example system in which the above solutions hold and this damping effect does not occur can easily be chosen, however, by significantly increasing a_1 while keeping a_2/a_1 constant.

2.3.1 Apsidal motion due to general relativity

The apsidal motion in the inner binary system due to general relativity (GR), $\dot{g}_{1,\mathrm{GR}}$, can be derived from the Schwarzschild metric, employing the Killing vectors associated with conservation of angular momentum and conservation of energy (see Appendix B for more details). The canonical expression for this apsidal motion is given by (see e.g. Fabrycky & Tremaine 2007):

$$\dot{g}_{1,\mathrm{GR}} = \frac{3}{c^2 a_1 \left(1-e_1^2\right)} \left[\frac{G_N(m_1+m_2)}{a_1}\right]^{3/2}, \tag{2.53}$$

where c is the speed of light. In order to derive Eq. 2.53, one needs to make the assumption that the eccentricity is small compared to unity. In cases where the inner orbit eccentricity is high, such as during eccentricity maximum in a Kozai resonance, the canonical expression is no longer valid in the strict sense and may therefore be inadequate. Nevertheless, this canonical expression has been used in previous works where Kozai cycles play an important role, e.g. Blaes et al. (2002) and Fabrycky & Tremaine (2007). In Appendix B this issue is addressed and it is investigated whether Eq. 2.53 is still valid for the most extreme conditions which we find in the population synthesis study (Chapter 5). These conditions are $e_1 \sim 1-10^{-5}$ for inner binary orbits of $a_1 \sim 1\,\mathrm{AU}$ and $e_1 \sim 1-10^{-8}$ for inner binary orbits of $a_1 \sim 10^3\,\mathrm{AU}$. We find that Eq. 2.53 is still valid if $\log_{10}(1-e_1) \gtrsim -8.3 - \log_{10}(a_1/\mathrm{AU}) + \log_{10}[(m_1+m_2)/M_\odot]$. This condition is satisfied for the two extreme conditions and we thus conclude that for the purposes of the population synthesis study it is justified to use Eq. 2.53.

2.3.2 Apsidal motion due to tidal bulges and rotation

In addition to relativistic apsidal motion which applies to point masses, the non-dissipative tidal bulges induced in physically extended stars in relatively close proximity also introduce apsidal motion. To lowest order in R_1/a_1 and R_2/a_1, where R_1 and R_2 are the radii of the primary and secondary inner orbit stars respectively, the total rate of the latter apsidal motion, $\dot{g}_{1,\mathrm{tide}}$, is given by (e.g. Smeyers & Willems 2001):

$$\dot{g}_{1,\mathrm{tide}} = \dot{g}_{1,\mathrm{tide},1} + \dot{g}_{1,\mathrm{tide},2}; \quad \dot{g}_{1,\mathrm{tide},i} = \frac{15}{8} n_1 \frac{8+12e_1^2+e_1^4}{\left(1-e_1^2\right)^5} \left[\tilde{q}_i\, k_{\mathrm{am},i} \left(\frac{R_i}{a_1}\right)^5\right], \tag{2.54}$$

where $n_1 = 2\pi/P_1 = \left[G(m_1+m_2)/a_1^3\right]^{1/2}$ is the mean inner orbital motion, $k_{\mathrm{am},i}$ is the classical apsidal motion constant of star i (see Kopal 1946 for a definition) and $\tilde{q}_i \equiv m_{3-i}/m_i$. Furthermore, the intrinsic rotation of the stars causes deformation of the stars in the inner orbit and therefore apsidal motion of which the total rate $\dot{g}_{1,\mathrm{rotate}}$ is given by (Fabrycky & Tremaine, 2007)

$$\dot{g}_{1,\mathrm{rotate}} = \dot{g}_{1,\mathrm{rotate},1} + \dot{g}_{1,\mathrm{rotate},2}; \quad \dot{g}_{1,\mathrm{rotate},i} = \frac{n_1}{\left(1-e_1^2\right)} \left[(1+\tilde{q}_i)\, k_{\mathrm{am},i} \left(\frac{R_i}{a_1}\right)^5 \left(\frac{\Omega_i}{n_1}\right)^2\right], \tag{2.55}$$

where Ω_i is the angular spin frequency of star i. Here we assume that the spin vectors $\mathbf{\Omega}_1$ and $\mathbf{\Omega}_2$ of both stars in the inner orbit are parallel to the inner orbit angular momentum vector $\mathbf{G}_1$ (i.e. we assume coplanarity), which is consistent with the assumption made in the binary population synthesis code on which the triple algorithm in this work is based (Chapter 3).

2.3.3 Semi-analytic computation of $e_{1,\mathrm{max}}$

In the limit that energy is not dissipated, i.e. in the absence of tidal friction and/or gravitational wave emission, the maximum eccentricity reached during Kozai cycles, $e_{1,\mathrm{max}}$, can be computed semi-analytically in the quadrupole order approximation. Clearly energy is conserved in this limit and therefore the total Hamiltonians corresponding to the initial and final states may be equated. To our knowledge, the octupole order STD Hamiltonian contains too many degrees of freedom to obtain $e_{1,\mathrm{max}}$; this does not apply to the quadrupole order STD Hamiltonian. This limitation implies that the method does not apply when octupole order terms are important. A quantity which measures the importance of octupole terms relative to quadrupole order terms is the ratio ϵ_{oct} of the octupole quantity C_{oct} (Eq. 2.26) to the quadrupole quantity C_{quad} (Eq. 2.24) (Naoz et al., 2011). Disregarding the numerical factor of $15/4$ and the minus sign and introducing an additional factor of e_2, this quantity is given by[3]:

$$\epsilon_{\mathrm{oct}} = \frac{m_1-m_2}{m_1+m_2} \frac{a_1}{a_2} \frac{e_2}{1-e_2^2}. \tag{2.56}$$

[3]The motivation for the additional factor of e_2 in ϵ_{oct} comes from the fact that $\langle\langle R_{\mathrm{oct}}\rangle_2\rangle_1$ contains an overall factor of e_2 (cf. Eq. 2.28) which is not the case for $\langle\langle R_{\mathrm{quad}}\rangle_2\rangle_1$ (cf. Eq. 2.27).

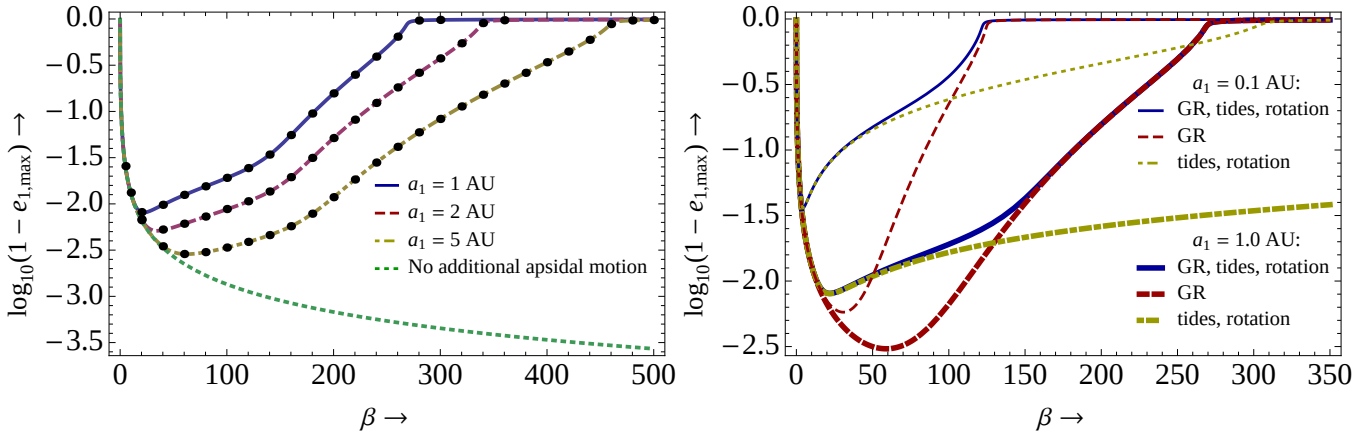

Figure 2.4: Maximum inner orbit eccentricity reached during Kozai cycles as function of $\beta \equiv a_2/a_1$ according to the method described in Sect. 2.3.3. Fixed triple parameters are as follows: $m_1 = 1.0\,M_\odot$, $m_2 = 0.5\,M_\odot$, $m_3 = 0.5\,M_\odot$, $R_1 = 1.0\,R_\odot$, $R_2 = 0.57\,R_\odot$, $e_{1,0} = 0.01$, $e_{2,0} = 0.30$, $\theta_0 = 0$, $g_{1,0} = 0^\circ$ and $k_{\rm am,1} = k_{\rm am,2} = 0.014$. Both inner orbit stars have spin periods of 10 days. In the left panel, the dotted curve shows the dependence in the absence of additional sources of motion. For the other three curves apsidal motion due to general relativity, tidal bulges and rotation is included, with three different values of a_1: $a_1 = 1.0$ AU (solid), $a_1 = 2.0$ AU (dashed) and $a_1 = 5.0$ AU (dot-dashed). Calculations of $e_{1,\max}$ according to direct numerical time integration of the STD equations of motion accurate to quadrupole order (with the same code used in Fig. 2.2) have also been shown. See Fig. 2.5 for a comparison with direct numerical time integration of the STD equations of motion accurate to octupole order. In the right panel thick curves correspond to $a_1 = 1.0$ AU and thin curves correspond to $a_1 = 0.1$ AU. In the solid curves apsidal motion due to both general relativity and tidal bulges and rotation is included. In the dashed curves apsidal motion due to general relativity alone is included. Lastly, in the dot-dashed curves apsidal motion due to tidal bulges and rotation alone is included.

The main parameters which determine the importance of the octupole order terms are therefore the relative inner binary mass difference $(m_1 - m_2)/(m_1 + m_2)$, the ratio a_1/a_2 and the outer orbit eccentricity. Typically $\log_{10}(|\epsilon_{\rm oct}|) \gtrsim -3$ indicates that octupole order terms are important, in which limit the eccentric Kozai mechanism applies (e.g. Lithwick & Naoz 2011). When this mechanism is important extremely high inner orbit eccentricities can be reached, far greater than predicted by quadrupole order terms alone. We will return to this mechanism in the example systems (Chapter 4) and in the population synthesis (Chapter 5).

The procedure to compute $e_{1,\max}$ within the limits described above is as follows. Excluding the constant inner and outer binary orbital energy terms, $-G_N m_1 m_2/(2a_1)$ and $-G_N m_3(m_1 + m_2)/(2a_2)$ respectively, and excluding the energies associated with the stellar spins, the total energy, i.e. the full Hamiltonian, is given by:

$$\mathcal{H}_{\rm tot} = \mathcal{H}_{\rm STD,\,quad} + \mathcal{H}_{\rm GR} + \mathcal{H}_{\rm tide} + \mathcal{H}_{\rm rotate}, \tag{2.57}$$

where $\mathcal{H}_{\rm STD,\,quad}$ is given by Eq. 2.31; $\mathcal{H}_{\rm GR}$ is given by (e.g. Blaes et al. 2002):

$$\mathcal{H}_{\rm GR} = \frac{G m_1 m_2}{a_1} \frac{3G(m_1 + m_2)}{c^2 a_1} \frac{1}{\left(1 - e_1^2\right)^{1/2}} \tag{2.58}$$

and the last two terms in Eq. 2.57 are taken from Fabrycky & Tremaine (2007):

$$\mathcal{H}_{\rm tide} = \mathcal{H}_{\rm tide,1} + \mathcal{H}_{\rm tide,2}; \quad \mathcal{H}_{{\rm tide},i} = \frac{G m_1 m_2}{a_1} \frac{1 + 3e_1^2 + \frac{3}{8}e_1^4}{\left(1 - e_1^2\right)^{9/2}} \left[\tilde{q}_i\, k_{{\rm am},i} \left(\frac{R_i}{a_1}\right)^5\right]; \tag{2.59}$$

$$\mathcal{H}_{\rm rotate} = \mathcal{H}_{\rm rotate,1} + \mathcal{H}_{\rm rotate,2}; \quad \mathcal{H}_{{\rm rotate},i} = \frac{G m_1 m_2}{a_1} \frac{1}{3\left(1 - e_1^2\right)^{3/2}} \left[(1 + \tilde{q}_i)\, k_{{\rm am},i} \left(\frac{R_i}{a_1}\right)^5 \left(\frac{\Omega_i}{n_1}\right)^2\right], \tag{2.60}$$

where $\tilde{q}_i \equiv m_{3-i}/m_i$. Note that the spin angular frequency Ω_i of each inner binary star is assumed to be constant.

From the quadrupole order equation of motion for e_1 (i.e. the quadrupole part of Eq. 2.39) it follows that e_1 is stationary ($\dot{e}_1 = 0$) for $g_1 = (\pi/2)\,k$, $k \in \mathbb{Z}$. Whenever $g_1 = 0$ or g_1 is a multiple of π (even k), the stationary point corresponds to a minimum in e_1. This follows from Fig. 2.3: even k correspond to $\cos(g_1) = \cos((\pi/2)\,k) = \pm 1$, which in turn correspond to minima in e_1, provided that g_1 circulates. On the other hand, if k is odd then the stationary point corresponds to $\cos(g_1) = 0$, which implies a minimum or a maximum in e_1 in the case that g_1 librates or a maximum in e_1 in the case that g_1 circulates. Note that the inclusion of the additional apsidal motion terms to the Hamiltonian does not affect these properties because these terms do not alter the equation for $\dot{e}_{1,\rm STD}$. This is because they do not imply any additional change of inner orbit angular momentum

G_1 for they are independent of g_1. We conclude that the state where the inner orbit eccentricity is at a maximum corresponds to $\cos(2g_1) = \cos(\pi k) = -1$ for odd k (in the case that g_1 librates, odd k can also correspond to a minimum eccentricity, but this value is easily distinguished from the maximum eccentricity). Furthermore, the corresponding value of $\theta = \cos(i_{\rm tot})$ is found from total angular momentum conservation of the triple system and given by Eq. 2.42. Thus the maximum eccentricity during Kozai cycles, $e_{1,\rm max}$, can be found in terms of the initial parameters by numerically solving (e.g. by means of the Newton-Raphson method) the algebraic equation $\mathcal{H}_{\rm tot} = \mathcal{H}_{\rm tot,0}$ for $e_1 = e_{1,\rm max}$ with $\cos(2g_1) = \cos(\pi k) = -1$ and θ given by Eq. 2.42. Here $\mathcal{H}_{\rm tot,0}$ is the total Hamiltonian corresponding to the initial state and is a function of the initial $e_{1,0}$, θ_0, $g_{1,0}$ and parameters appearing in Eqs. 2.58, 2.59 and 2.60.

As a demonstration of the method described above and to show the significance of the additional sources of apsidal motion, Fig. 2.4 shows $e_{1,\rm max}$ as function of the outer to the inner orbit semi-major axes a_2/a_1, which is constant during the dynamical evolution with the assumption of no dissipation. Since this quantity will turn out to be very important in the evolution of triples we will denote it with special symbol, i.e. $\beta \equiv a_2/a_1$. The parameters of the triple system are typical for a solar-mass hierarchical triple system in which the components are MS stars. Firstly, note that an expression for $e_{1,\rm max}$ as function of initial parameters and in the absence of additional sources of apsidal motion was derived in Sect. 2.2. This expression is independent of β. However, in this derivation the second term $\propto L_1/L_2 \propto \sqrt{a_1/a_2}$ in Eq. 2.42 was neglected. It turns out that if this second term is included the effect is to decrease $e_{1,\rm max}$. In other words, $e_{1,\rm max}$ decreases as $L_1/L_2 \propto \beta^{-1/2}$ increases. This dependence is shown by the dotted curve in Fig. 2.4 (left) for which the additional sources of apsidal motion are not included[4]. As $\beta \rightarrow \infty$ the second term in Eq. 2.42 becomes negligibly small and the previous result obtained in Sect. 2.4 applies, i.e. $e_{1,\rm max} = \left(1 - \frac{5}{3}\theta_0^2\right)^{1/2}$ if $e_{1,0} = 0$ (and $\theta_0^2 < \frac{3}{5}$).

Furthermore, when the additional sources of apsidal motion are included the effect is to detune the Kozai resonance and hence decrease $e_{1,\rm max}$. This is demonstrated by Fig. 2.4 (left), where contributions of apsidal motion due to general relativity, tidal bulges and rotation have been taken into account for three different values of a_1 (solid, dashed and dot-dashed curves). Depending on the value of a_1 these additional sources of apsidal motion can completely quench the Kozai resonance if β is sufficiently large. In addition, points from direct numerical time integration of the equations of motion accurate to quadrupole order are included in Fig. 2.4 (left) and show excellent agreement with the semi-analytical curves. For this system octupole order terms are generally not important, even for small β: only for $\beta \lesssim 18$ the octupole order integrations predict higher $e_{1,\rm max}$, but the differences are not significant (cf. Fig. 2.5).

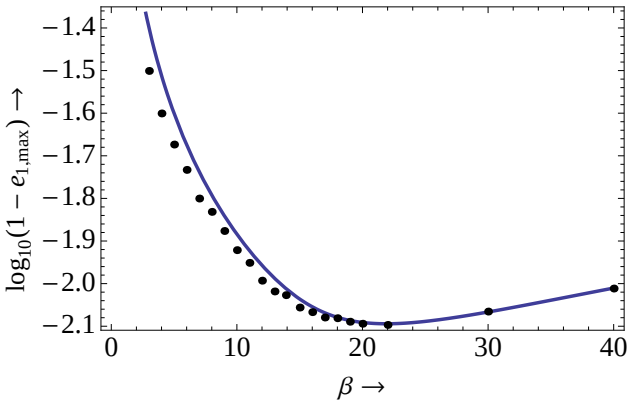

Figure 2.5: Maximum inner orbit eccentricity reached during Kozai cycles as function of $\beta \equiv a_2/a_1$ for small β for the same triple system as in Fig. 2.4. The solid curve applies to $a_1 = 1.0$ AU and is computed according to the method described in Sect. 2.3.3, i.e. it is accurate to quadrupole order. The individual points show direct numerical time integrations where octupole order terms are also included. For $\beta \lesssim 18$ there is a distinguishable difference between the quadrupole order and octupole order results, although this difference is small. Note that the system is no longer dynamically stable for $\beta \lesssim 5$ according to the stability criterion of Mardling & Aarseth (2001).

The individual contributions of additional apsidal motion due to general relativity on the one hand and tidal bulges and rotation on the other hand are illustrated in Fig. 2.4 (right), where curves are shown for $a_1 = 0.1$ AU and $a_1 = 1.0$ AU. In this example the contribution of the damping of the Kozai resonance due to tidal bulges and rotation dominates for $\beta \lesssim 100$, whereas the contribution due to general relativity dominates for $\beta \gtrsim 100$. Which of the two processes dominates is strongly dependent on the stellar radii and spin periods (cf. Eqs. 2.54 and 2.55). If the radii are very small (e.g. for compact objects) and/or the spin periods are long then the contribution due to tidal bulges and rotation is typically negligible. In the latter case, apsidal motion due to general relativity can still significantly detune the Kozai resonance. Note that for both contributions the damping effect increases in significance for smaller values of a_1. Thus for tight inner binary orbits the Kozai resonance can be effective only for a narrow range of β. This has important consequences for the evolution of triples as will become clear in the population synthesis study (Chapter 5).

[4]For this case (to quadrupole order, with no additional sources of apsidal motion and with Eq. 2.42) we have found an analytic expression for $e_{1,\rm max}$ as function of β. The general expression is very complicated, but for $e_{1,0} = 0$ it reduces to the following relatively simple expression: let $\gamma \equiv \frac{1}{2}\left(1 - e_2^2\right)^{-1/2} L_1/L_2 = \frac{1}{2}\left(1 - e_2^2\right)^{-1/2} \beta^{-1/2} \frac{m_1 m_2}{m_3(m_1+m_2)} \left(\frac{m_1+m_2+m_3}{m_1+m_2}\right)^{1/2}$ then $e_{1,\rm max} = \left\{1 - \frac{1}{8\gamma^2}\left[3 + 9\gamma^2 + 8\gamma\theta_0 - \left(9 + \gamma\left(48\theta_0 + \gamma\left(54 + \gamma^2 - 16\gamma\theta_0 - 16\theta_0^2\right)\right)\right)^{1/2}\right]\right\}^{1/2}$. The critical inclination for which $e_{1,\rm max} > e_{1,0} = 0$ is $\theta_0 = \left[\frac{3}{5}\left(1 + \frac{1}{15}\gamma^2\right)\right]^{1/2} - \frac{1}{5}\gamma < \left(\frac{3}{5}\right)^{1/2}$, i.e. the minimum mutual inclination angle for significant Kozai cycles is increased with respect to the case $\gamma = 0$. As $\gamma \rightarrow 0$, it can be shown that $e_{1,\rm max} \rightarrow \left(1 - \frac{5}{3}\theta_0^2\right)^{1/2}$, which is the familiar limit derived in Sect. 2.2.

Chapter 3

Hierarchical triple evolution algorithm

In previous studies of (coeval) stellar hierarchical triple systems usually a specific aspect of the evolution is studied. In particular, the coupling of Kozai cycles with tidal friction (KCTF) has been studied in the context of main sequence systems (Mazeh & Shaham, 1979; Eggleton & Kisseleva-Eggleton, 2001; Kisseleva-Eggleton & Eggleton, 2010; Fabrycky & Tremaine, 2007). Furthermore, the occurrence of extremely-high eccentricity cycles in relatively high mass (primary mass $m_1 = 7.0\,M_\odot$) triple systems has recently been studied by Shappee & Thompson (2012), where the effect of mass loss due to stellar evolution was taken into account. To our knowledge a comprehensive population synthesis study of triples, including a realistic description of the stellar evolution of the inner binary components and their binary interaction, has not been performed. Such a study is needed to gain quantitative understanding of the importance of Kozai cycles in triples at various stages in the evolution of the inner binary system. Because a relatively fast algorithm is required for such a population synthesis study and in order to ensure that the evolution of the inner binary system is treated adequately, we utilize an existing binary population synthesis code which has been extensively used and tested previously, `binary_c` (Izzard et al., 2004, 2006, 2009). To this code we have added a newly-developed module (hereafter `triple_c`) which takes into account the secular gravitational dynamics introduced by the tertiary in hierarchical triple systems. In this chapter we describe the details of this new algorithm: in Sect. 3.1 we give the equations which form the basis of the algorithm, in Sect. 3.2 we describe the implementation of the coupling of the secular gravitational dynamics to the binary population synthesis code and in Sect. 3.3 we include some information on how various required physical quantities are obtained. Examples of the new algorithm are given in Chapter 4 and the results of the population synthesis study are described in Chapter 5.

3.1 Equations

In Sect. 2 the basic theoretical background of the dynamics of hierarchical triple systems was introduced. To octupole order, these dynamics are described by Eqs. 2.37, 2.38, 2.39 and 2.40, in conjunction with conservation of total angular momentum which is expressed by Eq. 2.41. In addition there are sources of apsidal motion other than due to STD as discussed in Sect. 2.3. These dynamics are restricted to non-dissipative processes during which the inner and outer orbital energies remain constant. If the eccentricity in the inner binary system reaches high values due to Kozai cycles, however, dissipative processes, in particular tidal friction and gravitational wave emission (GWE), may become (very) important in the inner binary system. These processes are non-conservative and orbital and/or spin energy is dissipated either into the interior of the inner orbit stars or in the form of gravitational waves. It is therefore important to also incorporate such effects into the triple evolution algorithm. We address these processes below.

3.1.1 Tidal friction

Whenever the distances between the stars in hierarchical triple systems become comparable to the stellar radii, tidal effects may become important. For most hierarchical triple systems, tidal effects in the outer binary system are unimportant due to the large separation of the tertiary with respect to the inner binary components. In the inner binary system the separation between binary components is typically much smaller and hence tidal effects can be important. In the case of inner binary components with convective envelopes, the components may induce hydrostatic tidal bulges on each other. Dissipative convective motions in the stellar envelopes may then produce a misalignment of these tidal bulges with respect to the line joining the two centers of mass of the inner binary components. This misalignment causes a tidal torque which enables the exchange between stellar spin

and orbital angular momentum and energy. This exchange continues until circularization, synchronization and coplanarity are achieved (Hut, 1980). Because convective processes typically occur on short (i.e. dynamical) timescales, this mechanism for tidal friction, also known as the equilibrium tide (Zahn, 1977; Hut, 1981) is generally an effective mechanism. In the absence of a convective envelope, which is the case for MS stars with $m \gtrsim 1.25\,M_\odot$, a different, much less effective mechanism is responsible for the exchange between stellar spin and orbital angular momentum and energy. In the latter case, low-frequency gravity modes are excited by the time-varying tidal potential (the dynamical tide, Zahn 1975). Consequently damping of these modes near the surface of the star by radiation provides the torque necessary for the coupling between rotation of the spin and orbit. Similarly to the equilibrium tide, in the dynamical tide the final result of the tidal interaction is circularization, synchronization and coplanarity. Due to the much lower efficiency of energy dissipation in the dynamical tide compared to that in the equilibrium tide, the timescales of these processes are generally much longer.

Regardless of the mechanism which produces the necessary torque, the effect of tidal friction on the dynamical evolution of the orbital parameters can be described by the same equations, which are given by (Hut, 1981):

$$\begin{aligned}
\dot{a}_{1,\mathrm{TF}} &= \dot{a}_{1,\mathrm{TF},1} + \dot{a}_{1,\mathrm{TF},2}; \quad \dot{a}_{1,\mathrm{TF},i} = -6\,\frac{k_{\mathrm{am},i}}{T_i}\,\tilde{q}_i(1+\tilde{q}_i)\left(\frac{R_i}{a_1}\right)^8 \frac{a_1}{\left(1-e_1^2\right)^{15/2}}\left[f_1\left(e_1^2\right) - \left(1-e_1^2\right)^{3/2} f_2\left(e_1^2\right)\frac{\Omega_i}{n_1}\right];\\
\dot{e}_{1,\mathrm{TF}} &= \dot{e}_{1,\mathrm{TF},1} + \dot{e}_{1,\mathrm{TF},2}; \quad \dot{e}_{1,\mathrm{TF},i} = -27\,\frac{k_{\mathrm{am},i}}{T_i}\,\tilde{q}_i(1+\tilde{q}_i)\left(\frac{R_i}{a_1}\right)^8 \frac{e_1}{\left(1-e_1^2\right)^{13/2}}\left[f_3\left(e_1^2\right) - \frac{11}{18}\left(1-e_1^2\right)^{3/2} f_4\left(e_1^2\right)\frac{\Omega_i}{n_1}\right];\\
\dot{\Omega}_{i,\mathrm{TF}} &= 3\,\frac{k_{\mathrm{am},i}}{T_i}\,\frac{\tilde{q}_i^2}{r_{g,i}^2}\left(\frac{R_i}{a_1}\right)^6 \frac{n_1}{\left(1-e_1^2\right)^6}\left[f_2\left(e_1^2\right) - \left(1-e_1^2\right)^{3/2} f_5\left(e_1^2\right)\frac{\Omega_i}{n_1}\right],
\end{aligned} \tag{3.1}$$

where TF denotes tidal friction, $i \in \{1,2\}$ denotes the inner binary star number, $k_{\mathrm{am},i}$ is the apsidal motion constant, T_i is a typical time scale on which significant changes in the orbit take place through tidal evolution, $\tilde{q}_i = m_{3-i}/m_i$, $n_1 = 2\pi/P_1 = \left[G(m_1+m_2)/a_1^3\right]^{1/2}$ is the mean inner orbital motion, Ω_i is the spin frequency and $r_{g,i}^2 \equiv I_i/\left(m_i R_i^2\right)$ is the radius of gyration, where I_i denotes moment of inertia. The functions $f_k\left(e_1^2\right)$, $k \in \{1,2,3,4,5\}$, are functions of the square of the inner orbit eccentricity and their explicit expressions are given in Hut (1981). Note that we assume coplanarity for both inner orbit stars, consistent with the treatment in Hurley et al. (2002). The ratio k_i/T_i measures the strength of tidal friction due to the structure of the stars. In Sect. 3.3 we elaborate on how we obtain this quantity at various evolutionary stages of the inner binary stars.

3.1.2 Gravitational wave emission

Although in hierarchical triple systems the outer binary system is too wide for any significant gravitational wave emission (GWE), this process may be important in the much tighter inner binary system. As a consequence of the emission of gravitational waves the inner binary is circularized and shrinks, which processes are described quantitatively by (e.g. Blaes et al. 2002):

$$\dot{e}_{1,\mathrm{GWE}} = -\frac{304\,G_N^3 m_1 m_2 (m_1+m_2)\,e_1}{15c^5 a_1^4\left(1-e_1^2\right)^{5/2}}\left(1+\frac{121}{304}e_1^2\right); \tag{3.2}$$

$$\dot{a}_{1,\mathrm{GWE}} = -\frac{64\,G_N^3 m_1 m_2 (m_1+m_2)}{5c^5 a_1^3\left(1-e_1^2\right)^{7/2}}\left(1+\frac{73}{24}e_1^2+\frac{37}{96}e_1^4\right). \tag{3.3}$$

Typically, GWE is only important in rather tight inner binary systems, at least if e_1 is not very high. For circular orbits Eq. 3.3 is easily integrated to give a merger time as a function of the initial inner orbit semi-major axis $a_{1,0}$ of $t_{\mathrm{GWE,merge}} = 5c^5 a_{1,0}^4/\left[256 G_N^3 m_1 m_2 (m_1+m_2)\right]$. For a $0.6\,M_\odot + 0.6\,M_\odot$ binary system this gives $t_{\mathrm{GWE,merge}} = t_H = 13.7$ Gyr (i.e. a Hubble time) if $a_{1,0} \approx 0.012$ AU (corresponding to an orbital period of $P_1 \approx 0.42$ d). This merger time can be significantly reduced for highly eccentric orbits, however, e.g. as a consequence of Kozai cycles. The latter scenario has been investigated by Thompson (2011) who finds that inner binaries with orbital periods as high as $P_1 \sim 300$ d can still merge within a Hubble time if the triple parameters are chosen appropriately. In the present work, however, we find that the tertiary is too distant for this to be an important effect by the time GWE becomes important (i.e. when a_1 is sufficiently small), see also Chapters 5 and 6 and in particular Fig. 5.6.

3.1.3 System of first-order differential equations

The `triple_c` algorithm computes the change of various dynamical inner and outer orbit quantities according to the following system of ordinary differential equations:

$$\begin{cases} \dot{g}_1 &= \dot{g}_{1,\mathrm{STD}} + \dot{g}_{1,\mathrm{GR}} + \dot{g}_{1,\mathrm{tide}} + \dot{g}_{1,\mathrm{rotate}}; \\ \dot{g}_2 &= \dot{g}_{2,\mathrm{STD}}; \\ \dot{e}_1 &= \dot{e}_{1,\mathrm{STD}} + \dot{e}_{1,\mathrm{TF}} + \dot{e}_{1,\mathrm{GWE}}; \\ \dot{e}_2 &= \dot{e}_{2,\mathrm{STD}}; \\ \dot{a}_1 &= \dot{a}_{1,\mathrm{TF}} + \dot{a}_{1,\mathrm{GWE}}; \\ \dot{\theta} &= \frac{-1}{G_1 G_2}\left[\dot{G}_1\left(G_1 + G_2\theta\right) + \dot{G}_2\left(G_2 + G_1\theta\right)\right]; \\ \dot{\Omega}_1 &= \dot{\Omega}_{1,\mathrm{TF}}; \\ \dot{\Omega}_2 &= \dot{\Omega}_{2,\mathrm{TF}}, \end{cases} \tag{3.4}$$

where $\dot{g}_{1,\mathrm{STD}}$, $\dot{g}_{2,\mathrm{STD}}$, $\dot{e}_{1,\mathrm{STD}}$ and $\dot{e}_{2,\mathrm{STD}}$ are given by Eqs. 2.37, 2.38, 2.39 and 2.40 respectively, $\dot{g}_{1,\mathrm{GR}}$, $\dot{g}_{1,\mathrm{tide}}$ and $\dot{g}_{1,\mathrm{rotate}}$ are given by Eqs. 2.53, 2.54 and 2.55 respectively, $\dot{a}_{1,\mathrm{TF}}$, $\dot{e}_{1,\mathrm{TF}}$ and $\dot{\Omega}_{i,\mathrm{TF}}$ are given by Eq. 3.1 and $\dot{e}_{1,\mathrm{GWE}}$ and $\dot{a}_{1,\mathrm{GWE}}$ are given by Eqs. 3.2 and 3.3 respectively. The main assumption in these equations is that all processes that they describe are independent such that terms due to different processes may simply be added. It is important to note that both tidal friction and GWE act only to change a_1 and e_1 and therefore affect the magnitude and not the direction of $\mathbf{G}_1$, the orbital angular momentum vector of the inner binary system. This implies that θ is not affected by these processes. To compute the effect of STD on θ (i.e. the expression for $\dot{\theta}$), differentiate the relation $G_{\mathrm{tot}}^2 = G_1^2 + G_2^2 + 2G_1G_2\theta$ with respect to time, noting that G_{tot} due to STD is constant and subsequently solve for $\dot{\theta}$. The quantities $\dot{G}_1$ and $\dot{G}_2$ due to STD in the relation that follows are given by $\dot{G}_j = -G_j e_j \dot{e}_j / \left(1 - e_j^2\right)$. The latter follows from differentiation of G_j in Eq. 2.34 with respect to time, using that L_j due to STD remains constant.

3.2 Coupling to binary algorithm

The hierarchical triple evolution algorithm developed in this work couples the system of differential equations Eq. 3.4 with the existing rapid binary population synthesis algorithm `binary_c`, developed originally by Hurley et al. (2002) and further developed by Izzard et al. (2004, 2006, 2009). This binary star algorithm includes stellar evolution and a variety of binary interaction processes such as mass loss due to stellar winds, mass transfer and common-envelope evolution. We refer to Hurley et al. (2002) for further details of the binary population synthesis algorithm. The novel aspect of our approach is that the evolution of the inner binary system is taken into account through the coupling with `binary_c`. Also taken into account is the evolution of the tertiary, which is treated as being isolated such that its mass may be computed from single stellar evolution. The mass of the tertiary enters the differential equations Eq. 3.4 through the m_3-dependent quantities C_{quad}, C_{oct} and G_2. We restrict ourselves to hierarchical triple systems in which at all times the tertiary is sufficiently distant from the inner binary system that it does not fill its Roche-lobe in its orbit around the inner binary system as has been suggested in earlier studies (e.g. Iben & Tutukov 1999). Therefore the latter processes are not modeled in the triple algorithm.

The system of differential equations Eq. 3.4 is solved for the duration of each time step of the `binary_c` algorithm. In order to ensure proper convergence of the solutions of Eq. 3.4, which are quite stiff in nature, we use an ordinary differential equation (ODE) solver specifically designed to integrate stiff ordinary differential equations (Cohen & Hindmarsh, 1996). We have checked the results of our algorithm when not coupled with the `binary_c` code by computing the evolution of the same hierarchical triple systems as in Ford et al. (2000), Blaes et al. (2002) and Naoz et al. (2011) and have found good agreement. During each `binary_c` time step, quantities not included in the right hand side of Eq. 3.4 such as the inner binary masses and radii are assumed to be constant. Because the `binary_c` algorithm uses adaptive time steps to match the rate of binary evolution, it is always ensured that these quantities do not change significantly during each iteration of the triple evolution algorithm. In addition, the triple algorithm decreases the `binary_c` time step such that the inner orbital angular momentum G_1 does not change significantly. Thus, changes to the inner orbit semi-major axis and eccentricity due to STD coupled with tidal friction and GWE are relayed to the `binary_c` algorithm at appropriate times.

The version of `binary_c` used in this work enforces circularization at the onset of Roche Lobe overflow (RLOF) and common-envelope (CE) evolution. Although this assumption is generally justified for isolated binaries, in hierarchical triple systems high-amplitude eccentricity cycles could be induced even during these phases, in particular if the timescale of these cycles is comparable to or smaller than the timescales of mass transfer driven by RLOF. An accurate treatment of the latter processes in eccentric orbits is beyond the scope of this work (for recent work in this area we refer to Sepinsky et al. 2007) and so in this work the triple algorithm is disabled whenever mass transfer driven by RLOF or CE evolution ensues. Whenever the triple algorithm is active, it is ensured that tidal evolution and GWE in the inner binary system as calculated by `binary_c` do not change the inner orbital parameters, as these processes are taken into account by the triple module through the equations for $\dot{e}_1$ and $\dot{a}_1$ in Eq. 3.4. In this manner the coupling of eccentricity cycles with tidal friction and GWE in the inner orbit is calculated consistently.

If the ratio $\beta \equiv a_2/a_1$ is relatively large, the effects of STD are likely quenched by different processes in the inner binary system, in particular due to general relativistic apsidal motion in very tight inner binary systems, as has been illustrated in Sect. 2.3.3. In such situations it is not necessary to solve Eq. 3.4 as the STD-related terms are negligible and the inner binary evolution can therefore be handled fully by the existing `binary_c` code. In order to speed up computation, a criterion is therefore introduced which disables the ODE solver module and leaves the inner binary evolution up to `binary_c` in such cases. Specifically, for each iteration the ODE solver module is disabled if $\beta > 10\beta_{\rm crit,GR}$, where $\beta_{\rm crit,GR}$ is the value of β such that the periods associated with apsidal motion due to STD and general relativity are equal. An estimate of the period due to general relativistic apsidal motion is given by the reciprocal of Eq. 2.53, whereas an estimate of the period due to STD apsidal motion is given by[1] Eq. 2.52. Equating these two periods and ignoring factors of order unity, we find that the critical value of β for which GR apsidal motion dominates STD apsidal motion is given by:

$$\beta_{\rm crit,GR} \approx \left(\frac{c^2}{G_N}\right)^{1/3} a_1^{1/3} \left(\frac{m_3}{(m_1+m_2)^2}\right)^{1/3} \frac{\left(1-e_1^2\right)^{1/3}}{\left(1-e_2^2\right)^{1/2}} \approx 5\cdot 10^2 \left(\frac{a_1}{\rm AU}\right)^{1/3} \left(\frac{m_3}{M_\odot}\right)^{1/3} \left(\frac{m_1+m_2}{M_\odot}\right)^{-2/3} \frac{\left(1-e_1^2\right)^{1/3}}{\left(1-e_2^2\right)^{1/2}}. \tag{3.5}$$

Outer orbital expansion due to mass loss in either inner or outer binary systems is taken into account with the assumption of fast, isotropic winds (i.e. Jeans mode) such that $a_2(m_1+m_2+m_3)$ and e_2 remain constant (Huang, 1956, 1963). With this relation a new value of a_2 is computed from the changes of m_1, m_2 and m_3 during each time step of `binary_c`. The assumption implies that if the inner orbit components also lose mass in a fast isotropic wind such that $a_1(m_1+m_2)$ is constant and if the tertiary mass m_3 remains constant, then a_2 increases by a relatively smaller amount than a_1 increases, such that $\beta \equiv a_2/a_1$ decreases. We return to this important feature of triple evolution in Chapters 4 and 5.

Lastly, at each time step the triple system is checked for dynamical stability by means of the stability criterion formulated by Mardling & Aarseth (2001), which states that the system is stable if $\beta \equiv a_2/a_1$ satisfies:

$$\beta > \beta_{\rm crit} = \frac{2.8}{1-e_2}\left((1+q_2)\frac{1+e_2}{(1-e_2)^{1/2}}\right)^{2/5}(1-0.3i_{\rm tot}/\pi), \tag{3.6}$$

where $q_2 \equiv m_3/(m_1+m_2)$ and $i_{\rm tot}$ is expressed in radians. The factor depending on $i_{\rm tot}$ expresses the property that inclined triple systems tend to be more dynamically stable than coplanar ones. Whenever $\beta \leq \beta_{\rm crit}$, the STD equations are no longer strictly applicable and the triple algorithm is disabled. Subsequent evolution would have to be computed with a three-body integrator code, which is beyond the scope of this work (see e.g. Perets & Kratter 2012 for a study of triple systems which become dynamically unstable).

3.3 Evaluation of various physical quantities

In this section we include information on how various physical quantities occurring in Eq. 3.4 are evaluated in the `triple_c` algorithm. The ratio $k_{{\rm am},i}/T_i$, which is a measure for the strength of tidal friction (Sect. 3.1.1), is computed according to the same prescription which is used in `binary_c` (Hurley et al., 2002). In this prescription a distinction is made between convective, radiative and degenerate envelopes and the quantity k_i/T_i is computed based on results of Rasio et al. (1996), Zahn (1977) and Campbell (1984) for these three cases respectively. Typically for MS stars with radiative envelopes $k_i/T_i \sim 10^{-18}\,{\rm s}^{-1}$, for evolved stars with convective envelopes (i.e. giants) $k_i/T_i \sim 10^{-8}\,{\rm s}^{-1}$ and for degenerate stars $k_i/T_i \sim 10^{-15}\,{\rm s}^{-1}$ (see also the bottom right panel in Fig. 4.1). The gyration radii $r_{g,i}^2$, required for the expressions for $\dot{\Omega}_{i,\rm TF}$ (Eq. 3.1), are computed with a prescription in which the stars are split into two parts, consisting of the core and the envelope, detailed in Hurley et al. (2000) and Hurley et al. (2002). The quantities $k_{{\rm am},i}/T_i$ and $r_{g,i}^2$ are thus calculated from precisely the same prescription as in the `binary_c` code which is necessary for a consistent treatment.

The classical apsidal motion constant $k_{{\rm am},i}$ for star i in the inner binary orbit required for Eqs. 2.54 and 2.55 (note that in the above prescription of Hurley et al. (2002) the *ratio* $k_{{\rm am},i}/T_i$ is obtained and not $k_{{\rm am},i}$) is computed as a function of mass and time relative to the zero-age main sequence from detailed stellar models for metallicity $Z = 0.02$ calculated by Claret (2004). The run of $k_{{\rm am},i}$ with time is determined by means of linear relations scaled to the time spent during each evolutionary stage for all tabulated masses in Claret (2004). Subsequently, $k_{{\rm am},i}$ is calculated for arbitrary mass by means of linear interpolation between adjacent mass values. Furthermore, for low mass stars, i.e. $m_i < 0.7\,M_\odot$, the classical apsidal motion constant is taken to be $k_{{\rm am},i} = 0.14$ corresponding to $n = 3/2$ polytropes as an estimate for these (nearly) fully convective stars. For helium main sequence stars and white dwarfs, $k_{{\rm am},i}$ is calculated as function of mass by means of interpolations of tabulated data from Vila (1977). Lastly, for neutron stars, $k_{{\rm am},i}$ is calculated as function of mass and radius from the expression given in Hinderer (2008) and for black holes $k_{{\rm am},i} = 0$ as appropriate for non-spinning black holes.

[1] In this limit of relatively large β, Eq. 2.52 gives an adequate estimate of the Kozai period because in this limit the second term $\propto L_1/L_2$ in Eq. 2.42 and octupole order effects are not important.

Lastly, we detail some of the fixed binary evolution parameters used in this work. We choose quasi-solar metallicity, i.e. $Z = 0.02$. The initial spin periods of the inner orbit components are computed from a formula given by Hurley et al. (2000), which is fitted from data of the rotational speed of MS stars of Lang (1992). The common-envelope parameter $\alpha_{\rm CE}$ describes the efficiency of the conversion of orbital energy into binding energy with which to shed the envelope and it is set to the canonical value of $\alpha_{\rm CE} = 1$. In the $\alpha_{\rm CE}$ common-envelope description, an additional parameter λ is required, which is a dimensionless measure of the relative density distribution within the envelope; here it is determined by means of functional fits as detailed in Claeys et al. (2012). All other parameters intrinsic to the `binary_c` algorithm are also set to identical values as in Claeys et al. (2012).

Chapter 4

Example systems

To demonstrate the triple algorithm described in Chapter 3, we discuss in detail the evolution of two coeval stellar hierarchical triple systems which are typical examples of systems in our population synthesis study (Chapter 5) in which an inner binary carbon-oxygen (CO) white dwarf (WD) merger occurs through either a triple-induced circular mechanism (TICM) or a triple-induced eccentric mechanism (TIEM). These systems are selected from a triple sample in which the inner binary would not interact in the absence of a tertiary; we refer to Chapter 5 for more details.

4.1 CO WD TICM merger

We consider a hierarchical triple system with initial parameters $m_1 = 3.95\,M_\odot$, $m_2 = 3.03\,M_\odot$, $m_3 = 2.73\,M_\odot$, $a_1 = 19.7$ AU, $a_2 = 636.1$ AU, $e_1 = 0.23$, $e_2 = 0.82$, $i_{\rm tot} = 116.0°$, $g_1 = 28.5°$ and $g_2 = 249.6°$. Fig. 4.1 shows a_1, e_1, $\beta \equiv a_2/a_1$, $i_{\rm tot}$, $\epsilon_{\rm oct}$ and the tidal strength quantity k_i/T_i (Eq. 3.1) as a function of time. Here $\epsilon_{\rm oct}$ is the octupole parameter which quantifies the importance of octupole terms with respect to quadrupole terms and was introduced earlier in Sect. 2.3.3. In Fig. 4.1 the evolution is shown with both the triple algorithm enabled (triple case; solid curves) and disabled, leaving all inner binary evolution to `binary_c` (binary case; dashed curves). The latter binary case is equivalent to the situation in which there is no tertiary present. In the binary, case the inner orbit semi-major axis increases at the two moments when the inner binary stars evolve from AGB stars to CO WDs as a consequence of the associated wind mass loss. Here it is assumed that the wind mass loss is fast and isotropic such that $a_1(m_1 + m_2)$ remains constant. When either star in the inner binary system enters the RGB or AGB phase, it develops a convective envelope which increases the possibility for significant tidal fraction (cf. Sect. 3.1.1). In addition, the radii increase significantly. The change of envelope structure is reflected by a corresponding substantial increase of the tidal strength quantity k_i/T_i, as is shown by Fig. 4.1, where k_i/T_i is shown specifically during the primary AGB phase. Note that k_1/T_1 increases by 9 orders of magnitude during this phase and that it lasts for a relatively short time. Despite the large k_1/T_1 and radii, in the binary case there is no significant tidal friction due to the large a_1 and low e_1. Consequently in the binary case the CO WDs end their evolution in a wide binary of $a_1 \approx 84$ AU; note that during the evolution the stars did not interact.

In the triple case, Kozai cycles are induced in the inner orbit by the tertiary with $e_{1,\rm max} \approx 0.9$. Octupole order terms are important as $|\epsilon_{\rm oct}| \approx 10^{-2}$. Nevertheless, the eccentricity is not high enough to drive significant tidal friction during the MS because the tidal strength quantity is very small, $k_i/T_i \sim 10^{-18}\,{\rm s}^{-1}$. This is due to the fact that both inner binary stars have radiative envelopes. In addition, e_1 is not high enough for an orbital collision. During the primary RGB phase e_1 is not high enough to trigger significant tidal friction, but this is the case during the primary AGB phase starting at $t \approx 220.5$ Myr. Subsequently strong tidal friction circularizes the inner orbit during the time span of five Kozai cycles, where significant orbital shrinkage occurs at eccentricity maxima (Fig. 4.2). Consequently a_1 is reduced to $a_1 \approx 7$ AU and the orbit is completely circularized. Note that for complete circularization to occur, the duration of the phase in which k_1/T_1 is substantial must be sufficiently long compared to the Kozai period P_K, which is the case for this example system. In other cases, however, the Kozai period $P_K \propto (P_2/P_1)\,P_2$ (Eq. 2.52) can be much longer than the duration of the RGB/AGB phases, thus avoiding strong tidal friction even if the eccentricity maxima are high. After KCTF the ratio β has increased substantially to $\beta \sim 1200$, which is large enough to fully quench any subsequent eccentricity cycles (cf. Fig. 2.4). Consequently the mutual inclination angle $i_{\rm tot}$ is frozen to $i_{\rm tot} \approx 128°$.

Shortly after this episode of KCTF during the primary AGB phase in the triple case, the primary which swells to $R_1 \approx 600\,R_\odot$ fills its Roche Lobe and invokes common-envelope (CE) evolution, thus evolving to a CO WD and shrinking the orbit further to $a_1 \approx 1$ AU (Fig. 4.2). The secondary emerges from the CE as a MS star and continues its evolution. During its RGB phase the orbit is shrunk slightly due to tidal friction which explains the small kink in the plot of a_1 at $t \sim 10^{2.6}$ Myr in Fig. 4.1.

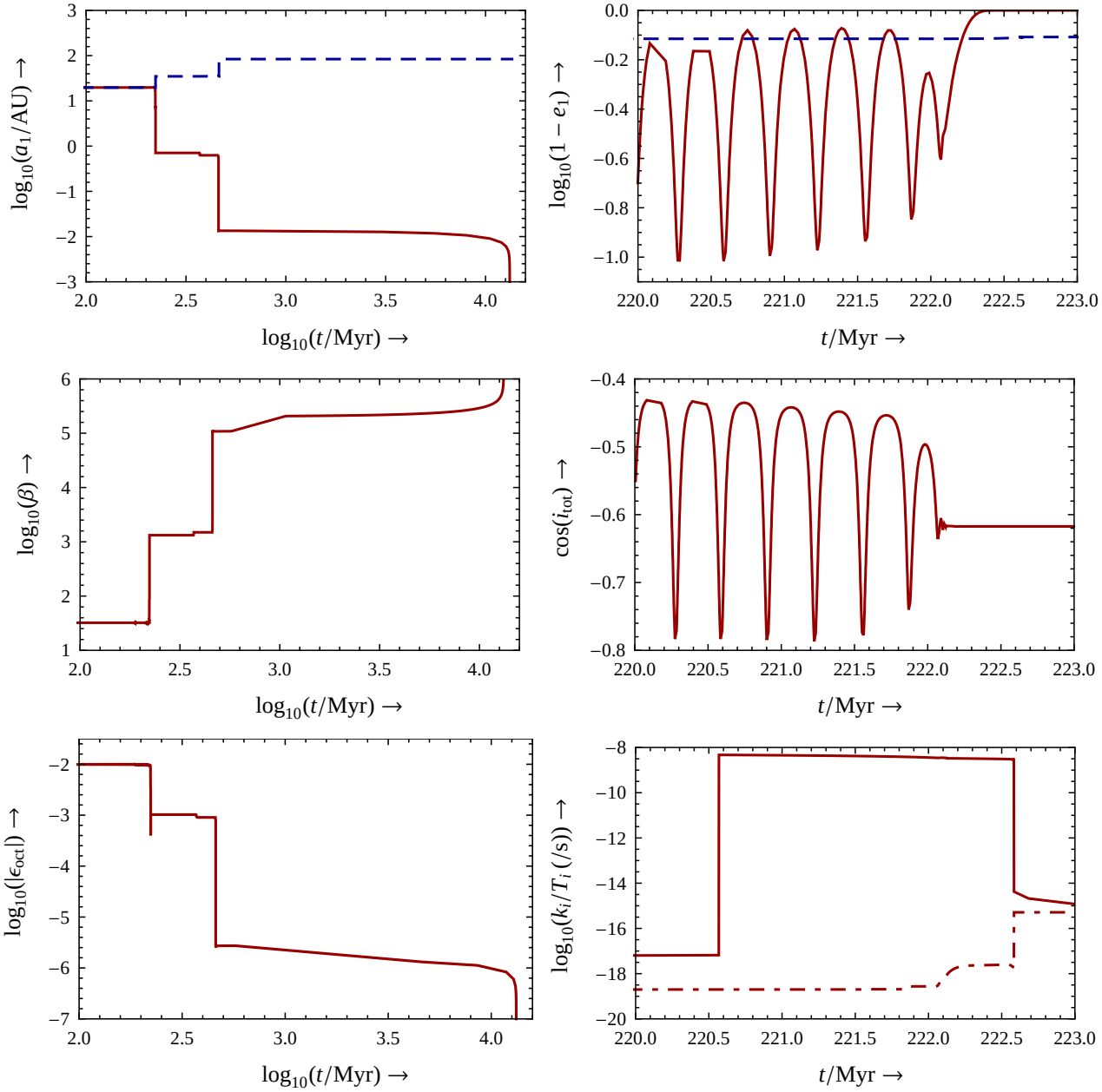

Figure 4.1: Several quantities of interest in the evolution of the TICM example system. Shown as a function of time are a_1, e_1, $\beta \equiv a_2/a_1$, $i_{\rm tot}$, $\epsilon_{\rm oct}$ (Eq. 2.56) and k_i/T_i. Solid lines: triple case; dashed lines: binary case. For the plot of k_i/T_i, the triple and binary cases are very similar; here the solid line applies to the primary ($i = 1$) and the dot-dashed line to the secondary ($i = 2$). Note that the evolution is not fully sampled in these plots which results in several kinks (in particular in the plots for e_1 and $i_{\rm tot}$) – more detailed calculations are performed internally in the triple algorithm but are not shown here (cf. Sect. 3.2).

At $t \sim 10^{2.7}$ Myr the secondary evolves to an AGB star, invoking a second CE phase. A close CO WD binary with $a_1 \sim 10^{-2}$ AU emerges from the CE. Due to gravitational wave emission (GWE), the system subsequently merges at $t \approx 10^{4.1}$ Myr in a circular orbit. We refer to the mechanism through which the merger occurs as the triple-induced circular mechanism (TICM) because the tertiary is (indirectly) responsible for driving a merger, although by the time the merger occurs the inner orbit has been completely circularized. The combined CO WD mass, 1.45 $M_\odot$, exceeds the Chandrasekhar mass, thus the merger potentially leads to a SN Ia (see also Sect. 5.4.2). A notable aspect of this scenario is that the tertiary affects the inner binary system only for the first ~ 220 Myr of the evolution,

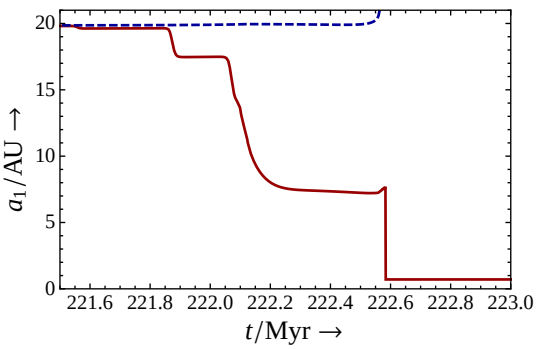

Figure 4.2: Detail of Fig 4.1 (top left).

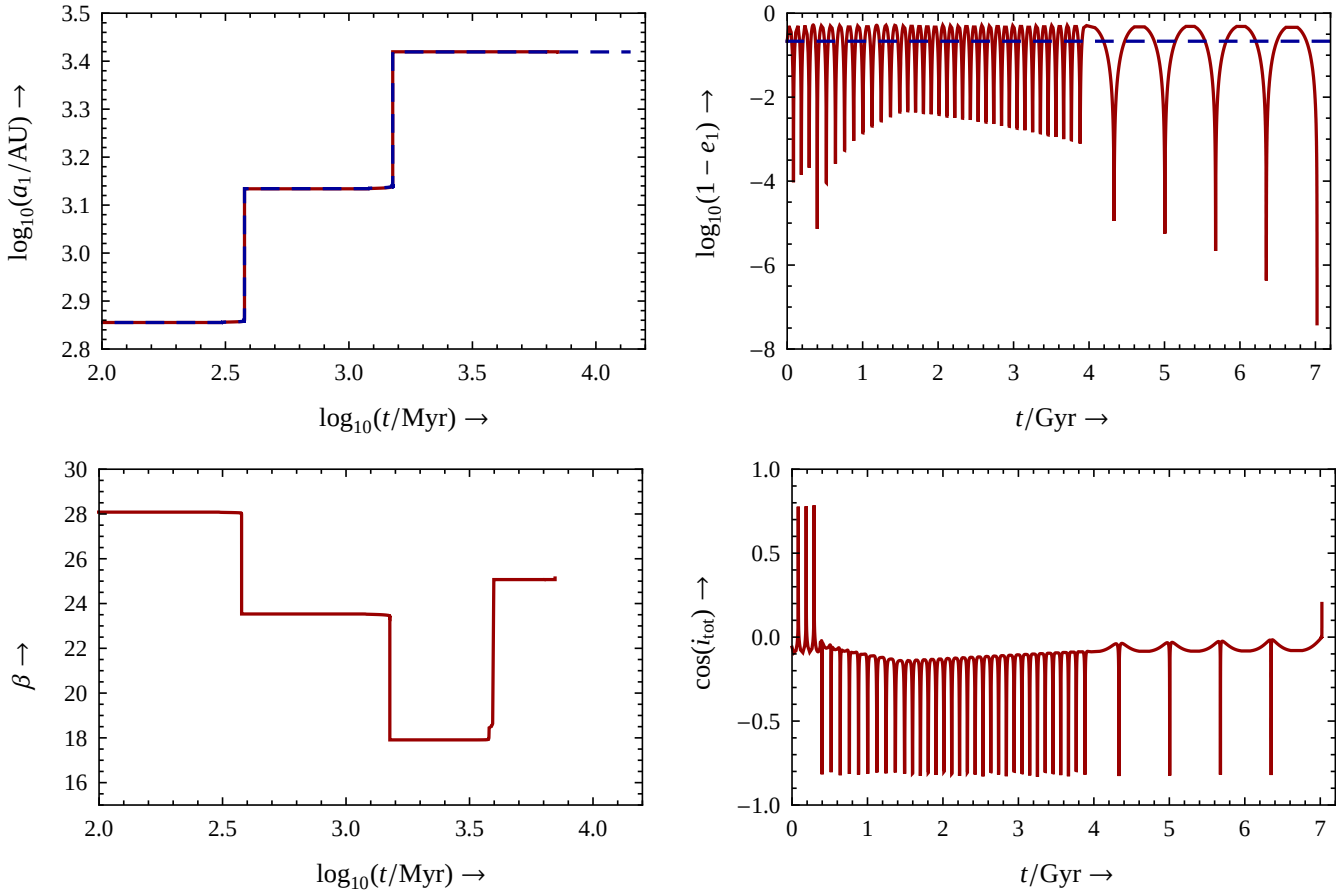

Figure 4.3: Quantities of interest for the TIEM example system, similar to Fig. 4.1.

which is only 1.7 % of the total lifetime of the inner binary system. Thus it is unlikely that the system is observed at a time when e_1 is high. Furthermore, due to mass loss in the inner and outer binary systems a_2 increases by over a factor of four compared to the initial value to $a_2 \approx 2750\,\mathrm{AU}$ at $t \approx 600\,\mathrm{Myr}$ while a_1 decreases significantly, thus making it difficult to observe the system as a hierarchical triple system after this time.

4.2 CO WD TIEM merger

The second example system has initial parameters $m_1 = 3.26\,M_\odot$, $m_2 = 2.00\,M_\odot$, $m_3 = 1.39\,M_\odot$, $a_1 = 716.6\,\mathrm{AU}$, $a_2 = 2.012 \cdot 10^4\,\mathrm{AU}$, $e_1 = 0.78$, $e_2 = 0.64$, $i_{\mathrm{tot}} = 93.4°$, $g_1 = 150.0°$ and $g_2 = 151.2°$. The evolution of a_1, e_1, $\beta \equiv a_2/a_1$ and i_{tot} for this system as function of time is shown in Fig. 4.3. The main difference in initial parameters in this example system compared to the previous TICM example system is that a_1 and a_2 are larger, although their ratio β is comparable. Due to the larger a_2 the Kozai period $P_K \approx 100\,\mathrm{Myr}$ is much longer. Consequently the primary RGB and AGB phases (which occur at $t \sim 10^{2.5}\,\mathrm{Myr}$ and $t \sim 10^{2.6}\,\mathrm{Myr}$ respectively) do not coincide with eccentricity maxima and there is no significant tidal friction during these phases, even though e_1 reaches higher maximum values compared to the TICM example. As the primary and secondary evolve to CO WDs the associated wind mass loss widens the orbit to $a_1 \approx 10^{3.42}\,\mathrm{AU}$. Although this inner binary wind mass loss increases a_2 as well, the ratio $\beta = a_2/a_1$ decreases with the assumption of fast isotropic winds such that $a_1(m_1 + m_2)$ and $a_2(m_1 + m_2 + m_3)$ are constant and if m_3 also remains constant. As a consequence the ratio β decreases significantly to $\beta \approx 18$ after the secondary has evolved to a CO WD. As the tertiary evolves to a CO WD and subsequently loses mass at $t \sim 10^{3.6}\,\mathrm{Myr}$, a_2 increases while a_1 stays constant, thus increasing β again. The latter process also increases the Kozai period and, somewhat surprisingly, the eccentricity cycles increase in amplitude. This process is associated with $\cos(i_{\mathrm{tot}})$ increasing slowly from negative values (retrograde orbit) to positive values (prograde orbit). At the moment of the orbital "flip" from retrograde to prograde at $t \approx 7.0\,\mathrm{Gyr}$, e_1 reaches a value of $1 - e_1 \approx 10^{-7.4}$, which is high enough to trigger an orbital collision even though $a_1 \approx 10^{3.42}\,\mathrm{AU} \approx 2630\,\mathrm{AU}$ is very large. This phenomenon of complex eccentricity modulations and orbital flips resulting into extremely high eccentricities is known as the eccentric Kozai mechanism (Lithwick & Naoz , 2011). It has also been studied in the context of systems in which mass loss is important (Shappee & Thompson, 2012) because mass loss significantly increases ϵ_{oct} (cf. Eq. 2.56). Intuitively it might be

expected that the extreme eccentricity of $e_1 \sim 1 - 10^{-7}$ as computed in this example system induces strong tidal friction in the CO WD system instead of triggering an orbital collision. For this example, however, the tidal strength quantity $k_i/T_i \sim 10^{-15}\,\mathrm{s}^{-1}$ as given by the Hurley et al. (2002) recipe is too small for significant tidal friction. Uncertainties in k_i/T_i for degenerate (and radiative) damping still exist, however, in particular for highly eccentric orbits. We have performed a test in which k_i/T_i for degenerate damping is multiplied by an artificial ad hoc factor of 10^3 to investigate the effect of much more effective degenerate damping. We find that the outcome is identical and thus we conclude that these uncertainties do not affect this system. We have performed similar tests for all systems in the population synthesis and find similar results; see Sect. 6.2 for more details.

Chapter 5

Triple population synthesis

Using the algorithm described in Sect. 3 we perform a population synthesis study of coeval stellar hierarchical triple systems. First we formulate the selection criteria of the specific triple population in Sect. 5.1 and based on these criteria we synthesize two triple populations by means of Monte Carlo methods in Sect. 5.2. These populations are subsequently evolved with the triple algorithm and the results are discussed in Sect. 5.3. We focus in more detail on triple-induced CO WD mergers, i.e. mergers induced by the secular gravitational influence of the tertiary, in Sect. 5.4.

5.1 Selection criteria

As mentioned in the introduction, in the present study we are mainly interested in inner binary mergers involving a CO WD. Hence we take an upper limit of the inner binary primary mass m_1 of $m_{1,u} = 6.5\,M_\odot$, which approximately captures the boundary between forming a CO WD and an oxygen-neon (ONe) WD in the case of single star evolution. The lower limit of m_1 is set to $m_{1,l} = 1.0\,M_\odot$ as any lower mass will not produce a significant number of CO WDs within a Hubble time for the chosen metallicity $Z = 0.02$. In addition we focus on triple systems with relatively wide inner binary systems, such that in the absence of a tertiary the inner binary stars do not interact during their evolution. With $1.0 < m_1/M_\odot < 6.5$, this implies that in the latter situation most systems consist of wide CO WD or CO WD + MS binaries after a Hubble time. The requirement of non-interactivity implies that neither star in the inner orbit fills its Roche Lobe during its evolution. This is achieved by choosing an inner orbit semi-major axis which is large enough to prevent Roche Lobe Overflow (RLOF) when the inner orbit stars attain their largest radius, i.e. during their AGB phases. In the absence of the tertiary tidal friction can act to shrink the orbit during this phase. If this happens prior to significant mass loss the inner orbital angular momentum is approximately conserved, hence also the inner orbit semi-latus rectum $l_1 \equiv a_1\left(1 - e_1^2\right)$ is conserved (cf. Eq. 2.34 with m_1 and m_2 constant). Therefore, in order to select non-interacting inner binary systems we select systems with initially $l_1 > l_{1,l} = 12\,\mathrm{AU}$, such that after tidal friction the inner orbit semi-major axis is at least larger than 12 AU, which is large enough to prevent RLOF for binaries in the mass range $1.0 < m_1/M_\odot < 6.5$.

A possible method to obtain the initial triple parameters is to directly sample from data of observed triple systems. Fig. 5.1 (top) shows the observed sample of 725 triple systems of Tokovinin (2008) in the (P_1, P_2)-diagram. A clear paucity of systems with inner orbital periods between $\log_{10}(P_1/\mathrm{d}) = 2$ and $\log_{10}(P_1/\mathrm{d}) = 4$ is present, which is likely due to the difficulty of detecting such systems in the regime between spectroscopic and visual binaries. Our selection criteria of inner binary systems with $1.0 < m_1/M_\odot < 6.5$ and $l_1 > 12\,\mathrm{AU}$ decrease the number of systems from 725 to 165, where a value of $\log_{10}(P_1/\mathrm{d}) = 4$ is taken to represent the dividing value $l_{1,l} = 12\,\mathrm{AU}$. The number of remaining systems is not large enough for direct sampling, therefore we choose to utilize the method of Monte Carlo sampling from distributions which are based on observed distributions. In order to gain information on the uncertainties of our results we use two distinct sampling methods, which are described below.

5.2 Sampling methods

The first triple sampling method (TSM1) is based on the supposition that a hierarchical triple system is composed of two uncorrelated binary systems. The main advantage of this approach is that the statistics of binary parameters are known with greater certainty than those of triple systems. A primary mass $1.0 < m_1/M_\odot < 6.5$ is sampled from a Kroupa et al. (1993) IMF, i.e. with slope -2.70. Subsequently two mass ratios, $q_1 \equiv m_2/m_1$ and $q_2 \equiv m_3/(m_1 + m_2)$, are sampled independently from a uniform

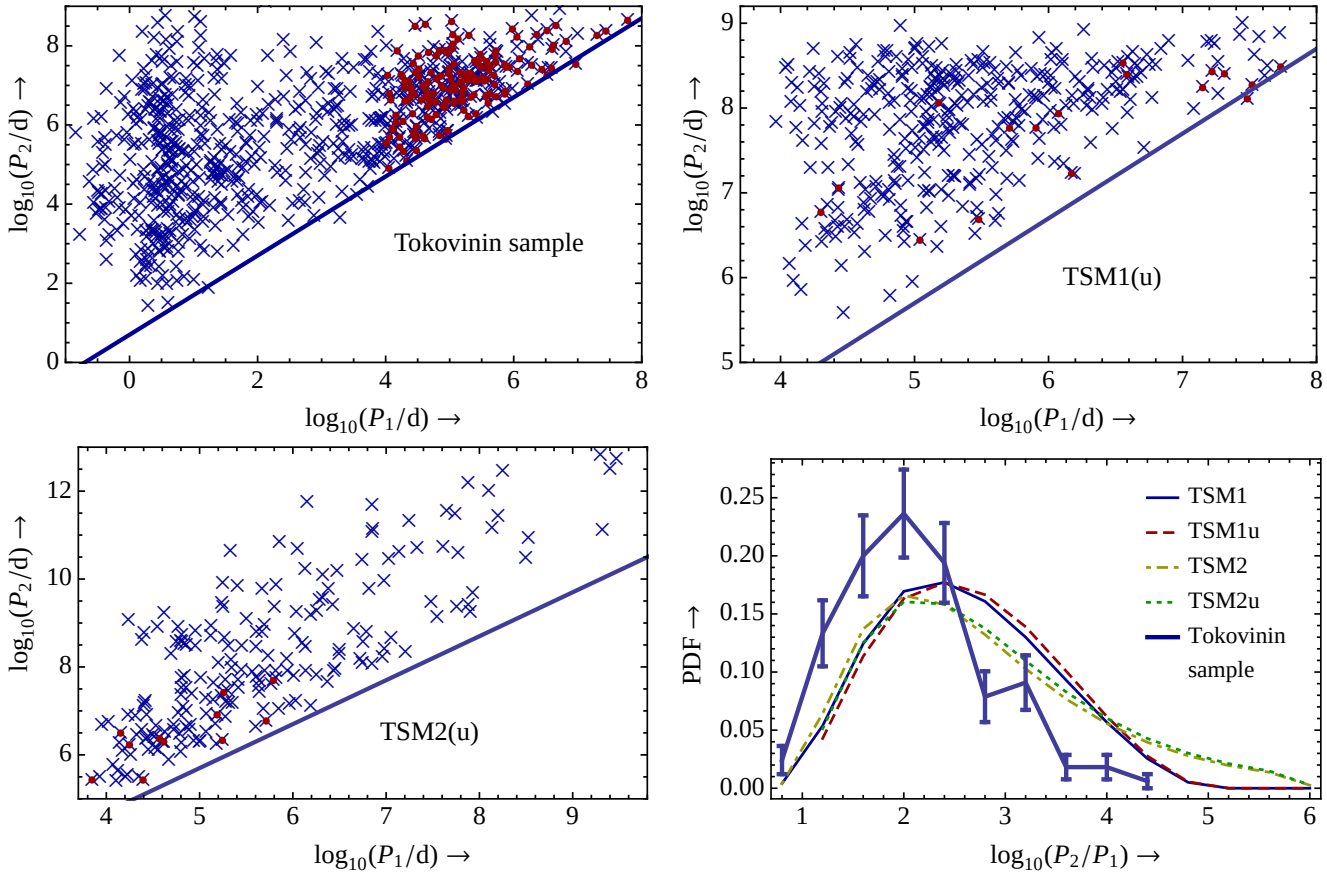

Figure 5.1: Inner (P_1) and outer (P_2) orbital periods of triple systems of the observed triple sample of Tokovinin (2008) (top left) and the two synthetic triple samples described in Sect. 5.2 (top right and bottom left). In the former observational sample, systems satisfying our selection criteria are denoted with •. In the latter synthetic samples, • denotes the systems which undergo an early MS inner binary merger or destabilization and hence are not likely to be observed. The solid lines correspond to $P_2/P_1 = 5$ and represent the typical critical value for dynamical stability. In the bottom right panel, the probability density function (PDF) of P_2/P_1 is shown for the Tokovinin sample satisfying the selection criteria (thick solid curve; error bars based on Poisson statistics are included), TSM1 (solid curve), TSM1u (dashed curve), TSM2 (dot-dashed curve) and TSM2u (dotted curve).

distribution such that $0 < q_j \leq 1$ (where $j \in \{1, 2\}$), $m_2 > 0.01\,M_\odot$ and $m_3 > 0.01\,M_\odot$, consistent with Claeys et al. (2012). The lower limit on the stellar masses is in accordance with the limit found by Kouwenhoven et al. (2007). The secondary and tertiary masses are subsequently computed from these mass ratios. We sample e_1 and e_2 from a thermal distribution $\mathrm{d}N/\mathrm{d}e_j = 2e_j$ as is appropriate for $P_j > 10^3$ d binaries (Kroupa & Burkert, 2001). Two semi-major axes are then sampled from a distribution which is flat in $\log_{10}(a_j)$, the smaller of which is designated a_1 and the larger of which is designated a_2. The lower and upper limits a_l and a_u in the distribution of the semi-major axes are $a_l = 5\,R_\odot$ and $a_u = 5 \cdot 10^6\,R_\odot$ for both inner and outer orbits (Kouwenhoven et al., 2007). From these systems we reject those which do not satisfy $l_1 = a_1\left(1 - e_1^2\right) > l_{1,l} = 12\,\mathrm{AU}$. Lastly, we sample the initial mutual orbital inclination angle i_tot from a distribution which is uniform in $\cos(i_\mathrm{tot})$ with $-1 < \cos(i_\mathrm{tot}) < 1$ and the initial arguments of periastron of both orbits, g_1 and g_2, from a uniform distribution with $0 < g_j < 2\pi$. From the triple systems obtained in this manner, we subsequently reject the systems which are not dynamically stable based on the stability criterion of Mardling & Aarseth (2001), consistent with our triple evolution algorithm (cf. Sect. 3.2).

In the second triple sampling method (TSM2) we use the multiple system recipe developed by Eggleton (2009). This recipe is designed to reproduce the properties of a set of 4558 stellar systems with Hipparcos magnitude brighter than 6 collected by Eggleton & Tokovinin (2008). It is followed until the second bifurcation, effectively selecting the multiple systems which are triple. The parameters given by the recipe are m_1, m_2, m_3, P_1 and P_2. The primary mass distribution in this recipe is designed to resemble the Salpeter distribution at large masses and turns over for masses below $0.3\,M_\odot$. The mass ratio distribution is approximately flat and the P_2 distribution has a broad peak around 10^5 d. We refer to Eggleton (2009) for further details. The corresponding semi-major axes are computed from Kepler's third law. The parameters not prescribed by the recipe are i_tot, e_j and g_j, which are sampled from the same distributions as in TSM1. Similarly to the method in TSM1, systems are rejected if $l_1 \leq l_{1,l} = 12\,\mathrm{AU}$ and if they do not satisfy the stability criterion of Mardling & Aarseth (2001).

Fig. 5.1 (top right & bottom left) shows the period-period diagram for a small sample (360 systems) of the TSM1 and

TSM2 populations. Note that the upper boundaries of P_1 and P_2 in both populations are quite different. In TSM1, P_1 and P_2 are limited by a_l and a_u, whereas in TSM2 such sharp boundaries do not exist. In TSM2 there exists an upper boundary of P_2 which is dependent on P_1, because in this sampling method the largest ratio P_2/P_1 is given by $P_2/P_1 = 2 \cdot 10^6$. This maximum period ratio has no physical origin and the consequences are minimal as such wide outer binary systems are very rare. Fig. 5.1 (top right & bottom left) also shows the systems which according to our triple algorithm experience a merger in the inner binary system or a destabilization early on the MS (see also Sect. 5.3). Such systems are not likely part of any observed sample of hierarchical triple systems. The populations with these systems removed are denoted by TSM1u and TSM2u respectively.

In Table 5.1 the distributions of the masses and orbital periods of the Tokovinin sample with our selection criteria applied are compared with the two sampled populations. In addition, Fig. 5.1 (bottom right) shows the distribution of P_2/P_1 of these systems. Due to the relatively steep slope of -2.70 in the mass distribution in TSM1 the mean masses in TSM1 are low compared to those in TSM2, for which a Salpeter-like slope of -2.23 applies for $m_1 > 1.0\,M_\odot$. The orbital periods of TSM1 and TSM2 show reasonable agreement, the orbital periods and their ratio being on average somewhat higher in TSM2 compared to those in TSM1. The number of systems with a MS merger or MS destabilization is relatively small and therefore these do not significantly affect the expected observed triple population. The distributions of the orbital periods and their ratio of the Tokovinin sample show fair agreement with those of the sampled populations, although the outer orbital periods in the Tokovinin sample are clearly smaller. This may well be due to observational bias because very long orbital periods in the order of 10^7 days or longer are very difficult to measure. The masses show poorer agreement, although selection effects in the observational sample may also play a role as it is likely that many relatively faint triple systems escape detection, thus biasing the observations to higher masses and higher mass ratios. Apart from selection effects it must be taken into account that the number of systems in the Tokovinin sample that satisfy our selection criteria is limited and thus the errors are relatively large, as demonstrated by the error bars in Fig. 5.1 (bottom right).

	Tokovinin		TSM1		TSM1u	
	Mean	SD	Mean	SD	Mean	SD
$m_1/M_\odot$	2.36	1.23	1.85	1.01	1.85	1.02
$m_2/M_\odot$	1.69	0.94	0.93	0.79	0.95	0.80
$m_3/M_\odot$	1.53	1.39	1.36	1.23	1.37	1.24
$\log_{10}(P_1/\mathrm{d})$	5.13	0.73	5.47	0.81	5.44	0.79
$\log_{10}(P_2/\mathrm{d})$	7.04	0.76	7.87	0.75	7.89	0.73
			TSM2		TSM2u	
			Mean	SD	Mean	SD
$m_1/M_\odot$			2.17	1.24	2.18	1.24
$m_2/M_\odot$			1.09	0.93	1.11	0.93
$m_3/M_\odot$			1.59	1.43	1.61	1.44
$\log_{10}(P_1/\mathrm{d})$			5.77	1.29	5.78	1.31
$\log_{10}(P_2/\mathrm{d})$			8.28	1.61	8.36	1.62

Table 5.1: Mean and standard deviation (SD) of masses and orbital periods of the Tokovinin (2008) sample satisfying the selection criteria and of both sampled triple populations TSM1 and TSM2. TSM1u and TSM2u refer to the populations where the inner binary MS mergers and MS destabilizations are excluded. The relatively sharp boundaries in the orbital periods in TSM1 compared to TSM2 are reflected by the relatively small standard deviations.

5.3 Results: main channels

We sample $N_{\mathrm{calc}} = 2 \cdot 10^6$ triple systems for both populations TSM1 and TSM2, making a total of $4 \cdot 10^6$ systems. Using the triple algorithm described in Sect. 3 these systems are evolved from $t = 0$, with all three components starting as ZAMS stars, to a Hubble time $t = t_H = 13.7\,\mathrm{Gyr}$. In order to retain sufficient resolution in higher-mass systems ($2.0 < m_1/M_\odot < 6.5$) we split both TSM1 and TSM2 into two parts of $1 \cdot 10^6$ systems, one with $1.0 < m_1/M_\odot < 2.0$ and one with $2.0 < m_1/M_\odot < 6.5$. In the results given below systems in each part are given appropriate weights determined by the mass function of m_1 to account for the fact that the actual number of systems in the $1.0 < m_1/M_\odot < 2.0$ range is larger than that in the $2.0 < m_1/M_\odot < 6.5$ range. For TSM1 the relative weights are 0.722 and 0.278 for both parts respectively; for TSM2 these relative weights are 0.603 and 0.397 (see also Appendix C). Several key events in the evolution are kept track of, most notably the onset of significant Kozai cycles with tidal friction (KCTF), common-envelope (CE) evolution, a merger in the inner binary system and a destabilization of the triple system. We thus obtain a catalogue of the evolutionary outcomes, where we distinguish between three main channels: inner binary mergers, no inner binary mergers and triple destabilizations. In a very small number of systems (55 and 44 for TSM1 and TSM2 respectively) the calculation of the evolution cannot be completed due to convergence errors in the ordinary differential equation solver routine; these systems are excluded from the results below. In these cases the errors occur just prior to MS merger or RGB + MS merger. Since the affected systems constitute a tiny fraction of all systems for which a MS merger or RGB + MS merger applies, this does not affect our conclusions.

Table 5.2 shows the probabilities of the main channels. Fig. 5.2 shows more detailed information on the likelihood of

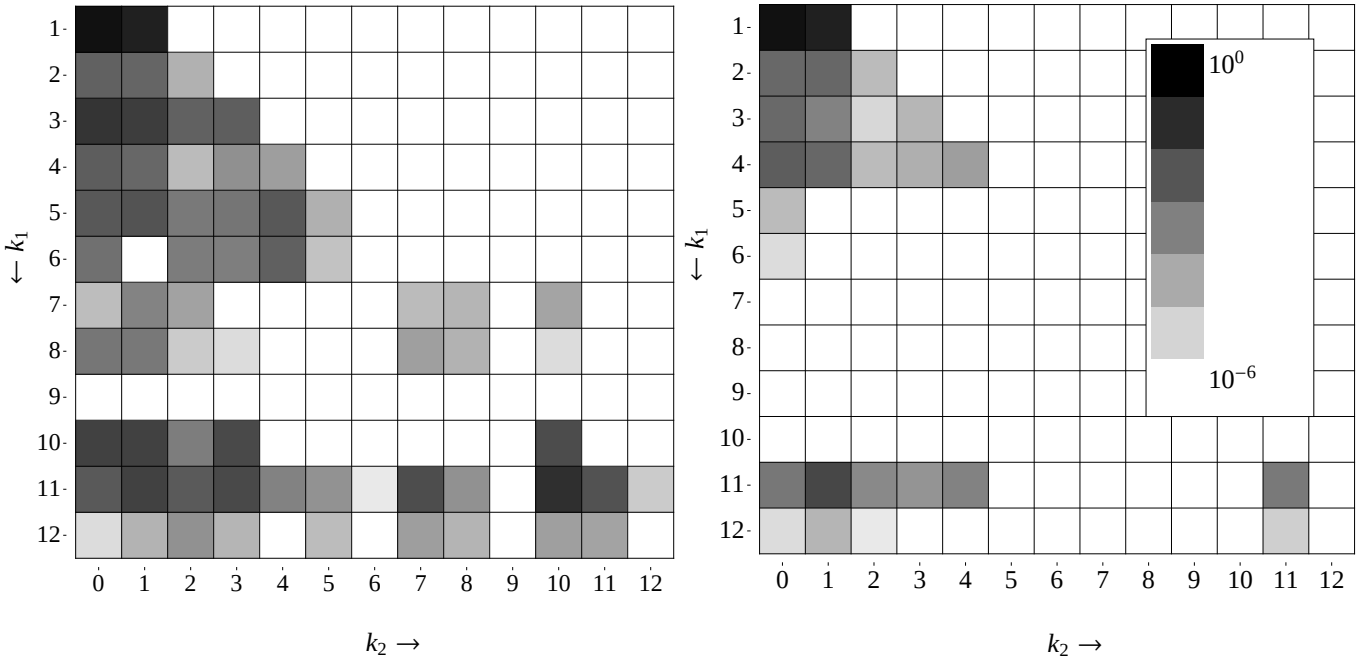

Figure 5.2: Left: the number of systems in TSM1 which merge for each occurring combination of stellar types just prior to merging, normalized to the total number of merger systems (which constitute $\sim$ 8% of all triple sampled triple systems). Right: the number of systems in TSM1 in which the merger occurs through the triple induced eccentric mechanism (TIEM), again normalized to the total number of merger systems. The stellar types are identical to the ones used in Hurley et al. (2002) and are repeated for convenience Table 5.3.

the different combinations of mergers, where the stellar types are given in Table 5.3. A post-MS merger is defined as a merger between a post-MS (non-compact object) primary and any secondary, whereas a compact object merger is defined as a merger between a compact object primary and any secondary. In addition to the probabilities of the channels, information on the occurrence of KCTF, CE evolution and the nature of the merger is given by means of the quantities $f_{\rm KCTF}$, $f_{\rm CE}$ and $f_{\rm TIEM}$. Here $f_{\rm KCTF}$ is defined as the fraction of systems in each channel in which $|\dot{e}_{1,\rm STD}| > 10^{-18}\,{\rm s}^{-1}$ (such that there is a significant change in e_1 due to STD in a Hubble time) and $0.1\,|\dot{e}_{1,\rm TF}| < |\dot{e}_{1,\rm STD}| < |\dot{e}_{1,\rm TF}|$ (i.e. $\dot{e}_{1,\rm STD}$ and $\dot{e}_{1,\rm TF}$ are of comparable order of magnitude). This may happen at various points in the evolution and it is strongly influenced by the envelope structure of the inner binary stars because this determines the effectiveness with which tidal energy can be dissipated. In particular if any inner binary star possess a convective envelope strong tidal friction is likely if e_1 is also high due to Kozai cycles. The former is true in particular for low-mass MS stars, HG/RGB stars and AGB stars. In Table 5.2 a distinction for $f_{\rm KCTF}$ is made between the types of the star in which tidal energy is dissipated for the duration of KCTF. Furthermore, $f_{\rm CE}$ is defined as the fraction of systems in each channel in which common-envelope (CE) evolution is at some point invoked. This includes both CE evolution triggered by a highly eccentric orbit and CE evolution triggered by Roche-Lobe overflow (in circular orbits). The fraction $f_{\rm CE}$ includes the possibility for multiple phases of CE evolution. Lastly, the quantity $f_{\rm TIEM}$ is defined as the fraction of systems in each channel in which the merger occurs due to an eccentric collision, i.e. in which a triple-induced eccentric mechanism (TIEM) applies (see Sect. 4.2). We define such a collision to occur if the inner binary periastron distance is smaller than or equal to the sum of the inner binary radii, i.e. if $a_1(1-e_1) \leq R_1 + R_2$ and when in the corresponding circular case there would not be a collision, i.e. $a_1 > R_1 + R_2$.

The most important feature of Table 5.2 is that in $\sim$ 8% of all systems an inner binary merger occurs, in $\sim$ 6% of all systems no inner binary merger occurs but the orbit is shrunk significantly and that in $\sim$ 10% of all systems a dynamically instability occurs. This

k	Description
0	MS ($m \lesssim 0.7\,M_\odot$)
1	MS ($m \gtrsim 0.7\,M_\odot$)
2	Hertzsprung Gap (HG)
3	Red Giant Branch (RGB)
4	Core Helium Burning (CHeB)
5	Early Asymptotic Giant Branch (EAGB)
6	Thermally Pulsing AGB (TPAGB)
7	Naked Helium Star MS (He MS)
8	Naked Helium Star Hertzsprung Gap (He HG)
9	Naked Helium Star Giant Branch (He GB)
10	Helium white dwarf (He WD)
11	Carbon-oxygen white dwarf (CO WD)
12	Oxygen-neon white dwarf (ONe WD)
13	Neutron Star (NS)
14	Black Hole (BH)
15	Massless remnant

Table 5.3: Description of the different stellar types used in Fig. 5.2. Identical to the types used in Hurley et al. (2002).

	P		$f_{\rm KCTF}$										$f_{\rm CE}$		$f_{\rm TIEM}$	
	MS		PHG/PRGB		PAGB		SHG/SRGB		SAGB							
	TSM1	TSM2	TSM1	TSM2	TSM1	TSM2	TSM1	TSM2	TSM1	TSM2	TSM1	TSM2	TSM1	TSM2	TSM1	TSM2
Merger	**8.054**	**7.743**	0.018	0.012	0.242	0.233	0.147	0.212	0.029	0.025	0.001	0.001	0.408	0.463	0.607	0.561
• On MS → single MS	**4.547**	**3.986**	0.010	0.007	—	—	—	—	—	—	—	—	0.001	0.001	0.991	0.994
→ CO WD	4.377	3.717	0.007	0.005	—	—	—	—	—	—	—	—	0.001	0.001	0.994	0.996
→ ONe WD	0.071	0.128	0.000	0.000	—	—	—	—	—	—	—	—	0.000	0.000	1.000	1.000
→ CC SN → NS	0.064	0.124	0.000	0.000	—	—	—	—	—	—	—	—	0.000	0.000	1.000	1.000
• Post-MS	**1.379**	**1.467**	0.035	0.022	0.650	0.569	0.209	0.283	0.110	0.089	0.000	0.000	1.000	1.000	0.130	0.146
• HG + MS (2)	0.074	0.093	0.131	0.054	0.135	0.095	—	—	—	—	—	—	1.000	1.000	0.798	0.904
• RGB + MS (3)	0.755	0.693	0.048	0.038	0.901	0.896	—	—	—	—	—	—	1.000	1.000	0.045	0.046
• CHeB + MS (4)	0.082	0.094	0.000	0.000	0.025	0.023	—	—	—	—	—	—	1.000	1.000	1.000	1.000
• AGB + MS (5)	0.177	0.266	0.000	0.000	0.213	0.172	0.905	0.925	—	—	—	—	1.000	1.000	0.002	0.002
• AGB + CHeB (4)	0.112	0.146	0.000	0.000	0.260	0.240	0.795	0.818	0.289	0.294	—	—	1.000	1.000	0.000	0.000
• Compact Object	**2.128**	**2.290**	0.024	0.014	0.496	0.423	0.420	0.534	0.039	0.028	0.003	0.003	0.893	0.924	0.098	0.072
• He WD + MS (3)	0.471	0.376	0.007	0.005	0.994	0.986	0.000	0.000	—	—	—	—	1.000	1.000	0.000	0.000
• He WD + RGB (7)	0.156	0.139	0.079	0.059	0.903	0.916	0.000	0.000	0.000	0.000	—	—	1.000	1.000	0.000	0.000
• He WD + He WD (7)	0.126	0.110	0.000	0.000	0.986	0.979	0.000	0.000	0.087	0.060	0.000	0.000	1.000	1.000	0.000	0.000
• CO WD + MS (5)	0.297	0.282	0.106	0.067	0.188	0.276	0.198	0.291	—	—	—	—	0.277	0.435	0.607	0.486
• CO WD + HG (5)	0.060	0.099	0.027	0.011	0.444	0.473	0.559	0.606	0.023	0.012	—	—	1.000	1.000	0.082	0.046
• CO WD + RGB (5)	0.149	0.188	0.004	0.006	0.287	0.253	0.790	0.852	0.069	0.032	—	—	1.000	1.000	0.018	0.009
• CO WD + CHeB (4)	0.007	0.008	0.000	0.000	0.000	0.000	0.132	0.153	0.012	0.010	—	—	1.000	1.000	1.000	1.000
• CO WD + HeMS (8)	0.124	0.178	0.000	0.000	0.127	0.090	0.918	0.932	0.063	0.042	0.000	0.000	1.000	1.000	0.000	0.000
• CO WD + He WD (8)	0.618	0.746	0.001	0.000	0.257	0.202	0.793	0.845	0.063	0.038	0.000	0.000	1.000	1.000	0.000	0.000
• CO WD + CO WD	0.095	0.128	0.000	0.000	0.130	0.104	0.719	0.786	0.145	0.105	0.025	0.022	0.873	0.899	0.121	0.091
No merger	**81.717**	**81.400**	0.002	0.001	0.067	0.046	0.205	0.191	0.015	0.011	0.027	0.026	0.047	0.046	—	—
• $a_{1,f}/\mathrm{AU} > 12$	75.535	75.836	0.000	0.000	0.029	0.015	0.178	0.162	0.010	0.007	0.024	0.022	0.000	0.000	—	—
• $10^{-2} < a_{1,f}/\mathrm{AU} < 12$	5.614	5.104	0.005	0.003	0.536	0.470	0.562	0.614	0.080	0.071	0.081	0.090	0.611	0.655	—	—
• $a_{1,f}/\mathrm{AU} < 10^{-2}$	0.569	0.460	0.150	0.096	0.510	0.490	0.330	0.416	0.033	0.025	0.001	0.001	0.794	0.855	—	—
Triple destabilization	**10.228**	**10.857**	0.000	0.000	0.001	0.001	0.024	0.030	0.000	0.000	0.001	0.001	0.000	0.000	—	—
• On MS	3.680	3.722	0.000	0.000	—	—	—	—	—	—	—	—	0.000	0.000	—	—
• Post-MS	4.635	5.124	0.000	0.000	0.001	0.001	0.027	0.031	0.000	0.000	0.000	0.000	0.000	0.000	—	—
• AGB + MS	4.036	4.603	0.000	0.000	0.001	0.001	0.030	0.034	—	—	—	—	0.000	0.000	—	—
• Compact Object	1.913	2.011	0.000	0.000	0.002	0.001	0.064	0.085	0.002	0.002	0.003	0.004	0.000	0.000	—	—
• CO WD + MS	0.888	0.769	0.000	0.000	0.002	0.002	0.036	0.049	—	—	—	—	0.000	0.000	—	—
• CO WD + AGB	0.751	0.977	0.000	0.000	0.002	0.000	0.097	0.115	0.004	0.002	0.007	0.007	0.000	0.000	—	—
• CO + CO WD	0.122	0.122	0.000	0.000	0.002	0.001	0.066	0.092	0.001	0.002	0.009	0.005	0.000	0.000	—	—

Table 5.2: Probabilities P (in per cent) of various evolutionary channels for both sampled triple populations. Any two objects in the first column refer to inner binary components. For the post-MS and compact object mergers, the integer numbers in brackets denote the stellar type of the remnant according to the binary evolution algorithm which occurs most frequently. We refer to Table 5.3 for the meaning of the stellar types and of abbreviations used and to Fig. 5.2 for a complete overview of all occurring combinations of stellar types prior to merger. In the no merger channels, $a_{1,f}$ denotes a_1 at $t = t_H$. The quantities $f_{\rm KCTF}$, $f_{\rm CE}$ and $f_{\rm TIEM}$ denote the fraction of systems within each channel for which significant KCTF, common-envelope (CE) evolution and the triple-induced eccentric mechanism (TIEM) applies respectively. For $f_{\rm KCTF}$, a distinction is made between the types of the star in which significant tidal energy is dissipated: MS (both stars are MS or the primary is a compact object and the secondary is a (low-mass) MS star); PHG/PRGB/PAGB (primary star is a HG/RGB/AGB star) and SHG/SRGB/SAGB (secondary star is a HG/RGB/AGB star). A long dash (—) indicates that this particular combination is not applicable.

means that in $\sim$ 24% of all systems the tertiary significantly alters the inner binary evolution. Taking into account that triple systems in which the inner binary components merge during the MS ($\sim$ 4%) or in which the triple system becomes dynamically unstable during the MS ($\sim$ 4%) are not likely to be observed (cf. Sect. 5.3.1), this estimate is reduced by $\sim$ 8%. This implies that the tertiary significantly alters the inner binary evolution in $\sim$ 16%/(1 − 0.08) $\sim$ 17% among the "observable" triples. Furthermore, the results for TSM1 and TSM2 are generally similar. The number of destabilizations is higher in TSM2, most likely due to the fact that TSM2 contains more systems with very low β compared to TSM1, cf. Fig. 5.1 (bottom right). To provide insight into the dependence of the probabilities of the main channels on the initial parameters we show in Fig. 5.3 these probabilities (expressed as fractions) as function of all initial parameters except g_2, for which we find no significant dependence. The various channels are discussed in more detail below.

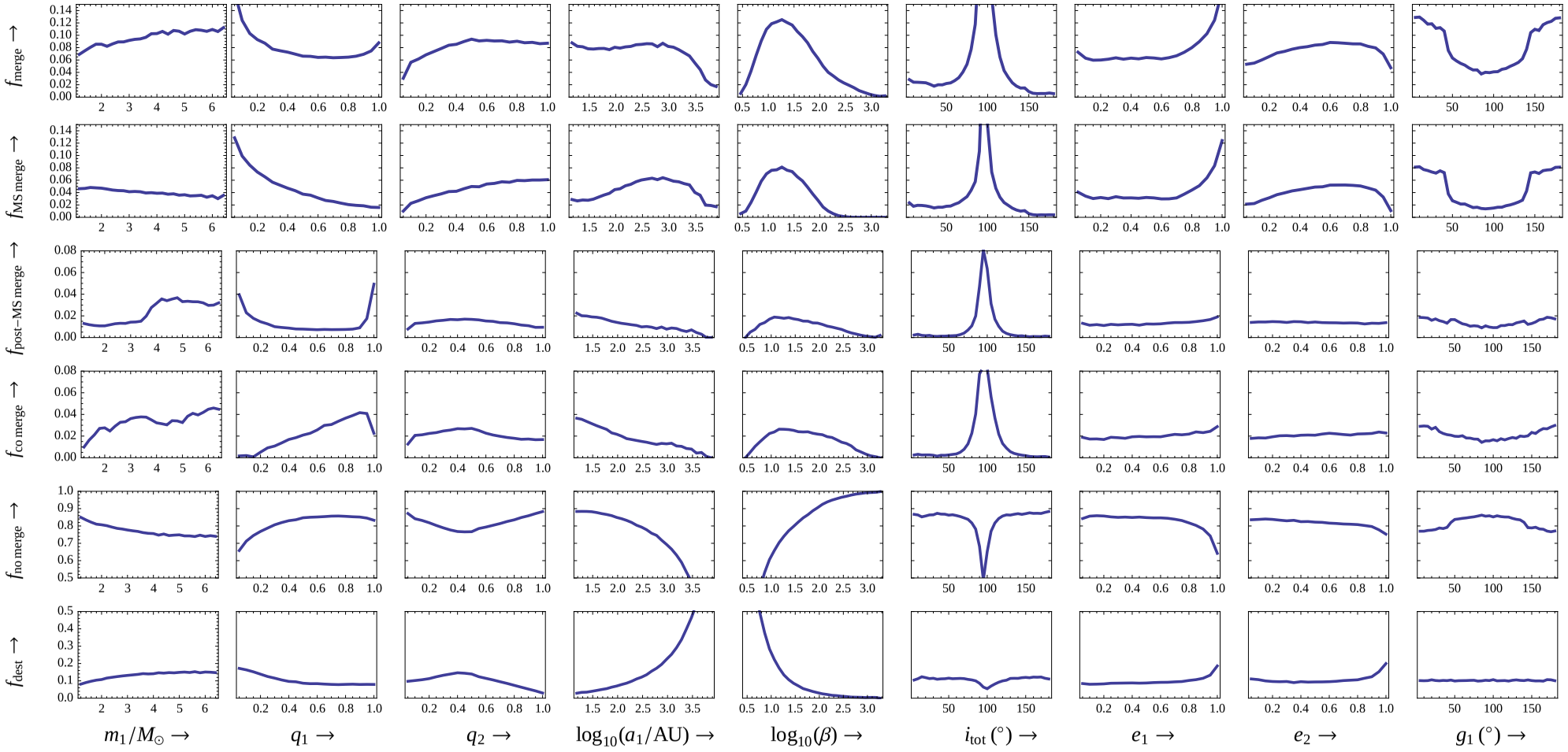

Figure 5.3: Probabilities of the main channels, expressed as fractions of all systems, as a function of initial parameters for TSM1; $q_1 \equiv m_2/m_1$, $q_2 \equiv m_3/(m_1+m_2)$ and $\beta \equiv a_2/a_1$. Abbreviations used: co - compact object; dest - destabilization.

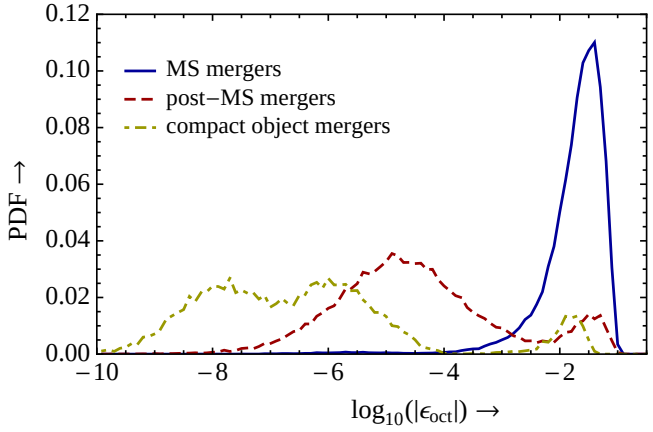

Figure 5.4: Distribution of the octupole parameter $\epsilon_{\rm oct}$ (Eq. 2.56) prior to merger for the TSM1 population, distinguishing between MS mergers (solid curve), post-MS mergers (dashed curve) and compact object mergers (dot-dashed curve).

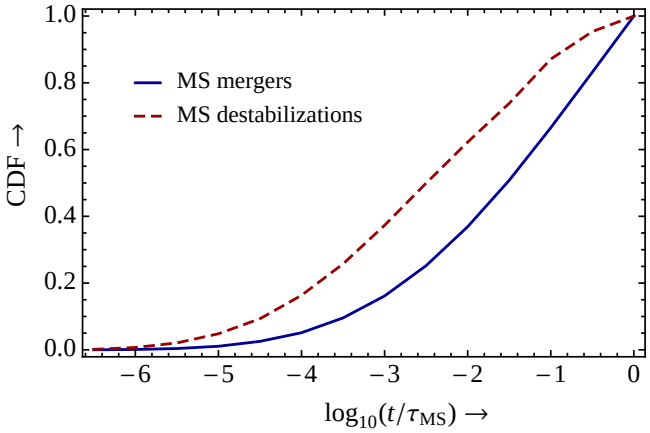

Figure 5.5: Cumulative distributions for TSM1 of the time t of MS merger t (solid curve) or MS destabilization (dashed curve), normalized to the MS timescale which is estimated as $\tau_{\rm MS} = 10\,(m_1/M_\odot)^{-2.8}$ Gyr.

5.3.1 Inner binary mergers

Due to high-amplitude eccentricity cycles induced in the inner orbit the components in the inner binary may at some point merge, either directly as a consequence of an orbital collision through the triple-induced eccentric mechanism (TIEM) or indirectly as a result of strong tidal friction induced by high eccentricity, possibly invoking common-envelope (CE) evolution. In the latter case the inner binary may either merge directly after the CE or survive the CE in a relatively tight orbit and subsequently merge as a result of orbital energy loss due to gravitational wave emission (GWE). Fig. 5.3 shows that these mergers typically have initial mutual inclination angles close to $i_{\rm tot} = 90°$, which is intuitively correct as the Kozai mechanism is most effective for highly inclined systems (cf. Fig. 2.4). Note that a maximum in $f_{\rm merge}$ occurs at inclinations slightly above $i_{\rm tot} = 90°$, i.e. for retrograde orbits. This is consistent with Shappee & Thompson (2012) who find an asymmetry in $\cos(i_{\rm tot})$ towards negative values for the probability of the eccentric Kozai mechanism to occur. In addition the systems which merge typically have relatively small β compared to the systems which do not, with the initial β peaking at $\beta \sim 10^{1.3} \approx 20$. Other general trends in $f_{\rm merge}$ are that this fraction increases with increasing e_1 for $e_1 \geq 0.7$ (higher e_1 imply higher eccentricity maxima) and in addition $f_{\rm merge}$ increases for increasing outer binary mass ratios $q_2 = m_3/(m_1 + m_2)$ (higher q_2 also imply higher eccentricity maxima because $C_{\rm quad}/G_1 \propto m_3/\sqrt{m_1 + m_2}$, cf. Eqs. 2.37, 2.38, 2.39 and 2.40). We separate further discussion into mergers occurring on the MS, after the MS and mergers involving a primary compact object.

MS mergers As Table 5.2 demonstrates, most mergers occur on the MS and for almost all of the latter the merger occurs through an eccentric collision. In the latter case, $-4 \lesssim \log_{10}(1-e_1) \lesssim -5$. In the `binary_c` algorithm it is assumed that the result of the merger is a single MS star with mass $m_1 + m_2$; depending on the latter value, the final remnant is either a CO WD (most cases), an ONe WD or a neutron star (NS) (following a core-collapse supernova). Fig. 5.4 shows the distribution of the octupole parameter $\epsilon_{\rm oct}$ (cf. Eq. 2.56) prior to merger for the main merger channels. It shows that octupole terms are very important for MS mergers because these typically have $\log_{10}(|\epsilon_{\rm oct}|) \sim -1.5$ prior to merger, which is large enough for octupole order terms to be important in the secular three-body dynamics (STD). This relatively large $\epsilon_{\rm oct}$ is due to a combination of initially small ratios $\beta \equiv a_2/a_1$, small inner binary mass ratios $q_1 \equiv m_2/m_1$ and high outer orbit eccentricities e_2. This is demonstrated by Fig. 5.3 which shows that the fraction of MS mergers $f_{\rm MS\,merge}$ decreases significantly with increasing q_1 and is peaked towards relatively small β around $0.5 < \log_{10}(\beta) < 2.0$. Furthermore $f_{\rm MS\,merge}$ increases with e_2, although it decreases again for $e_2 \gtrsim 0.8$ which is probably because systems with low β and high e_2 are likely to become dynamically unstable (compare the dependence of $f_{\rm dest}$ on e_2 in Fig. 5.3). It might be expected that MS mergers are more likely to occur for small initial a_1 as a tighter orbit makes an eccentric collision more likely. However, we find that MS mergers on average have relatively large initial a_1 with a maximum of $f_{\rm MS\,merge}$ around $a_1 \sim 10^{2.8}$ AU $\approx 6 \cdot 10^2$ AU (cf. Fig. 5.3). This implies that the effect of increasing the eccentricity maxima with increasing a_1 and hence decreasing β (cf. Sect. 2.3.3) is stronger than the effect that eccentric collisions become less likely with increasing a_1 if e_1 were fixed. The dependence of $f_{\rm MSmerge}$ on m_1 is quite weak, although a slight decrease with increasing m_1 is noticeable, which is possibly due to the fact that eccentricity maxima generally decrease with increasing inner binary masses. The latter effect is apparently stronger than the effect that MS radii increase with m_1 and thus a collision would be more likely for the same e_1. Lastly, a tendency of large $f_{\rm MS\,merge}$ for g_1 around 0° or 180° is evident in Fig. 5.3, which can be explained by the fact that circulating Kozai cycles (initially satisfying $\cos^2(g_1) > 3/5$) tend to have larger eccentricity maxima than librating ones (initially satisfying $\cos^2(g_1) < 3/5$); see e.g. Ford et al. (2000). For post-MS and compact object mergers this dependence

on g_1 is much weaker because for these systems octupole order terms are an average less important (cf. Fig. 5.4).

As Table 5.2 shows, for a small fraction of MS mergers (0.009 of all MS mergers for TSM1) the merger does not occur through the TIEM mechanism and hence the merger occurs in a circular orbit (i.e. the triple-induced circular mechanism applies). Instead KCTF is responsible for strong orbital shrinkage leading to a tight inner orbit, eventually resulting in a merger in a circular orbit due to GWE within a Hubble time. The fraction of MS merger systems in which the TICM applies (0.009 for TSM1) is indeed comparable to the fraction of MS merger systems which satisfy our KCTF criterion on the MS (0.010 for TSM1) and the same applies to TSM2. We find that strong KCTF on the MS occurs only in low-mass inner binary systems ($m_1 < 1.25\,M_\odot$) because inner binary components with these masses have convective envelopes which are much more effective at dissipating tidal energy than radiative envelopes found in higher-mass MS stars (in the algorithm used, $1.25\,M_\odot$ marks the boundary between stars with convective and radiative envelopes).

The TIEM mergers, which constitute the bulk of MS mergers, occur relatively early on the MS, with the majority of mergers ($\sim 70\%$) occurring within 10% of the primary MS lifetime, see Fig. 5.5. This is due to the fact that in many cases the collision occurs during the first few Kozai cycles, which typically have timescales of a few Myr which is a small fraction of the MS lifetime of the primary stars considered in the triple sample. The time of merger is thus mainly determined by the Kozai period $P_K \propto (P_2/P_1)\,P_2$ and hence the orbital periods. We indeed find that the distribution of the times of MS merger is very similar to the initial distribution of the Kozai periods. The fact that most MS mergers occur relatively early on the MS makes it unlikely to observe the progenitor triple systems. A similar conclusion applies to MS destabilizations (Sect. 5.3.3).

Post-MS mergers For any merger after the MS, an evolutionary change in the inner binary system plays a key role in the mechanism that leads to the merger. The radius expansion during the primary Hertzsprung Gap (HG) is responsible for an eccentric collision for most mergers during this phase. Note that in such an event the `binary_c` algorithm invokes CE evolution contrary to the MS TIEM mergers. For $\sim 20\%$ of the HG + MS mergers strong KCTF triggered by the substantial increase of the tidal strength quantity k_i/T_i during the primary HG phase, leads to substantial orbital circularization and shrinkage to $a_1 \sim 0.4$ AU. Subsequently CE evolution is invoked leading to a triple-induced circular merger (TICM). Similarly, one might expect primary RGB + secondary MS mergers to occur mainly through the TIEM as the primary RGB phase is accompanied with a substantial increase in radius. However, the large increase in the tidal strength quantity k_i/T_i during this phase is responsible for strong KCTF which completely circularizes and shrinks the inner orbit to $a_1 \sim 0.3$ AU which is small enough to invoke CE evolution and thus result in a TICM merger. Consequently the TICM dominates for RGB + MS mergers. During the primary core helium burning (CHeB) phase tides are once again relatively unimportant and most mergers during this phase are driven by radius expansion in conjunction with eccentricity cycles, in all cases leading to a TIEM merger. For RGB + RGB mergers (not included in Table 5.2) the TICM applies. For these systems an immediate merger occurs after KCTF and CE evolution. Due to the fact that KCTF with two RGB stars is particularly effective, the post-MS fraction $f_{\text{post-MS merge}}$ shows a strong peak towards $q_1 = 1$ corresponding to the RGB + RGB mergers for which a high inner binary mass ratio is required as the RGB phase lasts for a relatively short time (Fig. 5.3). The merger mechanism for primary AGB mergers is similar to that of primary RGB mergers, i.e. the TICM. The secondary at this point is most likely a MS or a CHeB star; mergers between AGB and RGB/AGB stars are also possible (Fig. 5.2) but these are rather unlikely due to the fact that the latter phases last for a relatively short time, making it unlikely that KCTF during the primary AGB phase coincides with the secondary RGB/AGB phase. For primary AGB mergers KCTF is effective mainly during the primary AGB phase, although in $\sim 25\%$ of these systems KCTF during the primary RGB phase is also important. After KCTF a CE is invoked; due to the fact that the orbit at this point is relatively tight the inner binary does not survive the CE phase and an AGB star (in case of AGB + MS merger) or CHeB star (in case of AGB + CHeB merger) remains.

Fig. 5.3 shows that post-MS mergers typically have relatively small β similarly to MS mergers, although $f_{\text{post-MS merge}}$ shows a clear tail for larger β which is not present in the dependence of $f_{\text{MS merge}}$ on β (for compact object mergers this tail is even more prominent). As discussed before, for MS mergers a_1 should be sufficiently large that the eccentricity maxima are high enough for collision. This does not apply to post-MS mergers, where effective tidal friction is the more important effect which requires a_1 to be small. For the systems with large a_1 and potentially (very) high eccentricity maxima, i.e. those with low β and high mutual inclination angles, strong tidal effects are expected to be important. Such systems are most likely to have experienced an orbital collision already on the MS. Thus $f_{\text{post-MS merge}}$ decreases with increasing a_1.

Compact object mergers In cases where KCTF during the RGB/AGB phases is less effective, a merger can be avoided when the most evolved state of the primary is an AGB star. In such cases a merger can occur when the primary has evolved to a WD, i.e. a compact object merger. Such a merger can occur through CE evolution triggered by KCTF, resulting in a tight orbit of $a_1 \lesssim 10^{-2}$ AU and thus a merger due to GWE within a Hubble time (TICM). In some cases multiple CE phases are triggered and the evolution is more complicated although we find that in all cases, the ratio β after CE is large enough such that any subsequent Kozai cycles do not occur. In the latter cases the Kozai mechanism is completely suppressed by other sources of apsidal motion, most notably apsidal motion due to general relativity (cf. Eq. 2.53). To further illustrate this point, Fig. 5.6 shows the distribution of $\beta \equiv a_2/a_1$ prior to and after the first CE for all systems in which CE evolution occurs. After the first CE $\beta \sim 10^5$, which is much

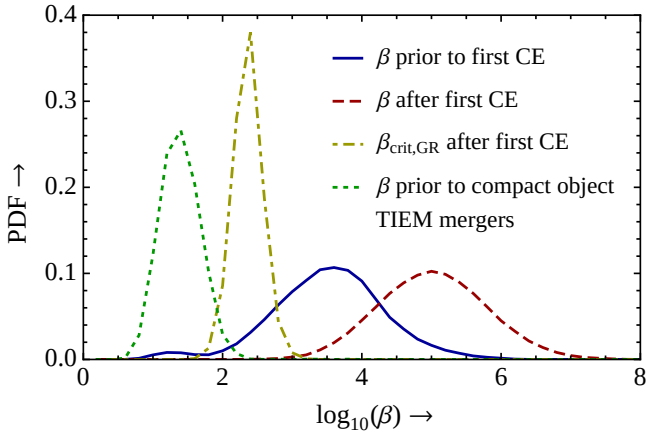

Figure 5.6: Distribution for TSM1 of $\beta = a_2/a_1$ prior to (solid curve) and after (dashed curve) first CE for all systems in which CE evolution occurs. Also shown is the distribution of $\beta_{\rm crit,GR}$ (Eq. 3.5) for the systems in which CE occurs, just after the CE (dot-dashed curve). Lastly, the dotted curve shows β prior to merger for all compact object TIEM mergers.

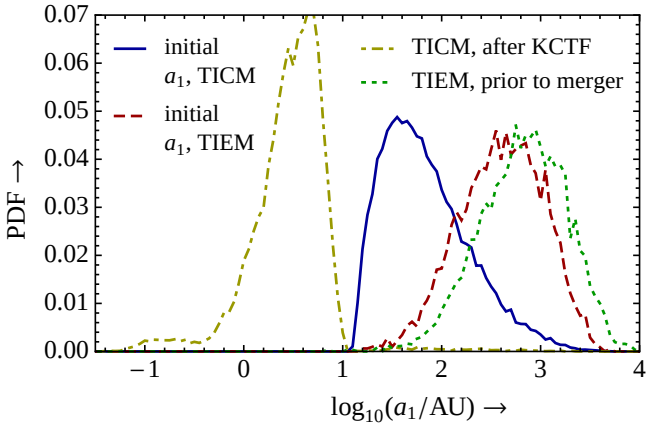

Figure 5.7: Distribution for TSM1 of the initial a_1 for compact object TICM (solid curve) and TIEM (dashed curve) mergers. In addition, the distributions are shown of a_1 after KCTF during primary AGB for which this is applicable, all of which are TICM merger systems (dot-dashed curve) and of a_1 just prior to a compact object eccentric merger in TIEM merger systems (dotted curve). Note that the systems having $a_1 \sim 10^{-1}$ AU after primary AGB KCTF are those in which KCTF occurred also during an earlier stage, most notably the primary RGB phase.

larger than the critical value $\beta_{\rm crit,GR}$ (cf. Eq. 3.5) for which general relativity dominates in these systems (Fig. 5.6, dot-dashed curve). Note that the dot-dashed curve in Fig. 5.6 shows the distribution of $\beta_{\rm crit,GR}$ just after the CE.

A relatively frequent channel in which CE evolution is triggered by KCTF is the channel leading to a He WD + MS merger. In this channel relatively strong KCTF during the primary RGB phase shrinks the inner orbit to $a_1 \sim 0.3$ AU, thus triggering the first CE which leaves a He WD + MS star binary with $a_1 \sim 10^{-2}$ AU which merges due to GWE. Alternatively, if KCTF during the primary RGB phase is less strong and shrinks the inner orbit to $a_1 \sim 0.6$ AU, the He WD + MS star inner binary after CE is wide enough for the secondary to evolve to an RGB star, thus invoking a second CE phase resulting in a He WD + RGB merger. If KCTF during the primary RGB is weaker still it leaves an inner orbit with $a_1 \sim 1$ AU, which is large enough for two subsequent CE phases after which a He WD + He WD binary remains which merges due to GWE. He WD + HG and He WD + RGB mergers are believed to be important channels leading to carbon-rich K-type giants, known as early-type R stars (Izzard et al., 2007). Similar paths apply to TICM mergers with higher initial primary masses, resulting not in primary He WD mergers but primary CO WD mergers instead. The most likely primary CO WD merger is that with a secondary He WD ($\sim 0.6\%$ of all systems). Such mergers have been discussed as progenitors of H-deficient carbon-rich supergiants known as RCrB stars (Tisserand et al., 2009).

Alternatively, strong KCTF during the MS and post-MS evolution of the primary and secondary star can also be avoided. The main parameter which determines whether or not strong KCTF occurs during these phases is a_1 as illustrated in Fig. 5.7. Many systems which are initially wider than $a_1 \sim 10^2$ AU avoid pre-compact object KCTF and subsequently a_1 increases due to wind mass loss in the primary as it evolves from an AGB star to a CO WD. With the assumption of a fast and isotropic wind, $a_1(m_1+m_2)$ remains constant during this short episode of wind mass loss. Similarly $a_2(m_1 + m_2 + m_3)$ remains constant. If the tertiary does not lose mass during this phase (which is statistically unlikely because the transition from AGB stars to WDs occurs relatively quickly) this implies that the ratio $\beta = a_2/a_1$ *decreases*. Consequently triple configurations are produced with the primary inner binary component a CO WD and with relatively small β, namely narrowly distributed around $\beta \sim 15$, cf. Fig. 5.6 (dotted curve). Octupole order effects are very important in such systems as is reflected in the small peak around $\log_{10}(|\epsilon_{\rm oct}|) \sim 10^{-2}$ for compact object merger systems in Fig. 5.4 (dot-dashed curve). In addition, because at this stage the inner orbit semi-major axis is relatively large (typically $a_1 \sim 10^3$ AU, cf. Fig. 5.7) there is no significant damping of Kozai cycles due to additional sources of apsidal motion. Consequently in such systems "flips" can occur during which the outer orbit switches from prograde to retrograde and vice versa. During these flips extremely-high eccentricities can be reached (e.g. Naoz et al. 2011; Shappee & Thompson 2012), in our calculations as high as $1 - e_1 \sim 10^{-8}$. In most cases these high eccentricities lead to orbital collisions, i.e. mergers through the TIEM. The value of the eccentricity required for such a collision is determined by a_1 and the radius and hence the type/mass of the secondary object (mainly a MS star, a CHeB star or a CO WD) and varies between $1 - e_1 \approx 10^{-3}$ (CHeB companion), $1 - e_1 \approx 10^{-5}$ (MS companion) and $1 - e_1 \approx 10^{-7}$ (CO WD companion). Alternatively, in a relatively small number of systems and mainly for CO WD + low-mass MS systems the high eccentricities do not lead to eccentric collisions but induce very strong tidal friction in the low-mass secondary which possesses a convective envelope, thus circularizing and

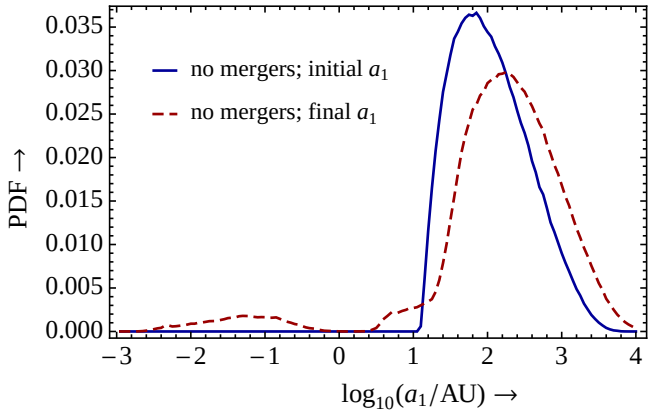

Figure 5.8: Distribution for TSM1 of the initial a_1 (solid curve) and the final a_1 (dashed curve) of all no merger systems.

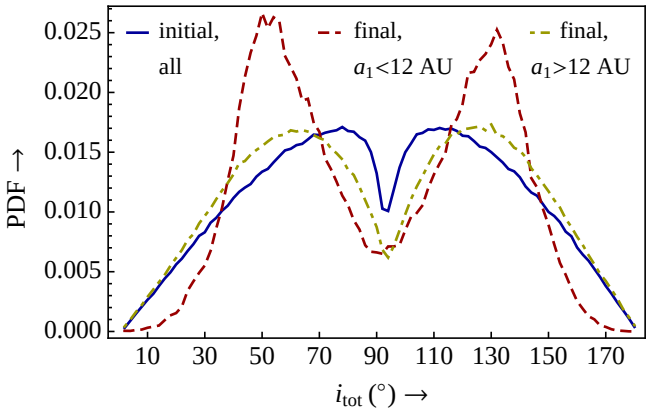

Figure 5.9: Distribution for TSM1 of the initial mutual inclination angle for the no merger systems (solid curve) and the final mutual inclination angle for the no merger systems with final $a_1 < 12$ AU (dashed curve) and $a_1 > 12$ AU (dot-dashed curve).

shrinking the inner orbit to $a_1 \sim 10^{-2}$ AU. These cases correspond to the MS f_{KCTF} fractions for the CO WD + MS merger channel and the no merger channel with $a_{1,f} < 12$ AU in Table 5.2. Depending on the precise values of a_1 and the masses the subsequent tight binary merges within a Hubble time due to GWE or a merger does not occur within a Hubble time. The latter systems constitute $\sim 20\%$ of the tightest inner binary systems which do not merge within a Hubble time ($a_{1,f} < 10^{-2}$ AU in Table 5.2). They may be recognized in Table 5.2 as the no merger systems with $a_{1,f} < 10^{-2}$ AU in which CE does not occur. The CO WD + CO WD merger systems are of particular astrophysical interest and are discussed in more detail in Sect. 5.4.

5.3.2 No inner binary mergers

If the initial mutual inclination angle is not close to 90° and/or the initial β is relatively large then the maximum eccentricity induced by Kozai cycles during the evolution is not high enough to eventually cause a merger. This is demonstrated by Fig. 5.3 which shows that $f_{\mathrm{no\,merge}}$ increases strongly with increasing β (even $f_{\mathrm{no\,merge}} \to 1$ for sufficiently large β) and that highly inclined systems are unlikely not to merge. Furthermore, $f_{\mathrm{no\,merge}}$ increases with decreasing a_1 which might be somewhat counterintuitive. This can be understood by considering that as a_1 decreases β is also generally larger, thus decreasing the eccentricity maxima. Although a merger does not occur for these systems, it is possible that the inner orbit is shrunk significantly due to KCTF as illustrated by Table 5.2: in $\sim 6\%$ of all systems, the final inner orbit semi-major axis is smaller than 12 AU, which is the minimum possible value in the absence of the tertiary (cf. Sect. 5.2). In the majority of these systems the main points in the evolution at which KCTF is important are the primary RGB and AGB phases, occurring in roughly equal proportion. Fig. 5.8 compares the initial and final distributions of a_1. The final distribution of a_1 shows a broad peak mainly due to strong KCTF around $a_{1,f} \sim 10^{-1.5}$ AU ≈ 0.03 AU ($P_1 \sim 2$ d). For the tightest of these systems ($a_{1,f} < 10^{-2}$ AU) it is also possible that very high eccentricity cycles lead to a tidal capture if the systems consists of a CO WD + low-mass MS star. The latter systems are very similar to compact object merger TIEM systems, with the exception that the companion is a low-mass MS star which possesses a convective envelope (Sect. 5.3.1; compact object mergers). Furthermore, the final distribution of a_1 shows a gap around $a_{1,f} \sim 1$ AU. This gap separates systems in which KCTF is followed by a CE ($a_{1,f} < 1$ AU) and in which a CE does not occur after KCTF ($a_{1,f} > 1$ AU). In the latter case KCTF is responsible for an enhancement of systems near final values of $a_1 \sim 10$ AU (cf. Fig. 5.8). If a CE occurs then this affects the final configuration of the inner binary system. This is shown in Table 5.4 where the likelihoods are shown of the most important inner binary configurations at the end of the evolution for the no merger systems. A distinction is made between the three groups with $a_{1,f} > 12$ AU ("wide"), $10^{-2} < a_{1,f}/\mathrm{AU} < 12$

	Wide		Tight		Very tight	
	TSM1	TSM2	TSM1	TSM2	TSM1	TSM2
CO + CO WD	0.370	0.428	0.189	0.209	0.010	0.016
CO WD + MS	0.599	0.535	0.503	0.494	0.391	0.392
CO + He WD	0.000	0.000	0.077	0.093	0.255	0.293
He + He WD	0.000	0.000	0.014	0.013	0.058	0.049
He WD + MS	0.000	0.000	0.188	0.159	0.284	0.246

Table 5.4: Likelihood of the most important inner binary configurations at the end of the evolution for the no merger systems. The no merger systems are divided into three groups, based on the final value of a_1: wide ($a_1 > 12$ AU), tight ($10^{-2} < a_1/\mathrm{AU} < 12$) and very tight ($a_1 < 10^{-2}$ AU). The fractions are relative to the total number of systems in each group. Note that in each column these fractions do not add to unity because not all final configurations are included in the table.

("tight") and $a_{1,f} < 10^{-2}$ AU ("very tight"). A CE does not occur in the wide systems and therefore these mainly end as CO WD + MS and CO WD + CO WD systems. In the case of a CE there is also a possibility for forming a He WD. The tighter systems can therefore also end as CO WD + He WD, He WD + He WD and He WD + MS systems.

The no merger systems are interesting from an observational point of view because the hierarchical structure remains intact during the entire evolution and the process of KCTF affects the mutual inclination angle. Typically during episodes of KCTF e_1 gradually approaches its maximum value in the Kozai cycle, followed by rapid circularization; the mutual inclination angle during this process tends to remain at its value associated with the eccentricity maximum, i.e. close to one of the two critical values determined by $\cos^2(i_{\rm tot}) = 3/5$. Therefore an observational marker of systems in which KCTF has once been important is a mutual inclination angle close to these critical values, as has been pointed out previously by Fabrycky & Tremaine (2007). Fig. 5.9 shows the initial and final mutual inclination angles for the no merger systems, distinguishing between final $a_1 > 12$ AU and $a_1 < 12$ AU. The initial distribution shows a clear lack of systems near $i_{\rm tot} \approx 90^\circ$ as also illustrated by Fig. 5.3. Systems for which strong KCTF applies at some point in the evolution (final $a_1 < 12$ AU) end with mutual inclination angles which are strongly peaked towards the critical values, whereas for systems in which KCTF is weaker or does not act at all (final $a_1 > 12$ AU), these peaks are much less prominent. In other words, we expect triple systems with tight inner orbits to show a markedly different inclination distribution than those with much wider inner orbits.

5.3.3 Triple destabilizations

If the initial β is particularly low, typically $\beta \lesssim 10$ (cf. Fig. 5.3), then the triple system may at some point in the evolution become dynamically unstable. Subsequent evolution is not modeled by our triple evolution algorithm because the secular evolution equations no longer apply in this case and N-body simulations are needed for an accurate description of the dynamical evolution. This scenario has been studied in detail in Perets & Kratter (2012), where it is referred to as the triple evolution dynamical instability. In our simulations, the destabilization occurs mainly during the MS or when the primary is an AGB star or a CO WD, cf. Table. 5.2.

In the case of MS destabilization, the triple system is initially marginally stable (i.e. only just satisfies Eq. 3.6) but due to octupole-order terms of the STD, which are important since β is (very) small and/or e_2 is high, e_2 varies periodically until it reaches a value high enough for destabilization of the triple system, i.e. $\beta \leq \beta_{\rm crit}$ (cf. Eq. 3.6). The time when this occurs is determined by the Kozai period P_K. Similarly to the MS mergers, this occurs relatively early in the evolution with most (90%) destabilizations occurring within 10% of the primary MS lifetime, cf. Fig. 5.5.

In the other cases destabilization is triggered by mass loss in the inner orbit, which, if fast and isotropic, acts to decrease β (i.e. the same mechanism discussed in the context of compact object TIEM mergers in Sect. 5.3.1) to a point where $\beta \leq \beta_{\rm crit}$. This happens when the primary loses a significant amount of mass as it evolves from the AGB phase to a WD and similarly when this happens to the secondary. In a small number of cases both inner binary components are CO WDs when the instability occurs and since there exists a finite probability of collision in the triple evolution dynamical instability (~ 0.1 as found by Perets & Kratter 2012) this could potentially lead to a CO WD collision. The implications of this scenario are investigated further in Sect. 5.4.

5.4 Results: triple-induced CO WD mergers

Of the inner binary merger systems, the double CO WD mergers are of particular astrophysical interest as some of such mergers are considered as an important progenitor channel for type Ia supernovae (SNe Ia) (Webbink, 1984; Iben & Tutukov, 1984). In the latter channel the merger results in a violent thermonuclear explosion due to CO burning in degenerate regions. The following two arguments support such a scenario. Firstly, the amount of energy released in the burning of the CO material is comparable to that found in SNe Ia. Secondly, because CO WDs contain no significant amount of hydrogen the explosion event is expected not to produce any spectral hydrogen lines, which is also consistent with SNe Ia. Due to this astrophysical relevance we describe below in Sect. 5.4.1 in more detail the channels leading to CO WD mergers found in our population synthesis study. Note that in the absence of the tertiary, such channels would not exist for the triple populations TSM1 and TSM2, i.e. these channels are all induced by the secular gravitational influence of the tertiary. In binary population synthesis studies these channels are therefore not taken into account. Subsequently we compute the expected rate of SNe Ia due to the triple-induced scenarios and compare our results to those of a binary population synthesis study and to observations in Sect. 5.4.2 .

5.4.1 Triple-induced CO WD merger channels

We find that inner binary CO WD mergers (momentarily excluding the possibility for triple destabilization scenarios, see below) occur through two main mechanisms: either the merger occurs in a tight circular orbit with GWE driving the merger (the TICM) or the merger is the consequence of an eccentric collision in a highly eccentric orbit (the TIEM). The TIEM channel applies to $\sim 10\%$ of all CO WD mergers (Table 5.2), i.e. the TICM channel is the dominant one. As discussed before in Sect. 5.3.1,

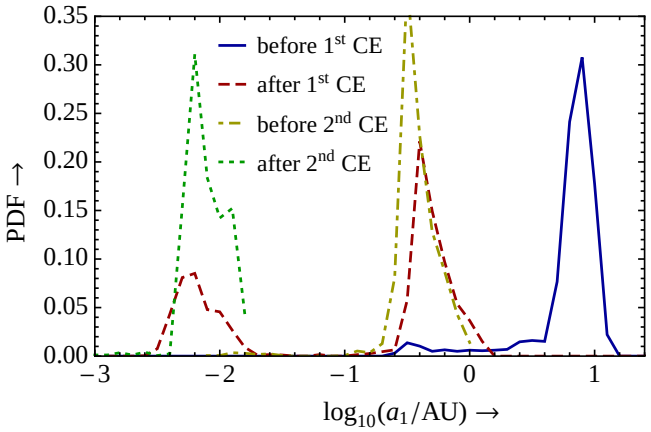

Figure 5.10: Distribution for TSM1 of a_1 for the CO WD merger systems which go through CE evolution. Solid: before first CE (i.e. after KCTF); dashed: after first CE. For those systems in which a second CE applies, the dot-dashed curve shows a_1 before the second CE and the dotted curve shows a_1 after the second CE.

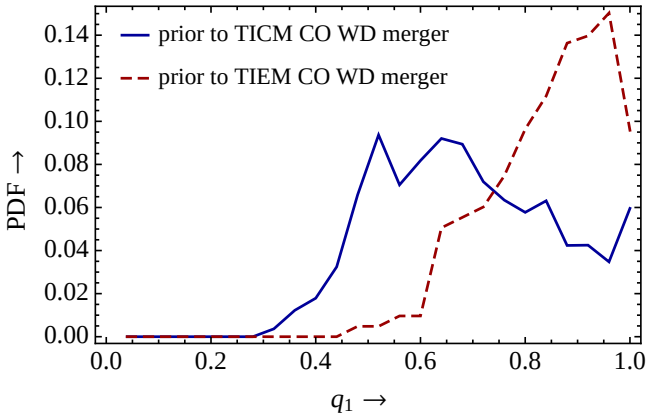

Figure 5.11: Distribution for TSM1 of the inner orbit mass ratio $q_1 = m_2/m_1$ just prior to CO WD merger, for the TICM (solid curve) and TIEM (dashed curve) mergers.

the main difference between the TICM and TIEM channels with regard to the initial parameters is that in the former initially $10^1 \lesssim a_1/\mathrm{AU} \lesssim 10^2$ while in the latter initially $10^2 \lesssim a_1/\mathrm{AU} \lesssim 10^3$ (Fig. 5.7, solid and dashed curves). Because tidal friction is strongly dependent on a_1 (cf. Eq. 3.1) this aids in avoiding KCTF during the giant phases in the TIEM systems while in the TICM systems KCTF causes substantial shrinkage of the inner orbit and so invokes CE evolution (Fig. 5.7, dot-dashed curves).

In the CO WD TICM systems, KCTF during the primary AGB phase leaves an inner binary AGB + MS system or an AGB + CHeB system with $a_1 \sim 10^{0.8} \approx 6\,\mathrm{AU}$ (Fig. 5.10, solid curve). Whether the secondary is a MS or a CHeB star after the primary AGB KCTF phase depends on the initial mass ratio $q_1 = m_2/m_1$: for the former initially $0.4 \lesssim q_1 \lesssim 0.9$ while for the latter initially $0.9 \lesssim q_1 \lesssim 1$. When the primary swells up during the AGB phase CE evolution is invoked, leaving either a CO WD + MS binary with $a_1 \sim 10^{-0.5}\,\mathrm{AU} \approx 0.3\,\mathrm{AU}$ (in case of a MS companion prior to CE) or a CO WD + He MS/HG binary with $a_1 \sim 10^{-2.5}\,\mathrm{AU} \approx 3 \cdot 10^{-3}\,\mathrm{AU}$ (in case of a CHeB companion prior to CE), cf. Fig 5.10 (dashed curve). In the latter case both the primary and the secondary are stripped of their envelopes resulting in a (much) tighter orbit; the secondary then evolves from a He MS/HG star to a CO WD. Subsequently a second CE is invoked, during which the inner binary system either mergers directly or survives the CE and merges due to GWE. In the case of a MS companion prior to the first CE, a second CE is invoked when the secondary evolves to an RGB/AGB star, leaving a tight CO WD + He MS/HG binary in which eventually a CO WD merger occurs (Fig. 5.10, dotted curve). Note that after the first CE the tertiary has no more influence on the inner binary system because $\beta \gg \beta_{\mathrm{crit,GR}}$ after this point in the evolution (cf. Fig. 5.6).

Fig. 5.11 shows the distribution of the mass ratio $q_1 \equiv m_2/m_1$ prior to the CO WD merger for both TICM and TIEM mergers. For the TICM mergers, this ratio is broadly distributed between ~ 0.5 and ~ 0.8. On the other hand, for TIEM mergers the distribution of q_1 prior to merger is more peaked towards unity. This can be understood as follows: if q_1 is relatively low, a system with initial parameters that are otherwise similar to those of TIEM CO WD merger systems is more likely to experience a primary CO WD TIEM merger with a MS or CHeB secondary star, cf. Table 5.2. For the latter systems the initial q_1 is indeed distributed around $0.2 \lesssim q_1 \lesssim 0.9$ and the mass ratio is typically not strongly affected during the evolution in TIEM systems because in such systems CE evolution is avoided.

In a very small number of systems (about 0.6% of all CO WD merger systems for TSM1) the evolution is very similar to that of the TIEM channel with the exception that the high eccentricity after formation of the double CO WD system does not lead to an orbital collision but instead triggers one or more episodes of very strong and brief gravitational wave emission (GWE). During the moment(s) that e_1 is extremely high ($1 - e_1 \lesssim 10^{-6}$) GWE leads to sudden orbital shrinkage reducing a_1 by a few per cent. If a_1 has become small enough the high eccentricity leads to a brief episode of orbital shrinkage due to GWE to a tight orbit of $a_1 \sim 10^{-2}$ AU. By this time the orbit has been circularized due to GWE (cf. Eq. 3.2). The final merger thus occurs due to GWE in a circular orbit and therefore these systems are interpreted as TICM systems, although the progenitor evolution is quite different from TICM systems in which a CE occurs.

In addition to the inner binary CO WD mergers, another triple-induced channel leading to CO WD mergers involves triple destabilizations which occur when the inner binary system consists of two CO WDs. In most of the latter systems the tertiary is also a CO WD at the moment of destabilization. In subsequent close three-body encounters it is possible that a CO WD collision occurs. Note that such a merger is expected to be physically similar to TIEM mergers, although in the latter case the triple system remains formally stable until the merger event. Perets & Kratter (2012) find that a collision occurs in $\sim 10\%$ of all destabilization cases. Adopting this fraction, we expect this channel to lead to CO WD mergers in $\sim 0.01\%$ of all systems.

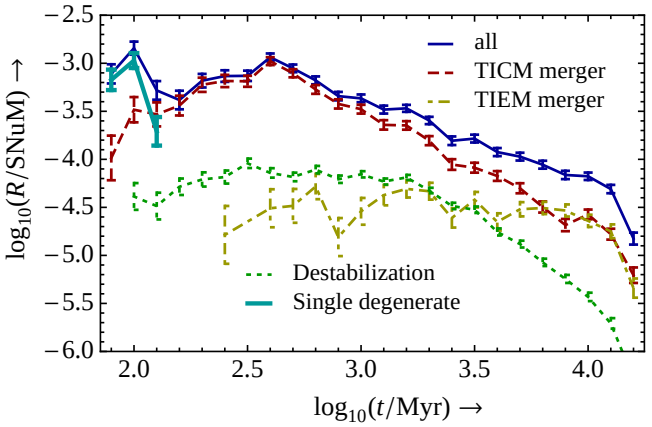

Figure 5.12: Delay time distribution (DTD) for TSM1 of the triple-induced inner binary CO WD merger and destabilization channels, which in an optimistic scenario all lead to SNe Ia. Shown are the rates in SNuM (per $10^{10}\,M_\odot$ per century) due to the combined inner binary CO WD merger channels (solid curve), due to super-$M_{\rm Ch}$ TICM mergers (dashed curve), due to sub-$M_{\rm Ch}$ and super-$M_{\rm Ch}$ TIEM mergers (dot-dashed curve) and due to CO WD collisions induced by triple destabilizations assuming that in 10% of all inner binary CO WD destabilizations, a collision subsequently occurs (dotted curve). Lastly, triple-induced contributions from the single degenerate channel are shown (thick solid curve).

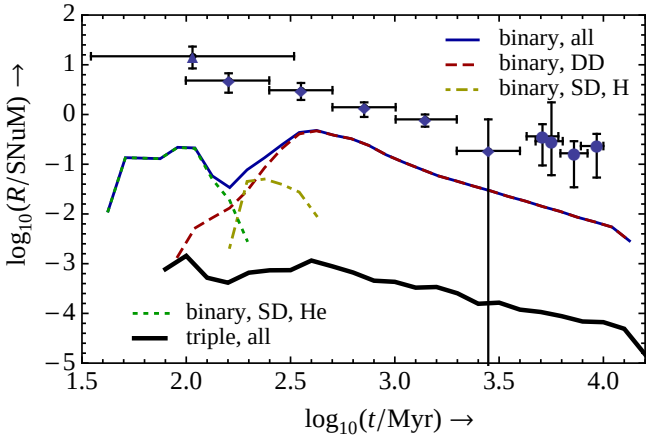

Figure 5.13: SNe Ia DTD according to all triple-induced channels of Fig. 5.12 (thick solid curve) and according to a binary population synthesis study (Claeys et al., 2012), with the total rate (solid curve), double degenerate (DD) rate (dashed curve), single degenerate (SD) hydrogen donor rate (dot-dashed curve) and single degenerate helium donor rate (dotted curve). In addition, observed SNe Ia rates (points with error bars) are shown from Totani et al. (2008), Maoz & Badenes (2010) and Maoz et al. (2010) (triangle, diamonds and filled circles respectively).

5.4.2 Expected SNe Ia rates

It is uncertain whether a CO WD merger leads to a SN Ia, even if the combined mass of the CO WDs exceeds the Chandrasekhar mass $M_{\rm Ch} \approx 1.44\,M_\odot$, which is the maximum mass for a carbon-oxygen gas supported by electron degeneracy pressure. The mechanism through which the merger occurs is an important factor in the efficiency of the explosion mechanism. For mergers occurring in circular orbits (i.e. in which the TICM applies) some hydrodynamical simulations indicate that during the merger the secondary is quickly disrupted, finally leading to the formation of a single CO WD surrounded by an accretion disk (e.g. Guerrero et al. 2004). In the merger process degeneracy is lifted, quenching a thermonuclear runaway situation. However, other studies show that a sub-luminous SN Ia may be formed if the mass ratio is larger than $q_1 = m_2/m_1 = 0.8$ (e.g. Pakmor et al. 2011). For head-on collisions on the other hand, which are very similar to highly eccentric collisions (i.e. in which the TIEM applies), evidence exists that they are more likely to result in a SN Ia even for sub-$M_{\rm Ch}$ encounters. This is due to the high relative speed on the order of the escape speed, 10^3 km/s, which causes shocks that aid the ignition of the thermonuclear explosion. In the simulations of Rosswog et al. (2009) all simulated equal-mass CO WD encounters with $m_1 = 0.6\,M_\odot$ and $m_1 = 0.9\,M_\odot$ lead to thermonuclear explosions and the resulting light curves and spectra resemble those of observed SNe Ia. For small mass ratios Rosswog et al. (2009) find that an explosion is avoided, with the critical mass ratio being at least $q_1 = 2/3$ (their Table 1). In the simulations of Raskin et al. (2010), however, mass ratios as low as $q_1 = 0.6$ still lead to a SN Ia (their Table 2). The total mass prior to merger $m_1 + m_2$ also determines the efficiency of forming a SN Ia as both Rosswog et al. (2009) and Raskin et al. (2010) find that a $0.5\,M_\odot + 0.5\,M_\odot$ CO WD encounter does not lead to a SN Ia whereas encounters with CO WDs more massive than $0.6\,M_\odot + 0.6\,M_\odot$ do. Note that the latter case is still sub-$M_{\rm Ch}$.

	f	
	TSM1	TSM2
TICM	**0.879**	**0.909**
• $m_1 + m_2 < M_{\rm Ch}$	0.503	0.441
• $0 < q_1 \leq 0.8$	0.312	0.310
• $0.8 < q_1 \leq 1$	0.192	0.131
• $m_1 + m_2 > M_{\rm Ch}$	0.376	0.467
• $0 < q_1 \leq 0.8$	0.350	0.440
• $0.8 < q_1 \leq 1$	0.026	0.028
TIEM	**0.121**	**0.091**
• $m_1 + m_2 < M_{\rm Ch}$	0.056	0.035
• $0 < q_1 \leq 0.8$	0.011	0.008
• $0.8 < q_1 \leq 1$	0.045	0.027
• $m_1 + m_2 > M_{\rm Ch}$	0.065	0.056
• $0 < q_1 \leq 0.8$	0.033	0.033
• $0.8 < q_1 \leq 1$	0.032	0.023

Table 5.5: Probabilities of various triple-induced CO WD merger channels, expressed as fractions of the total number of CO WD mergers (excluding the CO WD destabilization scenario).

In Table 5.5 probabilities are given of various subpopulations of the triple-induced CO WD mergers, expressed as fractions of the total number of CO WD mergers (excluding the CO WD destabilization scenario). Based on the above discussion we distinguish between mergers with

mass ratios q_1 above and below the value $q_1 = 0.8$. Mergers with $0 < q_1 \leq 0.8$ are unlikely to result in SNe Ia, whereas for those with $0.8 < q_1 \leq 1$ such an outcome is more probable. For TICM mergers the total mass should also exceed $M_{\rm Ch}$ whereas for TIEM mergers we do not impose such a constraint because we find that the lowest total mass for any TIEM merger exceeds 1.1 $M_\odot$. Table 5.5 shows that many TICM mergers have relatively low mass ratios as was also shown by Fig. 5.11. The fact that TICM mergers typically have low q_1 prior to merger suggests that many of these mergers do not lead to SNe Ia. Note, however, that the precise value of the critical mass ratio is uncertain. Moreover, in binary population synthesis studies such a distinction between mass ratios is usually not made.

In order to relate the expected rate of triple-induced SNe Ia to the binary population synthesis study of Claeys et al. (2012) and observations we normalize the number of systems in which a SN Ia is expected to occur to the part of the galactic mass represented by the sampled triple systems. Note that the sampled triple populations constitute only a small fraction of all triple systems. In addition we must assume specific values for the binary and triple fractions of the galactic population. The binary fraction $\alpha_{\rm bin}$ is a function of mass and is found to range between $\alpha_{\rm bin} = 0.56$ for solar-like stars (Raghavan et al., 2010) to $\alpha_{\rm bin} \geq 0.7$ for O & B stars (Kouwenhoven et al., 2007). In order to simplify the calculation we assume an intermediate constant value of $\alpha_{\rm bin} = 0.60$. Statistics on the triple fraction $\alpha_{\rm tr}$, which is similarly a strong function of mass, are less well-constrained. The observed triple fractions range from 0.11 for solar-like stars (Raghavan et al., 2010; Rastegaev, 2010) to 0.5 for more massive B stars (Remage Evans, 2011). Again neglecting the mass dependence we take a conservative intermediate constant value $\alpha_{\rm tr} = 0.25$. With these fractions we calculate a total mass represented by the number of triple systems we have calculated and with which we normalize the SNe Ia rates for TSM1. We express the result in rate per $10^{10}\,M_\odot$ per century (SNuM); we refer to Appendix C for more details on this procedure and explicit numbers. Fig. 5.12 shows these rates as a function of time, i.e. the delay time distribution (DTD), after an assumed starburst at $t = 0$. We make a distinction between super-$M_{\rm Ch}$ CO WD TICM mergers (dashed) and CO WD TIEM mergers (dot-dashed). In addition the expected rate due to CO WD destabilizations is included (dotted curve) assuming that in 10% of all CO WD destabilizations a collision and hence possibly a SN Ia results (Perets & Kratter, 2012). In an optimistic scenario (i.e. ignoring any constraints with respect to the mass ratio prior to merger), all of these are expected to lead to a SN Ia. Lastly, we estimate the contribution due to the single degenerate channel in which a single CO WD accretes material from a MS companion until it reaches $M_{\rm Ch}$. We identify systems in which a SNe Ia is expected to occur due to this single degenerate channel based on specific regions in the (m_2, a_1) space. Detailed simulations (Claeys et al., 2012) give predictions for these regions; if a CO WD is formed with a MS/RGB companion (mass m_2) and the parameters lie within these regions in the (m_2, a_1) space then the final result is expected to be a SNe Ia. Note that we have also computed the triple-induced DTD for TSM2 and find very similar results to those of TSM1.

Fig. 5.12 shows that the main contribution to the triple-induced rate is the super-$M_{\rm Ch}$ CO WD TICM merger channel, with a substantial but short contribution due to the single degenerate channel at $\sim 100\,$Myr. The channel due to destabilizations does not contribute significantly at any time. The CO WD TIEM merger channel contributes significantly to the combined triple-induced rate at late times ($t \sim 10\,$Gyr), whereas it does not at earlier times. This is due to the fact that after double CO WD formation the Kozai period P_K is typically quite long (the distribution of P_K peaks around $P_K \sim 0.3\,$Gyr, see also Sect. 4.2) and it typically takes at least a few cycles before an orbital flip occurs (cf. Fig. 4.3, bottom right panel). Such an orbital flip is almost invariably required to attain eccentricities high enough for a collision ($1 - e_1 \lesssim 10^{-7}$).

Furthermore we show in Fig. 5.13 the expected triple-induced SNe Ia rate according to all channels discussed above (thick curve) and results from the binary population synthesis study of Claeys et al. (2012). Furthermore observed rates are included from Totani et al. (2008), Maoz & Badenes (2010) and Maoz et al. (2010). For the binary population synthesis study a distinction is made between the double degenerate (DD) channel (super-$M_{\rm Ch}$ CO WD merger with any mass ratio, occurring invariably after CE evolution) and the single degenerate (SD) channel (a single CO WD accreting mass from a MS/HG/RGB companion until it reaches $M_{\rm Ch}$ and explodes), the latter with either a hydrogen-rich or helium-rich donor star. Fig. 5.13 shows that the triple-induced DTD generally follows the same shape as the binary population synthesis DTD, with a rate proportional to t^{-1} for times later than $t \sim 10^{2.6}\,$Myr (the best fitting slope for $t > 10^{2.6}\,$Myr is -0.96). The triple-induced rates are much lower than the binary population synthesis rates, however: the former are typically a factor of ~ 10 to $\sim 10^3$ lower than the binary population synthesis rates, which in turn are typically a factor of ~ 10 lower than the observed rates. The triple-induced channels are therefore of some importance but they do not solve the problem that the predicted SNe Ia rates are too low compared to the observed ones (see also Maoz & Mannucci 2012 and Wang & Han 2012). The present study does not give a complete picture of the triple-induced rate, however, and we will return to this point in the discussion in Chapter 6.

Chapter 6

Discussion

In this chapter we compare some of our findings from the population synthesis study (Chapter 5) with other studies (Sect. 6.1). Furthermore, we discuss the assumptions made and uncertainties in this work in Sect. 6.2. Lastly, we make suggestions for further study in Sect. 6.3.

6.1 Comparisons to other studies

6.1.1 Effect of mass loss on Kozai cycles

The effect of mass loss due to stellar evolution on the secular dynamical evolution of triples (i.e. Kozai cycles) has recently been studied by Shappee & Thompson (2012; hereafter ST12). ST12 performed N-body integrations of triples with fixed masses $m_1 = 7.0\,M_\odot$, $m_2 = 6.5\,M_\odot$ and $m_3 = 6.0\,M_\odot$ and fixed $a_1 = 10\,\mathrm{AU}$ and $a_2 = 250\,\mathrm{AU}$, with $\cos(i_{\mathrm{tot}})$, e_1, e_2 and g_1 in an equally spaced grid. Mass loss during the primary AGB phase is modeled with a relation which is linear in time, where the final WD mass is determined by the initial-final mass relation of Kalirai et al. (2008). Similarly to our study ST12 make the assumption of fast and isotropic wind mass loss in both binary systems such that $a_1(m_1 + m_2)$ and $a_2(m_1 + m_2 + m_3)$ remain constant. Unlike our study, however, ST12 do not model the processes of apsidal motion due to general relativity, tidal bulges and rotation, gravitational wave emission and tidal friction (cf. Chapter 3). To capture the importance of tidal friction an ad hoc tidal radius is introduced. Whenever the inner binary separation is smaller than this tidal radius it is assumed that tidal friction is important. This ad hoc tidal radius is adjusted with different evolutionary phases of the primary in an attempt to capture the different strengths of tidal forces, analogous to (but likely less accurate than) our approach where the tidal strength quantity k_i/T_i is computed from tidal theory where a main distinction is made between convective, radiative and degenerate damping (cf. Sect. 3.3). Furthermore, in contrast to our study ST12 do not take into account binary interactions such as CE evolution (cf. Sect. 3.2). Nevertheless, because ST12 accurately model the triple dynamics by means of an N-body code and take into account stellar evolutionary changes it is interesting to see how their results roughly compare with ours. In this comparison it should also be taken into account that in our study all triple parameters are sampled by means of Monte Carlo methods, whereas ST12 assume fixed masses and semi-major axes.

ST12 find that there is about 10% probability for close encounters (periastron distance comparable to the stellar radii) during the MS, which is roughly in agreement with the 5% MS mergers found in this study (cf. Table 5.2). ST12 also find that octupole order effects are important for these MS systems, which is consistent with our study (cf. Fig. 5.4). Furthermore, ST12 find that eccentricity cycles are important during the giant phase (with close encounters occurring in $\sim 30\%$ of all systems), which is consistent with our study where we find that $\sim 24\%$ of all systems experience strong KCTF during the RGB/AGB phases. Lastly, ST12 find that $\sim 10\%$ of all systems become dynamically unstable which is also consistent with our results (cf. Table 5.2).

6.1.2 Effect of mass loss on triple dynamical instability

The scenario of a triple dynamical instability has recently been studied in detail by Perets & Kratter (2012; hereafter PK12). PK12 determine which fraction of triple systems with $1.0 < m_1/M_\odot < 20$ become dynamically unstable during their evolution by means of a stability criterion. Subsequently PK12 investigate the further evolution by means of N-body simulations and determine the fraction of systems in which a collision between two (or more) components occurs. Although the evolution *after* dynamical stability is beyond the scope of our study, it is interesting to compare their fraction of systems which become

dynamically unstable with ours. This is because PK12 sample a triple population by means of a method which is qualitatively similar to the sampling method of our population TSM1 (cf. Sect. 5.2) and because their treatment of mass loss is similar.

In the sampling method of PK12 both inner and outer binary parameters are generated by means of Monte Carlo sampling from observed binary distributions. The assumed binary distributions in PK12 are not identical to ours, however. Firstly, in PK12 the period distribution for primary masses $m_1 < 3\,M_\odot$ is a Gaussian (Raghavan et al., 2010) and for $m_1 > 3\,M_\odot$ it is flat in $\log_{10}(P_j)$, whereas in our study for TSM1 the period distribution is flat in $\log_{10}(P_j)$ independent of the primary mass. Also note that PK12 sample a full range of inner and outer orbital periods whereas in our study a selection is made to $a_1\left(1-e_1^2\right) > 12\,\mathrm{AU}$. Secondly, PK12 assume a Salpeter IMF with $1.0 < m_1/M_\odot < 20$, whereas we assume a Kroupa IMF with $1.0 < m_1/M_\odot < 6.5$ for TSM1. Also PK12 increase the weight of the $3.0 < m_1/M_\odot < 20$ subsample by a factor of five to account for the dependence of the triple fraction on mass (this factor of five is motivated by observations, see PK12). We do not employ such an increased weight for higher mass primaries. Thirdly, PK12 sample mass ratios from a Gaussian distribution for low mass primaries and a power law for high mass primaries while we assume flat distributions. The remaining parameters are sampled similarly in both studies: both sample e_j from thermal distributions and $i_{\rm tot}$ from a distribution which is uniform in $\cos(i_{\rm tot})$. Despite these differences in assumed binary distributions the triple sample of PK12 and our TSM1 sample should be roughly comparable. Note that in addition to the sampling method described above, PK12 also directly use observed triple data from Tokovinin (2008). We did not use such a method because of the limited number of systems in the Tokovinin (2008) sample which remain after applying our selection criteria (cf. Sect. 5.1). In this comparison we shall therefore focus solely on results from the binary sampling method of PK12.

PK12 model the inner binary mass with the `binary_c` algorithm (Hurley et al., 2002) similar to our study. Note, however, that PK12 do not model the effect of Kozai cycles. Furthermore, the tertiary mass is modeled with the SSE code (Hurley et al., 2000) which is equivalent to the `binary_c` algorithm in single star mode. This method for the tertiary mass is identical to ours (cf. Sect. 3.2). PK12 then compute the effect of mass loss in the inner binary system and the tertiary on the outer orbit semi-major axis with the assumption of fast and isotropic wind, again similar to our study. The effect of this mass loss is to decrease the ratio $\beta \equiv a_2/a_1$ (as in Sect. 5.3.3), which decrease can drive a triple destabilization. Using the stability criterion of Valtonen et al. (2008) PK12 then determine the fraction $f_{\rm dest,\,PK12}$ of systems which become dynamically unstable (note, however, that PK12 find from their N-body simulations that only 33% of the systems which do not satisfy this stability criterion are truly dynamically unstable within their 0.5 Myr time integration). They find a fraction $f_{\rm dest,\,PK12} \sim 0.053$.

This fraction should be compared with our fraction $f_{\rm dest} \sim 0.102$ of all systems which become dynamically unstable in TSM1 (cf. Table 5.2). Note that among these systems are MS destabilizations, which are systems which are only marginally stable at system formation. The MS destabilizations are mainly driven by octupole order effects which increase e_2 early in the evolution such that $\beta_{\rm crit}$ increases (cf. Eq. 3.6 and Sect. 5.3.3). Such effects are not modeled in PK12. However, because systems which in our study destabilize early on the MS are only marginally stable, they would likely destabilize during the AGB phase which is associated with a decrease in β. The latter systems are taken into account in PK12. The fractions $f_{\rm dest,\,PK12}$ and $f_{\rm dest}$ are roughly comparable, although our fraction is distinctly higher. The main reason for this difference is likely due to different distributions of $\beta \equiv a_2/a_1$ in PK12 and our study because $f_{\rm dest}$ depends very sensitively on this distribution (see the dependence of $f_{\rm dest}$ on β in Fig. 5.3; note that this figure only shows the region $0 < f_{\rm dest} < 0.5$). In addition (but note that this is a small effect), PK12 use the stability criterion of Valtonen et al. (2008) whereas we use that of Mardling & Aarseth (2001) (cf. Sect. 3.2). On average the former gives slightly smaller values of $\beta_{\rm crit}$ than the latter[1] and in general the number of destabilizations decreases with decreasing $\beta_{\rm crit}$.

6.1.3 The role of the tertiary in CO WD mergers

As discussed before in Chapter 1, Thompson (2011; hereafter TH11) has recently suggested that high eccentricities induced by the tertiary in close CO WD binaries can significantly reduce the merger time due to GWE. TH11 models this effect of the tertiary and finds that binaries with orbital periods as high as $P_1 \sim 300\,\mathrm{d}$ can still merge due to GWE within a Hubble time if a relatively close and sufficiently inclined tertiary is present. In the absence of a tertiary the maximum orbital period for a merger due to GWE within a Hubble time for these CO WD binaries is $P_1 \sim 0.3\,\mathrm{d}$ (see e.g. Sect. 3.1.2). The scenario introduced by TH11 could significantly increase the expected observed rates of mergers of compact objects, in particular CO WD mergers. The latter mergers are considered as an important candidate progenitor channel for SNe Ia. TH11 does not take into account the evolution of the triple system prior to the formation of the CO WD binary, however. We have taken into account this prior evolution in the case of initially wide inner binaries with $a_1\left(1-e_1^2\right) > 12\,\mathrm{AU}$. Although we find that CO WD mergers due to GWE (in circular orbits) occur, these systems are unaffected by Kozai cycles after the first CE phase which precedes the formation of the close CO WD binary. This is due to the large ratio $\beta \equiv a_2/a_1$ after the CE phase such that Kozai cycles are quenched by general relativistic

[1] More quantitatively: the ratio between $\beta_{\rm crit}$ according to Valtonen et al. (2008) and Mardling & Aarseth (2001) is given by $\beta_{\rm crit,\,V08}/\beta_{\rm crit,\,MA01} = \frac{15}{14}\,(1+q_2)^{-1/15}\,(1-e_2)^{1/30}\,(1+e_2)^{-2/5}\left(\frac{7}{4}+\frac{1}{2}\cos(i_{\rm tot})-\cos^2(i_{\rm tot})\right)^{1/3}\left(1-\frac{0.3}{\pi}i_{\rm tot}\right)^{-1}$ ($i_{\rm tot}$ expressed in radians). If we assume a flat distribution in $0 < q_2 < 1$, a thermal distribution for e_2 and $i_{\rm tot}$ uniform in $\cos(i_{\rm tot})$ we find a mean weighted value $\langle\beta_{\rm crit,\,V08}/\beta_{\rm crit,\,MA01}\rangle \approx 0.98$.

apsidal motion (cf. Fig. 5.6). Note, however, that although Kozai cycles are not important after the CE they do play a key role in triggering the CE through orbital shrinkage due to KCTF during the primary giant phases.

Furthermore, we find a new channel leading to CO WD mergers in which the tertiary plays a key role and which has not been considered by TH11. In this channel the merger occurs through an eccentric collision (TIEM) after the formation of an inner binary CO WD system. Due to mass loss in the inner binary system as both the primary and secondary evolve to CO WDs the ratio $\beta \equiv a_2/a_1$ at this time is low, typically $\beta \sim 15$ (Fig. 5.6; dotted curve). This induces octupole order effects in which very high eccentricities occur during orbital flips (e.g. Fig. 4.2). Consequently an orbital collision can occur. Note that these orbital collisions are similar to head-on encounters which are normally expected to occur only in dense stellar systems such as the cores of globular clusters, whereas hierarchical triple systems are also common among field stars (e.g. Raghavan et al. 2010). As discussed in Sect. 5.4.2 these head-on encounters are likely to result in SNe Ia. Another CO WD merger channel in which the tertiary plays a key role is when a triple destabilization occurs. Note that this scenario has been investigated previously by PK12. If the inner binary is a CO WD binary at the time of destabilization, a possible outcome is a collision; PK12 find that the probability for a collision is $\sim 10\%$.

Because CO WD mergers are considered as an important progenitor channel for SNe Ia we have computed the expected SNe Ia rates due to the various triple-induced CO WD merger channels and normalized them to the part of the mass represented by the sampled triple population in Sect. 5.4.2. Fig. 5.13 shows these rates as function of time (for TSM1) in an optimistic scenario (i.e. in which the dependence of the mass ratio prior to merger on the efficiency of an explosion is neglected) and compares them with the rates according to the binary population synthesis study of Claeys et al. (2012) and observed rates from Totani et al. (2008), Maoz & Badenes (2010) and Maoz et al. (2010). As was discussed in Sect. 5.4.2 the triple-induced rates are much lower than the binary population synthesis rates and the observations. However, it needs to be taken into account that in our work inner binary systems with initially $l_1 \equiv a_1\left(1-e_1^2\right) < 12\,\mathrm{AU}$ are not modeled. It is likely that there is also a contribution from triple systems with initially tighter inner binaries. Therefore the rates due to a full triple population are likely higher than those presented in Fig. 5.13, especially when taking into account that in TSM1 only ~ 0.130 of all triple systems satisfy $l_1 > 12\,\mathrm{AU}$ (cf. Appendix C).

6.2 Assumptions and uncertainties

In this work many physical processes are modeled and due to the large number of uncertainties associated with these processes we were forced to make simplifying assumptions. Here we address some of these assumptions and uncertainties. In the triple algorithm used in this work the assumption of fast and isotropic wind mass loss is made (Sect. 3.2). This assumption is used to compute the effect of mass loss in the inner binary system and the tertiary on the outer orbit semi-major axis. If, however, the wind speed v_w of the mass-losing star in the inner binary system is comparable to the inner orbital speed $v_\mathrm{orb,1}$ then the winds are likely affected by its companion (e.g. Val-Borro et al. 2009). This may be the case for AGB stars, which have a relatively low wind speed of typically $v_\mathrm{w} \sim 10\,\mathrm{km\,s^{-1}}$ (e.g. Winters et al. 2003). In the case that $v_\mathrm{w} \sim v_\mathrm{orb,1}$ the mass loss in the inner binary system may no longer be fast and isotropic and consequently the assumption that $a_2(m_1+m_2+m_3)$ is constant no longer holds. In the inner binary system part of the mass lost in the wind is then accreted by the companion. As a result the expansion of the inner orbit is reduced with respect to the situation of fast and isotropic winds. More quantitatively, if the primary in a binary orbit loses mass then the effect on the semi-major axis is described by (Hurley et al., 2002)

$$\frac{\langle \delta a \rangle}{a} = -\frac{\delta m_1}{m_1+m_2} - \left(\frac{2-e^2}{m_2} + \frac{1+e^2}{m_1+m_2}\right)\frac{\langle \delta m_2 \rangle}{1-e^2}, \tag{6.1}$$

where brackets denote orbital averaging. If the companion does not accrete any mass then the second term in Eq. 6.1 is zero and Eq. 6.1 reduces to $a(m_1+m_2)$ being constant (note that $\delta m_1 < 0$). If, on the other hand, the companion accretes mass through wind from the primary then the increase of a is reduced due to the second term in Eq. 6.1, where $\langle \delta m_2 \rangle > 0$. Note that this effect on the inner orbit is taken into account in our triple algorithm because it is implemented in `binary_c`, where $\langle \delta m_2 \rangle$ is prescribed by the Bondi & Hoyle (1944) mechanism (Hurley et al., 2002). The effect is, however, not taken into account for the outer orbit. In the latter orbit part of the mass lost in the wind may be accreted by the tertiary if the wind is sufficiently slow compared to the outer orbital speeds. Consequently the expansion of the outer orbit is less than expected based on the assumption made in the triple algorithm. This would imply that during phases of strong mass loss in the inner binary system, notably during the primary and secondary AGB phases, there would be a stronger decrease in the ratio $\beta \equiv a_2/a_1$. Consequently in the systems in which β decreases during the AGB phases due to mass loss in the inner binary system we would expect more systems in which octupole order terms (and hence also orbital flips) are important after the AGB phase due to the smaller β. This would imply more eccentric merger systems (in particular eccentric CO WD merger systems) and more systems which become dynamically unstable during or after the AGB phase. However, we do not believe that this effect significantly changes our results. We find that systems in which wind mass loss during the AGB phase is responsible for decreasing the ratio β typically have large inner orbit semi-major axes, i.e. $a_1 \sim 10^{2.6}\,\mathrm{AU} \sim 400\,\mathrm{AU}$ (cf. Fig. 5.7, dashed curve). In this case the inner orbital speeds are slow,

$v_{\rm orb,1} = [G_N(m_1 + m_2)/a_1]^{1/2} \sim 3\,{\rm km\,s^{-1}} < v_{\rm w}$ (taking $m_1 + m_2 = 4\,M_\odot$ and $e_1 = 0$) and hence we expect the assumption of fast and isotropic winds to be reasonable.

Furthermore, uncertainties remain in the physics of tidal friction, in particular in the dynamical tide model where high eccentricities may induce complicated coupling of stellar oscillations with the tidal potential (Zahn, 2005). It is conceivable that such coupling in the case of high eccentricity could significantly increase the effectiveness of tidal friction and this could have important consequences for the our study. For example, we have found that MS mergers merge predominantly due to eccentric collisions (TIEM); only for a small number of systems with low-mass inner binary components, KCTF is effective at shrinking the orbit and hence resulting in a TICM merger. If tidal friction in stars possessing radiative envelopes in highly eccentric orbits were more effective than prescribed by the method used in this work (Hurley et al., 2002), for which k_i/T_i is independent of e_1, then KCTF could be effective in more systems. The details of such a dependence of e_1 on k_i/T_i are unclear. Nevertheless, in order to obtain a rough idea of the consequences of stronger tidal friction than assumed in Chapter 3 we have recalculated the evolution of the TSM1 population, artificially increasing the tidal strength quantities k_i/T_i by an ad hoc factor of 10^3 for the case of radiative damping. We find that this has virtually no effect: the probabilities of the main channels are unchanged, as is the proportion of systems which merge in eccentric orbits. Furthermore, we have performed the same test (i.e. multiplying k_i/T_i by an ad hoc factor of 10^3) for degenerate damping, for which also uncertainties remain. We similarly find that the artificial increase in k_i/T_i for degenerate damping does not change the results. It may thus be concluded that the uncertainties in radiative and degenerate damping do not significantly affect the results of our population synthesis study.

Uncertainties exist not only in our triple algorithm but also in the initial parameter distributions. For binary systems these parameters are reasonably constrained, although the distribution of the mass ratio q_1 remains uncertain. For triple systems on the other hand, the parameters are much less certain due to the small number of observed triple systems with reliable orbital distributions. In particular the initial distribution of the mutual inclination angle $i_{\rm tot}$ is virtually unknown, although efforts are on the way to better constrain this parameter (e.g. Lane et al. 2007 and Muterspaugh et al. 2008). Because of these uncertainties in the triple parameters we have sampled two distinct populations with different mass and orbital period distributions (cf. Table 5.1). Despite the differences with respect to the masses and orbital periods between these methods, we find that our results for both populations are very similar (cf. Table 5.2). Furthermore, the assumed distribution of $i_{\rm tot}$ is the same in TSM1 and TSM2. As Fig. 5.3 shows, our results are strongly dependent on this distribution, which is ill-constrained by observations. We emphasize, however, that our assumption of a uniform distribution of $\cos(i_{\rm tot})$ is reasonable and that there is no a priori reason to believe that the distribution of $i_{\rm tot}$ is significantly different from uniform in $\cos(i_{\rm tot})$.

6.3 Suggestions for further study

In order to gain further insight into the accuracy of the our triple algorithm, it would be valuable to perform detailed three-body simulations with a realistic treatment of tidal evolution of specific triple systems, in particular those in which the inner orbit eccentricity maxima are high. Such simulations could specifically be used to verify the extreme inner orbit eccentricities of $1 - e_1 \sim 10^{-8}$ in wide inner binary systems of $a_1 \sim 10^3$ AU found in CO WD TIEM merger systems in our study (see e.g. the example system in Sect. 4.2). Also it is of interest to investigate by means of a detailed treatment whether this high eccentricity leads primarily to an orbital collision (as found in this work) or to tidal capture or a short burst of gravitational wave emission. The latter two scenarios would lead to very tight circular orbits and subsequent mergers due to GWE. Note that we do find that the last scenario of strong GWE due to high eccentricities occurs in our population synthesis study (cf. Sect. 5.4.1), but it is very unlikely. Such detailed simulations could e.g. be carried out in the AMUSE framework (Portegies Zwart et al., 2009), coupling hydrodynamical, three-body codes and possibly stellar evolution codes.

Lastly, as mentioned previously, the triple sample considered in this work only contains relatively wide inner binary systems. In order to also simulate those triple systems with $l_1 < 12$ AU, the triple algorithm used would have to be extended to also include mass transfer in eccentric orbits, for which a formalism has been derived previously (e.g. Sepinsky et al. 2007).

Chapter 7

Conclusion

We have studied the evolution of coeval stellar hierarchical triple systems with intermediate mass (inner binary primary mass $1.0 < m_1/M_\odot < 6.5$) and initially relatively wide inner binary systems ($a_1[1-e_1^2] > 12$ AU) which would not interact in the absence of the tertiary component. For this purpose we have developed a secular gravitational hierarchical triple dynamics code and coupled this with an existing binary population synthesis algorithm. We have performed a population synthesis study and find that in 25% of these systems the process of Kozai cycles with tidal friction (KCTF) is important at some point in the evolution, most notably during the primary RGB and AGB phases. In particular, in $\sim$ 6% of all systems the inner binary is shrunk significantly, thus producing close CO WD and He WD binaries. In $\sim$ 8% of all systems the tertiary drives an inner binary merger among which mergers due to eccentric collisions are important ($\sim$ 60% of all mergers). Mergers on the MS occur most frequently ($\sim$ 4% of all systems) and octupole order terms in the secular-three body dynamics are important in driving high eccentricities, which in most cases are high enough for an orbital collision. For MS mergers tidal friction is typically weak due to the radiative structure of the stellar envelopes, such that KCTF occurs only in a small fraction of MS merger systems ($\lesssim 0.01$). Most inner binary post-MS and compact object mergers are driven by strong KCTF, substantially shrinking the orbit to $a_1 < 12$ AU and potentially invoking common-envelope evolution as either component grows significantly in size during the RGB/AGB phase. After any common-envelope phase we find that $\beta = a_2/a_1$ is always so large that the secular three-body dynamics are completely dominated by general relativistic apsidal motion and Kozai cycles are suppressed. We thus find that none of the triple systems considered in this sample lead to close CO WD binaries in which the GWE merger time is reduced by Kozai cycles, as has been suggested by Thompson (2011). In $\sim$ 10% of all compact object merger systems strong KCTF is avoided. In such systems, the increase in a_1 due to wind mass loss in the inner binary orbit significantly decreases the ratio $\beta \equiv a_2/a_1$, thus increasing the importance of octupole order effects. Consequently high-amplitude eccentricity cycles are induced, in particular during transitions between retrograde and prograde orbits and vice versa. Due to weak tidal friction in the majority of these systems (compact objects and/or MS/CHeB stars), these cycles likely lead to an orbital collision through the triple-induced eccentric mechanism (TIEM), which is a novel scenario in the evolution of hierarchical triples.

Among the inner binary mergers we find many possible combinations, thus showing that the tertiary, through its secular dynamical influence, introduces many new merger channels previously only considered in the context of isolated binary systems. We expect a relatively large number of MS mergers and destabilizations (the latter of which can indirectly lead to mergers) and these occur relatively early in the evolution. For the resulting merged MS stars to potentially become blue straggler stars (i.e. stars more luminous than stars at the MS turn-off point) the merger/destabilization would have to occur at a later time in the MS evolution. A relatively large number of the mergers systems ($\sim$ 2% of all systems) involve compact objects, thus introducing novel channels for many peculiar types of stars such as early-type R stars (Izzard et al., 2007) and RCrB stars (Tisserand et al., 2009). We have paid special attention to CO WD mergers and CO WD destabilizations because some of such systems are considered as an important candidate progenitor channel for SNe Ia. We have computed the expected rates of SNe Ia due to all plausible triple-induced channels and have compared these to the rates found in a binary population synthesis study and those from observations. We find that the triple-induced rates are approximately one to three orders of magnitude lower than those found in binary population synthesis studies. The triple-induced rates represent a lower limit, however, because the triple sample considered in this work is not complete with respect to m_1 and, more importantly, a_1. For a more complete study also initially closer inner binary systems should be included, from which there is also likely to be a significant contribution to the triple-induced SNe Ia rate. In addition, because the algorithm used in this work faces many uncertainties due to necessary simplifying assumptions in favor of computational speed, more detailed simulations of specific systems are warranted to evaluate its accuracy, in particular of those in which the eccentricity maxima are very high.

Acknowledgements

I would like to thank Onno Pols and Gijs Nelemans for their supervision in this master's project. In addition I would like to thank Joke Claeys for her invaluable help with the `binary_c` code and with the comparison of the triple-induced SNe Ia rates to her binary population synthesis rates. Also I would like to thank Carlo Abate, Alex Chiotellis, Evert Glebbeek, Pim van Oirschot and Silvia Toonen for their useful comments and suggestions during the (bi-)weekly group meetings held in Utrecht and Nijmegen. Lastly I would like to thank Leiden Observatory and in particular Erik Deul for the use of the Jupiter computer cluster, without which a population synthesis study of the present scope would not have been feasible.

Chapter 8

List of acronyms

AGB	–	asymptotic giant branch
CE	–	common-envelope
CHeB	–	core helium-burning
CO	–	carbon-oxygen
DTD	–	delay time distribution
GR	–	general relativity
GWE	–	gravitational wave emission
He	–	helium
HG	–	Hertzsprung gap
KCTF	–	Kozai cycles with tidal friction
MS	–	main sequence
NS	–	neutron star
ONe	–	oxygen-neon
RGB	–	red giant branch
RLOF	–	Roche-lobe overflow
SN(e) Ia	–	supernova(e) type Ia
STD	–	secular triple dynamics
TF	–	tidal friction
TICM	–	triple-induced circular mechanism
TIEM	–	triple-induced eccentric mechanism
TSM	–	triple sampling method
WD	–	white dwarf

Bibliography

Blaes, O., Lee, M.H., Socrates, A. 2002, ApJ, 578, 775

Bondi, H., Hoyle, F. 1944, MNRAS, 104, 273

Campbell, C.G. 1984, MNRAS, 207, 433

Claeys, J. et al., in preparation

Claret, A. 2004, A&A, 424, 919

Cohen, S.D., Hindmarsh, A.C. 1996, Computers in Physics, 10-2, 138

Eggleton, P.P. 2009, MNRAS, 399, 1471

Eggleton, P.P., Kisseleva-Eggleton, L., 2001, AJ, 562, 1012

Eggleton, P.P., Tokovinin, A.A. 2008, MNRAS, 389, 869

Fabrycky, D., Tremaine, S. 2007, ApJ, 669, 1298

Ford, E.B., Kozinsky, B., Rasio, F.A. 2000, ApJ, 535, 385

Gradshteyn, I.S., Ryzhik, I.M. Table of Integrals, Series, and Products, seventh edition. Academic Press, 2007. ISBN 978-0-12-373637-6

Guerrero, J., García-Berro, E., Isern, J. 2004, A&A, 413, 257

Harrington, R. S. 1968, AJ, 73, 190

Hinderer, T. 2008, ApJ, 677, 1216

Huang, S.S. 1956, AJ, 61, 49

Huang, S.S. 1963, AJ, 138, 471

Hurley, J.R. Pols, O.R., Tout, A. 2000, MNRAS, 315, 543

Hurley, J.R., Tout, C.A., Pols, O.R. 2002, MNRAS, 329, 897

Hut, P. 1980, A&A, 92, 167

Hut, P. 1981, A&A, 99, 126

Iben, I.J., Tutukov, A.V. 1984, ApJS, 54, 335

Iben, I.J., Tutukov, A.V. 1999, ApJ, 511, 324

Izzard, R.G., Tout, C.A., Karakas, A.I., Pols, O.R. 2004, MNRAS, 350, 407

Izzard, R.G., Dray, L.M., Karakas, A.I., Lugaro, M., Tout, C.A. 2006, A&A, 460, 565

Izzard, R. G., Jeffery, C. S., Lattanzio, J. 2007, A&A, 470, 661

Izzard, R.G., Glebbeek, E., Stancliffe, R.J., Pols, O.R. 2009, A&A, 508, 1359

Kalirai, J. S., Hansen, B. M. S., Kelson, D. D. et al. 2008, ApJ, 676, 594

Kinoshita, H., Nakai, H. 1999, CeMDA, 75, 125

Kisseleva-Eggleton, L., Eggleton, P.P. 2010, ASP, 435, 169

Kopal, Z. 1946, An introduction to the study of eclipsing stars, Cambridge, Mass., Harvard university press

Kouwenhoven, M.N.B., Brown, A.G.A., Portegies Zwart, S.F., Kaper, L. 2007, A&A, 474, 77

Kozai, Y. 1962, AJ, 67, 591

Kroupa, P., Tout, T.A., Gilmore, G. 1993, MNRAS, 262, 545

Kroupa, P., Burkert, A. 2001, ApJ, 555, 945

Lane, B.F., Muterspaugh, M.W., Fekel, F.C. et al. 2007, ApJ, 669, 1209

Lang K. R. 1992, Astrophysical Data. Springer-Verlag

Lidov, M. L. 1962, Planet. Space Sci., 9, 719

Lithwick, Y. Naoz, S. 2011, ApJ, 742, 94

Maoz, D., Badenes, C. 2010, MNRAS, 407, 1314

Maoz, D., Sharon, K., Gal-Yam, A. 2010, ApJ, 722, 1879

Maoz, D., Mannucci, F. 2012, arXiv:111.4492

Mardling, R.A., Aarseth, S.J. 2001, MNRAS, 321, 398

Mazeh, T., Shaham, J. 1979, A&A, 77, 145

Muterspaugh, M.W., Lane, B.F., Fekel, F.C. 2008, AJ, 135, 766

Naoz, S., Farr, W.M., Lithwick, Y., Rasio, F.A., Teyssandier, J. 2011, arXiv:1107.2414

Nelemans, G., Yungelson, L.R., Portegies Zwart, S.F., Verbunt, F. 2001, A&A, 365, 491

Pakmor, R., Hachinger, S., Röpke, F. K., Hillebrandt, W. 2011, A&A, 528, 117

Perets, H.B., Kratter, K.M. 2012, arXiv:1203.2914

Perlmutter, S. et al. 1999, ApJ, 517, 565

Portegies Zwart, S., McMillan, S., Harfst, S. et al. 2009, New Astronomy, 14, 369

Raghavan, D., McAlister, H.A. et al. 2010, ApJS, 190, 1

Rasio, F. A., Tout, C. A., Lubow, S. H., Livio, M. 1996, ApJ, 470, 1187

Raskin, C., Scannapieco, E., Rockefeller, G., Fryer, C., Diehl, S., Timmes, F. X. 2010, ApJ, 724, 111

Rastegaev, D.A. 2010, AJ, 140, 2013

Remage Evans, N. 2011, arXiv:1102.5316

Riess, A. et al. 1998, AJ, 116, 1009

Rosswog, S., Kasen, D., Guillochon, J., Ramirez-Ruiz, E. 2009, ApJL, 705, 128

Ruiter A.J., Belczynski, K., Fryer, C. 2009, ApJ, 699, 2026

Sepinsky, J.F., Willems, B., Kalogera, V., Rasio, F.A. ApJ, 702, 1387

Shappee, B.J., Thompson, T. A. 2012, arXiv:1204.1053

Smeyers, P., Willems, B. 2001, A&A, 373, 173

Thompson, T.A. 2011, AJ, 741, 82

Tisserand P. et al. 2009, A&A, 501, 985

Tokovinin, A., Thomas, S., Sterzik, M., Udry, S. 2006, A&A, 450, 681

Tokovinin, A. 2008, MNRAS, 389, 925

Totani, T. et al. 2008, PASJ, 60, 1327

Val-Borro, M., Karovska, M., Sasselov, D. 2009, AJ, 700, 1148

Valtonen, M., Karttunen, H. 2006, The Three-Body Problem, ed. Valtonen, M. & Karttunen, H.

Valtonen, M., Mylläri, A., Orlov, V., Rubinov, A. 2008, in IAU Symposium, Vol. 246, IAU Symposium, ed. E. Vesperini, M. Giersz, & A. Sills, 209 - 217

Vila, S.C. 1977, ApJ, 213,464

Wang, B., Han, Z. 2012, arXiv:1204.1155

Webbink, J.R. 1984, ApJ, 277, 355

Winters, J. M., Le Bertre, T., Jeong, K. S. et al. 2003, A&A, 409, 715

Zahn, J.P. 1975, A&A, 41, 329

Zahn, J.P. 1977, A&A, 57, 383

Zahn, J.P. 2005, ASP, 333,4

Zinnecker, H. 2008, Multiple Stars Across the H-R Diagram, ESO Astrophysics Symposia

Internal links (useful in the electronic version):

Appendices

Appendix A

Derivations in the hierarchical three-body problem: further details

A.1 Secular Hamiltonian

A.1.1 Expression for $\cos(\Phi)$

An expression is derived for the angle between the two relative binary vectors $\mathbf{r}_1$ and $\mathbf{r}_2$, Φ, in terms of the Euler angles (g_j, i_j, h_j), the magnitudes r_j and the true anomalies f_j. Let $\mathbf{r}_{\text{inv}}$ denote any vector expressed in the invariant coordinate system (X, Y, Z) and let $\mathbf{r}_{\text{orb}}$ denote this vector expressed in an orbital coordinate system (x, y, z). Starting from the orbital coordinate system (x, y, z), rotate around the z-axis by an angle g. Next, rotate around the X-axis by and angle i. Lastly, rotate around the Z-axis by an angle h. In mathematical terms, this reads:

$$\mathbf{r}_{\text{inv}} = \mathcal{R}_Z(h)\mathcal{R}_X(i)\mathcal{R}_z(g)\,\mathbf{r}_{\text{orb}}, \tag{A.1.1}$$

where $\mathcal{R}_k$ denotes the rotation matrix for rotation around any axis k. In terms of the magnitudes of the relative binary vectors and the true anomalies f_j, $\mathbf{r}_j$ expressed in its corresponding orbital frame, $\mathbf{r}_{\text{orb},j}$, is given by:

$$\mathbf{r}_{\text{orb},j} = r_j \begin{pmatrix} \cos(f_j) \\ \sin(f_j) \\ 0 \end{pmatrix}. \tag{A.1.2}$$

Since the orbital frames (x_1, y_1, z_1) and (x_2, y_2, z_2) do not coincide, $\cos(\Phi)$ is not given by $\hat{\mathbf{r}}_{\text{orb},1} \cdot \hat{\mathbf{r}}_{\text{orb},2}$. Instead, the position vectors $\mathbf{r}_{\text{orb},j}$ first need to be transformed to the common invariant coordinate system, such that $\cos(\Phi) = \hat{\mathbf{r}}_{\text{inv},1} \cdot \hat{\mathbf{r}}_{\text{inv},2}$. With the relevant rotation matrices, this transformation reads:

$$\begin{aligned}
\mathbf{r}_{\text{inv},j} &= r_j \mathcal{R}_Z(h_j)\mathcal{R}_X(i_j) \begin{pmatrix} \cos(g_j) & -\sin(g_j) & 0 \\ \sin(g_j) & \cos(g_j) & 0 \\ 0 & 0 & 1 \end{pmatrix} \begin{pmatrix} \cos(f_j) \\ \sin(f_j) \\ 0 \end{pmatrix} = r_j \mathcal{R}_Z(h_j)\mathcal{R}_X(i_j) \begin{pmatrix} \cos(g_j)\cos(f_j) - \sin(g_j)\sin(f_j) \\ \sin(g_j)\cos(f_j) + \cos(g_j)\sin(f_j) \\ 0 \end{pmatrix} \\
&= r_j \mathcal{R}_Z(h_j) \begin{pmatrix} 1 & 0 & 0 \\ 0 & \cos(i_j) & -\sin(i_j) \\ 0 & \sin(i_j) & \cos(i_j) \end{pmatrix} \begin{pmatrix} \cos(g_j + f_j) \\ \sin(g_j + f_j) \\ 0 \end{pmatrix} = r_j \begin{pmatrix} \cos(h_j) & -\sin(h_j) & 0 \\ \sin(h_j) & \cos(h_j) & 0 \\ 0 & 0 & 1 \end{pmatrix} \begin{pmatrix} \cos(g_j + f_j) \\ \cos(i_j)\sin(g_j + f_j) \\ \sin(i_j)\sin(g_j + f_j) \end{pmatrix} \\
&= r_j \begin{pmatrix} \cos(h_j)\cos(g_j + f_j) - \cos(i_j)\sin(h_j)\sin(g_j + f_j) \\ \sin(h_j)\cos(g_j + f_j) + \cos(i_j)\cos(h_j)\sin(g_j + f_j) \\ \sin(i_j)\sin(g_j + f_j) \end{pmatrix}.
\end{aligned} \tag{A.1.3}$$

Consequently:

$$\begin{aligned}
\cos(\Phi) = \hat{\mathbf{r}}_{\text{inv},1} \cdot \hat{\mathbf{r}}_{\text{inv},2} &= \cos(h_1)\cos(h_2)\cos(g_1 + f_1)\cos(g_2 + f_2) - \cos(h_1)\cos(g_1 + f_1)\cos(i_2)\sin(h_2)\sin(g_2 + f_2) \\
&- \cos(h_2)\cos(g_2 + f_2)\cos(i_1)\sin(h_1)\sin(g_1 + f_1) + \cos(i_1)\cos(i_2)\sin(h_1)\sin(h_2)\sin(g_1 + f_1)\sin(g_2 + f_2) \\
&+ \sin(h_1)\sin(h_2)\cos(g_1 + f_1)\cos(g_2 + f_2) + \sin(h_1)\cos(g_1 + f_1)\cos(i_2)\cos(h_2)\sin(g_2 + f_2) \\
&+ \sin(h_2)\cos(g_2 + f_2)\cos(i_1)\cos(h_1)\sin(g_1 + f_1) + \cos(i_1)\cos(i_2)\cos(h_1)\cos(h_2)\sin(g_1 + f_1)\sin(g_2 + f_2) \\
&+ \sin(i_1)\sin(i_2)\sin(g_1 + f_1)\sin(g_2 + f_2).
\end{aligned} \tag{A.1.4}$$

Regrouping terms and using the trigonometric identities $\cos(\alpha+\beta) = \cos(\alpha)\cos(\beta) - \sin(\alpha)\sin(\beta)$ and $\sin(\alpha+\beta) = \sin(\alpha)\cos(\beta) + \cos(\alpha)\sin(\beta)$ Eq. A.1.4 can be written in a more manageable form:

$$\begin{aligned}
\cos(\Phi) &= \cos(g_2+f_2)\left[\cos(h_1)\cos(h_2)\cos(g_1+f_1) - \cos(h_2)\cos(i_1)\sin(h_1)\sin(g_1+f_1) + \sin(h_1)\sin(h_2)\cos(g_1+f_1)\right.\\
&\quad \left. + \sin(h_2)\cos(i_1)\cos(h_1)\sin(g_1+f_1)\right] + \sin(g_2+f_2)\left[-\cos(h_1)\cos(g_1+f_1)\cos(i_2)\sin(h_2)\right.\\
&\quad + \cos(i_1)\cos(i_2)\sin(h_1)\sin(h_2)\sin(g_1+f_1) + \sin(h_1)\cos(g_1+f_1)\cos(i_2)\cos(h_2)\\
&\quad \left. + \cos(i_1)\cos(i_2)\cos(h_1)\cos(h_2)\sin(g_1+f_1) + \sin(i_1)\sin(i_2)\sin(g_1+f_1)\right]\\
&= \cos(g_2+f_2)\left[\cos(g_1+f_1)\cos(\Delta h) - \cos(i_1)\sin(g_1+f_1)\sin(\Delta h)\right] + \sin(g_2+f_2)\left[\cos(i_2)\cos(g_1+f_1)\sin(\Delta h)\right.\\
&\quad \left. + \sin(g_1+f_1)\left\{\cos(i_1)\cos(i_2)\cos(\Delta h) + \sin(i_1)\sin(i_2)\right\}\right], \qquad \text{(A.1.5)}
\end{aligned}$$

where for convenience $\Delta h \equiv h_1 - h_2$. Note that Eq. A.1.5 is invariant under the substitution of indices $1 \leftrightarrow 2$, as should be the case.

A.1.2 Relation between the longitudes of the ascending nodes

The relation $\Delta h = h_1 - h_2$, which may strictly be substituted only after deriving the equations of motion from the Hamiltonian, is a consequence of the choice of coordinate systems used, which is directly linked to conservation of total angular momentum. To prove the relation it is necessary to find an expression for the angular momentum vector $\mathbf{G}$ in terms of the angles (g, i, h) which specify the orientation of the binary orbit with respect to the invariant coordinate system, which must be done for both the inner and outer binary orbits[1]. For a binary orbit, the kinetic energy T is given by $T = \frac{1}{2}\mu\left(\dot{r}^2 + r^2\dot{f}^2\right)$, where μ is the reduced mass of the binary system and f the true anomaly. The potential energy does not depend on any velocities, therefore the magnitude of the angular momentum G (the conjugate momentum of the true anomaly f) is given by:

$$G = \frac{\partial \mathcal{H}}{\partial \dot{f}} = \frac{\partial T}{\partial \dot{f}} = \mu r^2 \dot{f}. \qquad \text{(A.1.6)}$$

Furthermore, the angular momentum in vector form, $\mathbf{G}$, may be computed from:

$$\mathbf{G} = \mu \mathbf{r} \times \dot{\mathbf{r}}, \qquad \text{(A.1.7)}$$

where $\mathbf{r}$ is to be expressed in the invariant coordinate system, cf. Eq. A.1.3. Since $\mathbf{r} = r\hat{\mathbf{r}}$, Eq. A.1.7 can also be expressed as:

$$\mathbf{G} = \mu \mathbf{r} \times \left(\dot{r}\hat{\mathbf{r}} + r\dot{\hat{\mathbf{r}}}\right) = \mu r^2 \hat{\mathbf{r}} \times \dot{\hat{\mathbf{r}}}. \qquad \text{(A.1.8)}$$

The quantity $\dot{\hat{\mathbf{r}}}$ is derived explicitly in the invariant coordinate system from Eq. A.1.3, using the fact that (at least for one orbital period) the motion remains fixed in the orbital plane such that $\dot{g} = \dot{h} = 0$:

$$\dot{\hat{\mathbf{r}}} = \dot{f}\begin{pmatrix} -\cos(h)\sin(g+f) - \cos(i)\sin(h)\cos(g+f) \\ -\sin(h)\sin(g+f) + \cos(i)\cos(h)\cos(g+f) \\ \sin(i)\cos(g+f). \end{pmatrix} \qquad \text{(A.1.9)}$$

Therefore, in the invariant coordinate system (X, Y, Z):

$$\begin{aligned}
\mathbf{G} &= \mu r^2 \dot{f} \begin{vmatrix} \hat{\mathbf{X}} & \hat{\mathbf{Y}} & \hat{\mathbf{Z}} \\ \cos(h)\cos(g+f) - \cos(i)\sin(h)\sin(g+f) & \sin(h)\cos(g+f) + \cos(i)\cos(h)\sin(g+f) & \sin(i)\sin(g+f) \\ -\cos(h)\sin(g+f) - \cos(i)\sin(h)\cos(g+f) & -\sin(h)\sin(g+f) + \cos(i)\cos(h)\cos(g+f) & \sin(i)\cos(g+f) \end{vmatrix}\\
&= \mu r^2 \dot{f}\left[\hat{\mathbf{X}}\left\{\sin(h)\sin(i)\cos^2(g+f) + \cos(h)\cos(i)\sin(i)\sin(g+f)\cos(g+f) + \sin(h)\sin(i)\sin^2(g+f)\right.\right.\\
&\quad \left. - \cos(h)\cos(i)\sin(i)\sin(g+f)\cos(g+f)\right\} - \hat{\mathbf{Y}}\left\{\cos(h)\sin(i)\cos^2(g+f) - \sin(h)\cos(i)\sin(i)\sin(g+f)\cos(g+f)\right.\\
&\quad \left. + \cos(h)\sin(i)\sin^2(g+f) + \sin(h)\cos(i)\sin(i)\cos(g+f)\sin(g+f)\right\} + \hat{\mathbf{Z}}\left\{-\cos(h)\sin(h)\cos(g+f)\sin(g+f)\right.\\
&\quad + \cos^2(h)\cos(i)\cos^2(g+f) + \sin^2(h)\cos(i)\sin^2(g+f) - \sin(h)\cos(h)\cos^2(i)\sin(g+f)\cos(g+f)\\
&\quad + \cos(h)\sin(h)\cos(g+f)\sin(g+f) + \cos^2(h)\cos(i)\sin^2(g+f) + \sin^2(h)\cos(i)\cos^2(g+f)\\
&\quad \left.\left. + \sin(h)\cos(h)\cos^2(i)\cos(g+f)\sin(g+f)\right\}\right]\\
&= \mu r^2 \dot{f}\left[\sin(i)\sin(h)\,\hat{\mathbf{X}} - \sin(i)\cos(h)\,\hat{\mathbf{Y}} + \cos(i)\,\hat{\mathbf{Z}}\right] = G\left[\sin(i)\sin(h)\,\hat{\mathbf{X}} - \sin(i)\cos(h)\,\hat{\mathbf{Y}} + \cos(i)\,\hat{\mathbf{Z}}\right]. \qquad \text{(A.1.10)}
\end{aligned}$$

[1] In the following, the indices j are suppressed.

Eq. A.1.10 applies to both binary orbits $j = 1$ and $j = 2$ with respect to the invariant coordinate system hence the total angular momentum of the three-body system, $\mathbf{G}_{\rm tot} \equiv \mathbf{G}_1 + \mathbf{G}_2$, is given by:

$$\begin{aligned}\mathbf{G}_{\rm tot} = \hat{\mathbf{X}}\left\{G_1\sin(i_1)\sin(h_1) + G_2\sin(i_2)\sin(h_2)\right\} + \hat{\mathbf{Y}}\left\{-G_1\sin(i_1)\cos(h_1) - G_2\sin(i_2)\cos(h_2)\right\} \\ + \hat{\mathbf{Z}}\left\{G_1\cos(i_1) + G_2\cos(i_2)\right\}.\end{aligned} \tag{A.1.11}$$

By definition the total angular momentum vector must be parallel to the Z-axis of the invariant coordinate system hence the X- and Y-components of $\mathbf{G}_{\rm tot}$ must vanish while the Z-component must be equal to $G_{\rm tot}$:

$$\begin{cases} G_1\sin(i_1)\sin(h_1) &= -G_2\sin(i_2)\sin(h_2); \\ G_1\sin(i_1)\cos(h_1) &= -G_2\sin(i_2)\cos(h_2); \\ G_{\rm tot} &= G_1\cos(i_1) + G_2\cos(i_2). \end{cases} \tag{A.1.12}$$

Division of the first two equations in Eq. A.1.12 then gives $\tan(h_1) = \tan(h_2)$, or $h_1 - h_2 = \pi$. Note that, if no external forces act, this relation must hold at all times because the total angular momentum vector $\mathbf{G}_{\rm tot}$ is conserved.

A.1.3 Averaging procedure

Transformations between mean, true and eccentric anomalies

We briefly state some relations between the mean, eccentric and true anomalies, here denoted by l, E and f respectively, which are required for the explicit integrations below. As can be found in any textbook on celestial mechanics for a binary orbit the distance r between the centre of mass and any point on the relative elliptic orbit is given in terms of the eccentric and true anomalies E and f as:

$$r/a = 1 - e\cos(E) = \frac{1-e^2}{1+e\cos(f)}. \tag{A.1.13}$$

Furthermore, using geometric arguments it may be shown that:

$$\sin(E) = \sqrt{1-e^2}\frac{\sin(f)}{1+e\cos(f)}; \qquad \cos(E) = \frac{\cos(f)+e}{1+e\cos(f)}; \tag{A.1.14}$$

these equations may also written in inverted form as:

$$\sin(f) = \sqrt{1-e^2}\frac{\sin(E)}{1-e\cos(E)}; \qquad \cos(f) = \frac{\cos(E)-e}{1-e\cos(E)}. \tag{A.1.15}$$

Lastly, we use the Kepler equation,

$$l = E - e\sin(E). \tag{A.1.16}$$

From Eq. A.1.16 it immediately follows that:

$$\mathrm{d}l = (1 - e\cos(E))\,\mathrm{d}E = (r/a)\,\mathrm{d}E, \tag{A.1.17}$$

which states the differential transformation between the mean and eccentric anomalies. Furthermore, differentiating both sides of the second equation of Eq. A.1.14, one finds:

$$-\sin(E)\,\mathrm{d}E = \frac{-\sin(f)(1+e\cos(f)) + e\sin(f)(\cos(f)+e)}{(1+e\cos(f))^2}\,\mathrm{d}f = -\sin(f)\frac{1-e^2}{(1+e\cos(f))^2}\,\mathrm{d}f,$$

which gives, after writing $\sin(E)$ in terms of f with the first equation of Eq. A.1.14:

$$-\sqrt{1-e^2}\frac{\sin(f)}{1+e\cos(f)}\,\mathrm{d}E = -\sin(f)\frac{1-e^2}{(1+e\cos(f))^2}\,\mathrm{d}f \Rightarrow \mathrm{d}E = \frac{\sqrt{1-e^2}}{1+e\cos(f)}\,\mathrm{d}f = \frac{1}{\sqrt{1-e^2}}\frac{r}{a}\,\mathrm{d}f. \tag{A.1.18}$$

Lastly, combining Eqs. A.1.17 and A.1.18, one finds:

$$\mathrm{d}l = \frac{1}{\sqrt{1-e^2}}\left(\frac{r}{a}\right)^2 \mathrm{d}f, \tag{A.1.19}$$

which states the differential transformation between the mean and true anomalies.

Quadrupole order

The quadrupole order term R_{quad}, Eq. 2.23, is first averaged over the outer orbital period for which it is convenient to integrate over the true anomaly:

$$\begin{aligned}\langle R_{\mathrm{quad}}\rangle_2 &= \frac{1}{2\pi}\int_0^{2\pi} R_{\mathrm{quad}}\,\mathrm{d}l_2 = 16\,C_{\mathrm{quad}}\left(1-e_2^2\right)^{3/2}\left(\frac{r_1}{a_1}\right)^2\frac{1}{2\pi}\int_0^{2\pi}\left(\frac{a_2}{r_2}\right)^3 \underbrace{\frac{1}{2}\left(3\cos^2(\Phi)-1\right)}_{=\widetilde{P}_2(\cos(\Phi))}\underbrace{\left(\frac{r_2}{a_2}\right)^2\frac{1}{\sqrt{1-e_2^2}}\,\mathrm{d}f_2}_{=\mathrm{d}l_2}\\
&= 8\,C_{\mathrm{quad}}\left(1-e_2^2\right)^{3/2}\left(\frac{r_1}{a_1}\right)^2\frac{1}{2\pi}\int_0^{2\pi}\frac{1+e_2\cos(f_2)}{1-e_2^2}\frac{1}{\sqrt{1-e_2^2}}\left(3\cos^2(\Phi)-1\right)\mathrm{d}f_2\\
&= 8\,C_{\mathrm{quad}}\left(\frac{r_1}{a_1}\right)^2\frac{1}{2\pi}\int_0^{2\pi}\left[1+e_2\cos(f_2)\right]\left[3\cos^2(\Phi)-1\right]\mathrm{d}f_2.\end{aligned} \tag{A.1.20}$$

With some trigonometric identities, $\cos(\Phi)$, Eq. A.1.5, is expressed in terms of $\cos(f_2)$ and $\sin(f_2)$ as:

$$\cos(\Phi) = \tilde{A}_a\cos(f_2) + \tilde{A}_b\sin(f_2); \quad \begin{cases}\tilde{A}_a &= Z_a\cos(f_1) + Z_b\sin(f_1);\\ \tilde{A}_b &= Z_c\cos(f_1) + Z_d\sin(f_1),\end{cases} \tag{A.1.21}$$

where Z_a, Z_b, Z_c and Z_d are defined in Eq. 2.29. Therefore:

$$\begin{aligned}\langle R_{\mathrm{quad}}\rangle_2 &= 8\,C_{\mathrm{quad}}\left(\frac{r_1}{a_1}\right)^2\frac{1}{2\pi}\int_0^{2\pi}\left[1+e_2\cos(f_2)\right]\left[3\tilde{A}_a^2\cos^2(f_2)+6\tilde{A}_a\tilde{A}_b\cos(f_2)\sin(f_2)+3\tilde{A}_b^2\sin^2(f_2)-1\right]\mathrm{d}f_2\\
&= 8\,C_{\mathrm{quad}}\left(\frac{r_1}{a_1}\right)^2\left[\frac{3}{2}\tilde{A}_a^2+\frac{3}{2}\tilde{A}_b^2-1\right].\end{aligned} \tag{A.1.22}$$

For the integration over the inner orbit it is convenient to transform to the eccentric anomaly (cf. Eqs. A.1.15 and A.1.17):

$$\begin{aligned}\langle\langle R_{\mathrm{quad}}\rangle_2\rangle_1 &= \frac{1}{2\pi}\int_0^{2\pi}\langle R_{\mathrm{quad}}\rangle_2\,\mathrm{d}l_1 = 8\,C_{\mathrm{quad}}\frac{1}{2\pi}\int_0^{2\pi}\left(\frac{r_1}{a_1}\right)^2\left[\frac{3}{2}\left(Z_a^2+Z_c^2\right)\cos^2(f_1)+3(Z_aZ_b+Z_cZ_d)\cos(f_1)\sin(f_1)\right.\\
&\left.+\frac{3}{2}\left(Z_b^2+Z_d^2\right)\sin^2(f_1)-1\right]\underbrace{\left(\frac{r_1}{a_1}\right)\mathrm{d}E_1}_{=\mathrm{d}l_1} = 8\,C_{\mathrm{quad}}\frac{1}{2\pi}\int_0^{2\pi}\left[1-e_1\cos(E_1)\right]^3\left[\frac{3}{2}\left(Z_a^2+Z_c^2\right)\left(\frac{\cos(E_1)-e_1}{1-e_1\cos(E_1)}\right)^2\right.\\
&\left.+3(Z_aZ_b+Z_cZ_d)\frac{\sqrt{1-e_1^2}\sin(E_1)(\cos(E_1)-e_1)}{(1-e_1\cos(E_1))^2}+\frac{3}{2}\left(Z_b^2+Z_d^2\right)\left(\frac{\sqrt{1-e_1^2}\sin(E_1)}{1-e_1\cos(E_1)}\right)^2-1\right]\mathrm{d}E_1\\
&= 8\,C_{\mathrm{quad}}\frac{1}{2\pi}\int_0^{2\pi}\left[1-e_1\cos(E_1)\right]\left[\frac{3}{2}\left(Z_a^2+Z_c^2\right)(\cos(E_1)-e_1)^2+3(Z_aZ_b+Z_cZ_d)\sqrt{1-e_1^2}\sin(E_1)(\cos(E_1)-e_1)\right.\\
&\left.+\frac{3}{2}\left(Z_b^2+Z_d^2\right)\left(1-e_1^2\right)\sin^2(E_1)-(1-e_1\cos(E_1))^2\right]\mathrm{d}E_1 = 8\,C_{\mathrm{quad}}\left[\frac{3}{2}\left(Z_a^2+Z_c^2\right)\frac{1}{2}\left(1+4e_1^2\right)\right.\\
&\left.+\frac{3}{2}\left(Z_b^2+Z_d^2\right)\left(1-e_1^2\right)\cdot\frac{1}{2}-\frac{1}{2}\left(2+3e_1^2\right)\right]\\
&= \boxed{C_{\mathrm{quad}}\left[6\left(Z_a^2+Z_c^2\right)\left(1+4e_1^2\right)+6\left(Z_b^2+Z_d^2\right)\left(1-e_1^2\right)-4\left(2+3e_1^2\right)\right]}.\end{aligned} \tag{A.1.23}$$

Eq. A.1.23 is simplified substantially if $\Delta h = \pi$ is substituted. With $\Delta h = \pi$, Eq. 2.29 gives $D_a = -1$, $D_b = D_c = 0$ and $D_d = -\cos(i_{\rm tot})$, where $i_{\rm tot} \equiv i_1 + i_2$ is the mutual inclination between the inner and outer binary orbits. Therefore:

$$\begin{aligned}\left(Z_a^2 + Z_c^2\right)\Big|_{\Delta h=\pi} &= \cos^2(g_1) + \cos^2(i_{\rm tot})\sin^2(g_1) = \frac{1}{2}\left(1+\cos(2g_1)\right) + \frac{1}{2}\cos^2(i_{\rm tot})\left(1-\cos(2g_1)\right); \\ \left(Z_b^2 + Z_d^2\right)\Big|_{\Delta h=\pi} &= \sin^2(g_1) + \cos^2(i_{\rm tot})\cos^2(g_1) = \frac{1}{2}\left(1-\cos(2g_1)\right) + \frac{1}{2}\cos^2(i_{\rm tot})\left(1+\cos(2g_1)\right)\end{aligned} \tag{A.1.24}$$

and:

$$\begin{aligned}\langle\langle R_{\rm quad}\rangle_2\rangle_1\big|_{\Delta h=\pi} &= C_{\rm quad}\Big[\Big\{\left(3(1+\cos(2g_1)) + 3\cos^2(i_{\rm tot})(1-\cos(2g_1))\right)\Big\}\left\{1+4e_1^2\right\} + \{3(1-\cos(2g_1)) \\ &\quad +3\cos^2(i_{\rm tot})(1+\cos(2g_1))\Big\}\left\{1-e_1^2\right\} - 4\left(2+3e_1^2\right)\Big] = C_{\rm quad}\Big[3 + 3\cos(2g_1) + 3\cos^2(i_{\rm tot}) \\ &\quad -3\cos^2(i_{\rm tot})\cos(2g_1) + 12e_1^2 + 12e_1^2\cos(2g_1) + 12e_1^2\cos^2(i_{\rm tot}) - 12e_1^2\cos^2(i_{\rm tot})\cos(2g_1) + 3 \\ &\quad -3\cos(2g_1) + 3\cos^2(i_{\rm tot}) + 3\cos^2(i_{\rm tot})\cos(2g_1) - 3e_1^2 + 3e_1^2\cos(2g_1) - 3e_1^2\cos^2(i_{\rm tot}) \\ &\quad -3e_1^2\cos^2(i_{\rm tot})\cos(2g_1) - 8 - 12e_1^2\Big] = C_{\rm quad}\Big[-2 + 6\cos^2(i_{\rm tot}) - 3e_1^2 + 15e_1^2\cos(2g_1) \\ &\quad -15e_1^2\cos^2(i_{\rm tot})\cos(2g_1) + 9e_1^2\cos^2(i_{\rm tot})\Big] \\ &= \boxed{C_{\rm quad}\Big[\left(2+3e_1^2\right)\left(3\cos^2(i_{\rm tot})-1\right) + 15e_1^2\sin^2(i_{\rm tot})\cos(2g_1)\Big]}.\end{aligned} \tag{A.1.25}$$

Octupole order

The octupole order perturbing term $R_{\rm oct}$, Eq. 2.25, is first averaged over the outer orbit employing the true anomaly:

$$\begin{aligned}\langle R_{\rm oct}\rangle_2 &= -\frac{1}{2\pi}\int_0^{2\pi} R_{\rm oct}\,{\rm d}l_2 = -\frac{32}{15}2\,C_{\rm oct}\left(1-e_2^2\right)^{5/2}\left(\frac{r_1}{a_1}\right)^3\frac{1}{2\pi}\int_0^{2\pi}\left(\frac{a_2}{r_2}\right)^4 \underbrace{\frac{1}{2}\left(5\cos^3(\Phi)-3\cos(\Phi)\right)}_{=\widetilde{P}_3(\cos(\Phi))}\underbrace{\left(\frac{r_2}{a_2}\right)^2\frac{1}{\sqrt{1-e_2^2}}\,{\rm d}f_2}_{={\rm d}l_2} \\ &= -\frac{32}{15}C_{\rm oct}\left(1-e_2^2\right)^{5/2}\left(\frac{r_1}{a_1}\right)^3\frac{1}{2\pi}\int_0^{2\pi}\left(\frac{1+e_2\cos(f_2)}{1-e_2^2}\right)^2\frac{1}{\sqrt{1-e_2^2}}\left(5\cos^3(\Phi)-3\cos(\Phi)\right){\rm d}f_2 \\ &= \frac{32}{15}C_{\rm oct}\left(\frac{r_1}{a_1}\right)^3\frac{1}{2\pi}\int_0^{2\pi}\left[1+e_2\cos(f_2)\right]^2\left[5\cos^3(\Phi)-\cos(\Phi)\right){\rm d}f_2.\end{aligned} \tag{A.1.26}$$

Employing Eq. A.1.21 and using that $(a+b)^3 = a^3 + 3a^2b + 3ab^2 + b^3$ one finds:

$$\begin{aligned}\langle R_{\rm oct}\rangle_2 &= -\frac{32}{15}C_{\rm oct}\left(\frac{r_1}{a_1}\right)^3\frac{1}{2\pi}\int_0^{2\pi}\left[1+e_2\cos(f_2)\right]^2\Big[5\tilde{A}_a^3\cos^3(f_2) + 15\tilde{A}_a^2\tilde{A}_b\cos^3(f_2)\sin(f_2) + 15\tilde{A}_a\tilde{A}_b^2\cos(f_2)\sin^2(f_2) \\ &\quad +5\tilde{A}_b^3\sin^3(f_2) - 3\tilde{A}_a\cos(f_2) - 3\tilde{A}_b\sin(f_2)\Big]\,{\rm d}f_2 = -\frac{32}{15}C_{\rm oct}\left(\frac{r_1}{a_1}\right)^3\left[\frac{3}{4}e_2\cdot 5\tilde{A}_a^3 + \frac{1}{4}e_2\cdot 15\tilde{A}_a\tilde{A}_b^2 - 3e_2\tilde{A}_a\right] \\ &= -8\,C_{\rm oct}e_2\left(\frac{r_1}{a_1}\right)^3\left[\tilde{A}_a^3 + \tilde{A}_a\tilde{A}_b^2 - \frac{4}{5}\tilde{A}_a\right].\end{aligned} \tag{A.1.27}$$

The integration over the inner orbit is performed with the eccentric anomaly:

$$\langle\langle R_{\rm oct}\rangle_2\rangle_1 = \frac{1}{2\pi}\int_0^{2\pi}\langle R_{\rm oct}\rangle_2\,{\rm d}l_1 = -8\,C_{\rm oct}e_2\frac{1}{2\pi}\int_0^{2\pi}\left(\frac{r_1}{a_1}\right)^3\left[\tilde{A}_a^3 + \tilde{A}_a\tilde{A}_b^2 - \frac{4}{5}\tilde{A}_a\right]\underbrace{\left(\frac{r_1}{a_1}\right){\rm d}E_1}_{={\rm d}l_1}. \tag{A.1.28}$$

Since all terms in $\tilde{A}_a^3$ and $\tilde{A}_a\tilde{A}_b^2$ involve products of $\cos(f_1)$ and $\sin(f_1)$ to third order (cf. Eq. A.1.21) these terms all contain a denominator which is third order in $1 - e_1\cos(E_1)$ (cf. A.1.15), i.e. $\tilde{A}_a^3 \propto 1/(1-e_1\cos(E_1))^3$ and $\tilde{A}_a\tilde{A}_b^2 \propto 1/(1-e_1\cos(E_1))^3$. Similarly, $\tilde{A}_a \propto 1/(1-e_1\cos(E_1))$. The required integrals for the proceeding calculation are therefore:

$$\frac{1}{2\pi}\int_0^{2\pi}(1-e_1\cos(E_1))\cdot\begin{cases}(\cos(E_1)-e_1)^3\ \mathrm{d}E_1 & =-\frac{5}{8}e_1\left(3+4e_1^2\right);\\ \sin^3(E_1)\,\mathrm{d}E_1 & =0;\\ (\cos(E_1)-e_1)^2\sin(E_1)\,\mathrm{d}E_1 & =0;\\ (\cos(E_1)-e_1)\sin^2(E_1)\,\mathrm{d}E_1 & =-\frac{5}{8}e_1;\end{cases}$$
$$\frac{1}{2\pi}\int_0^{2\pi}(1-e_1\cos(E_1))^3\cdot\begin{cases}(\cos(E_1)-e_1)\ \mathrm{d}E_1 & =-\frac{5}{8}e_1\left(3e_1^2+4\right);\\ \sin(E_1)\,\mathrm{d}E_1 & =0,\end{cases}$$

such that only terms proportional to $\cos^3(f_1)$, $\cos(f_1)\sin^2(f_1)$ and $\cos(f_1)$ in Eq. A.1.28 remain after averaging over the inner orbit. With Eq. A.1.21 the relevant terms are:

$$\begin{aligned}\tilde{A}_a^3 &= Z_a^3\cos^3(f_1)+3Z_aZ_b^2\cos(f_1)\sin^2(f_1)+...;\\ \tilde{A}_a\tilde{A}_b^2 &= [Z_a\cos(f_1)+Z_b\sin(f_1)]\left[Z_c^2\cos^2(f_1)+2Z_cZ_d\cos(f_1)\sin(f_1)+Z_d^2\sin^2(f_1)\right]\\ &= Z_aZ_c^2\cos^3(f_1)+\left(Z_aZ_d^2+2Z_bZ_cZ_d\right)\cos(f_1)\sin^2(f_1)+...,\end{aligned}\tag{A.1.29}$$

where the dots denote terms which vanish after integration. Hence:

$$\begin{aligned}\langle\langle R_{\rm oct}\rangle_2\rangle_1 &= -8\,C_{\rm oct}e_2\frac{1}{2\pi}\int_0^{2\pi}\Big\{[1-e_1\cos(E_1)]\left[(\cos(E_1)-e_1)^3\left(Z_a^3+Z_aZ_c^2\right)+\left(1-e_1^2\right)\sin^2(E_1)\,(\cos(E_1)-e_1)\left(3Z_aZ_b^2\right.\right.\\ &\quad\left.\left.+Z_aZ_d^2+2Z_bZ_cZ_d\right)\right]+[1-e_1\cos(E_1)]^3\left[-\frac{4}{5}Z_a\,(\cos(E_1)-e_1)\right]\Big\}\,\mathrm{d}E_1\\ &= -8\,C_{\rm oct}e_2\left[-\frac{5}{8}e_1\left(3+4e_1^2\right)Z_a\left(Z_a^2+Z_c^2\right)-\frac{5}{8}e_1\left(1-e_1^2\right)\left(3Z_aZ_b+Z_aZ_d^2+2Z_bZ_cZ_d\right)+\frac{4}{5}\frac{5}{8}e_1\left(3e_1^2+4\right)Z_a\right]\\ &= \boxed{C_{\rm oct}e_1e_2\left[Z_a\left\{5\left(3+4e_1^2\right)\left(Z_a^2+Z_c^2\right)-4\left(3e_1^2+4\right)\right\}+5\left(1-e_1^2\right)\left(3Z_aZ_b^2+Z_aZ_d^2+2Z_bZ_cZ_d\right)\right]}.\end{aligned}\tag{A.1.30}$$

With the substitution $\Delta h=\pi$, it can be shown[2] that Eq. A.1.30 is equivalent to Eq. 2.32.

A.1.4 Equations of motion

In this section equations for $\dot{g}_j$ and $\dot{e}_j$ are derived to quadrupole and octupole order. For the secular evolution equations for $\dot{g}_j$ and $\dot{e}_j$ derivatives of the secularly averaged perturbing term $\langle\langle R\rangle_2\rangle_1$ with respect to e_j, i_j and g_j are required. These derivatives commute with the substitution $\Delta h=\pi$, i.e. :

$$\left.\frac{\partial\langle\langle R\rangle_2\rangle_1}{\partial x}\right|_{\Delta h=\pi}=\frac{\partial\left(\langle_2\langle_1 R\rangle\rangle|_{\Delta h=\pi}\right)}{\partial x},\tag{A.1.31}$$

where $x\in\{e_j,i_j,g_j\}$ (see also Naoz et al. 2011). Thus it is sufficient to use Eqs. 2.31 and 2.32 instead of Eqs. 2.27 and 2.28. In the quadrupole order, not much complexity is introduced when using the left-hand side of Eq. A.1.31, however, and so this method is employed below for this order. This is different for the octupole order where the substitution into the perturbing term introduces a substantial simplification, hence the right-hand side of Eq. A.1.31 is employed below for this order.

Furthermore, to perform the differentiations with respect to G_j it is necessary to remark that the quantities $C_{\rm quad}$ and $C_{\rm oct}$ depend on G_2 through their dependence on e_2. These quantities are expressed in terms of L_j and G_j with Eq. 2.34 as follows:

$$C_{\rm quad}=\frac{G_N^2}{16}\frac{(m_1+m_2)^7}{(m_1+m_2+m_3)^3}\frac{m_3^7}{(m_1m_2)^3}\frac{L_1^4}{L_2^3G_2^3};\tag{A.1.32}$$

$$C_{\rm oct}=-\frac{15}{16}\frac{G_N^2}{4}\frac{m_1+m_2)^9}{(m_1+m_2+m_3)^4}\frac{m_3^8(m_1-m_2)}{(m_1m_2)^5}\frac{L_1^6}{L_2^3G_2^5}.\tag{A.1.33}$$

Note that differential equations for $\dot{h}_j$ also exist and can be derived straightforwardly. The secular equations for $\dot{g}_j$ and $\dot{e}_j$ are independent of h_j, however, therefore it is not necessary to include equations for $\dot{h}_j$ when solving the secular three-body dynamics equations. Hence the equations for $\dot{h}_j$ are not included here; refer to Naoz et al. (2011) for explicit expressions for $\dot{h}_j$ up to and including octupole order.

[2]This should be possible using appropriate trigonometric identities; in the present work we have checked this statement by means of direct substitution of various values of g_1, g_2, e_1 and $i_{\rm tot}$ into both expressions and in this manner find that they are equivalent.

Quadrupole order

From Eqs. 2.24 and 2.27 it follows that $\langle\langle R_{\rm quad}\rangle_2\rangle_1$ depends on e_1, e_2, g_1, i_1, i_2 and Δh. There is no dependence on g_2, which implies that $G_2 = L_2\sqrt{1-e_2^2}$ is constant, hence e_2 is constant as well. Furthermore, note that i_1 and i_2 depend on G_1 and G_2 through Eq. 2.36 and that e_1 is a function of G_1. Therefore, by the chain rule for differentiation:

$$\dot{g}_{1,\rm quad} = -\left.\frac{\partial\langle\langle R_{\rm quad}\rangle_2\rangle_1}{\partial G_1}\right|_{\Delta h=\pi} = -\left.\frac{\partial\langle\langle R_{\rm quad}\rangle_2\rangle_1}{\partial e_1}\frac{\partial e_1}{G_1}\right|_{\Delta h=\pi} - \left.\frac{\partial\langle\langle R_{\rm quad}\rangle_2\rangle_1}{\partial i_1}\frac{\partial i_1}{\partial G_1}\right|_{\Delta h=\pi} \tag{A.1.34}$$

(note that when differentiating with respect to G_1, G_2 and H_2 must remain constant such that i_2 must remain constant as well; therefore $\partial i_2/\partial G_1 = 0$). From Eq. 2.34, it follows that:

$$\frac{\partial e_1}{\partial G_1} = \frac{\partial}{\partial G_1}\left(\sqrt{1-\left(\frac{G_1}{L_1}\right)^2}\right) = \frac{-1}{\sqrt{1-(G_1/L_1)^2}}\frac{G_1}{L_1^2} = \frac{-1}{e_1}\frac{G_1}{G_1^2}(1-e_1^2) = -\frac{1-e_1^2}{e_1 G_1}. \tag{A.1.35}$$

From Eq. 2.27:

$$\frac{\partial\langle\langle R_{\rm quad}\rangle_2\rangle_1}{\partial e_1} = C_{\rm quad}\left[6\cdot 8\left(Z_a^2+Z_c^2\right)e_1 - 6\cdot 2\left(Z_b^2+Z_d^2\right)e_1 - 4\cdot 6e_1\right] = 12C_{\rm quad}e_1\left[4\left(Z_a^2+Z_c^2\right) - \left(Z_b^2+Z_d^2\right) - 2\right].$$

Therefore, with Eq. A.1.24:

$$\begin{aligned}\left.\frac{\partial\langle\langle R_{\rm quad}\rangle_2\rangle_1}{\partial e_1}\right|_{\Delta h=\pi} &= 12\,C_{\rm quad}e_1\left[2(1+\cos(2g_1)) + 2(1-\cos(2g_1))\cos^2(i_{\rm tot}) - \frac{1}{2}(1-\cos(2g_1)) - \frac{1}{2}(1+\cos(2g_1))\right.\\ &\left.\times\cos^2(i_{\rm tot}) - 2\right] = 12\,C_{\rm quad}e_1\left[2 + 2\cos(2g_1) + 2\cos^2(i_{\rm tot}) - 2\cos(2g_1)\cos^2(i_{\rm tot}) - \frac{1}{2}\right.\\ &\left.+\frac{1}{2}\cos(2g_1) - \frac{1}{2}\cos^2(i_{\rm tot}) - \frac{1}{2}\cos(2g_1)\cos^2(i_{\rm tot}) - 2\right]\\ &= 6\,C_{\rm quad}e_1\left[5\cos(2g_1) + 3\cos^2(i_{\rm tot}) - 5\cos(2g_1)\cos^2(i_{\rm tot}) - 1\right].\end{aligned} \tag{A.1.36}$$

From the definitions in Eq. 2.29 and Eq. 2.30, it follows that:

$$\begin{aligned}\frac{\partial\left(Z_a^2+Z_c^2\right)}{\partial i_1} &= 2\left(D_a\cos(g_1) - D_b\sin(g_1)\right)\left(\frac{\partial D_a}{\partial i_1}\cos(g_1) - \frac{\partial D_b}{\partial i_1}\sin(g_1)\right) + 2\left(D_c\cos(g_1) + D_d\sin(g_1)\right)\\ &\times\left(\frac{\partial D_c}{\partial i_1}\cos(g_1) + \frac{\partial D_d}{\partial i_1}\sin(g_1)\right) = 2\left(\cos(\Delta h)\cos(g_1) - \cos(i_1)\sin(\Delta h)\sin(g_1)\right)\\ &\times\sin(i_1)\sin(\Delta h)\sin(g_1) + 2\left\{\cos(i_2)\sin(\Delta h)\cos(g_1) + \sin(g_1)\left[\cos(i_1)\cos(i_2)\cos(\Delta h)\right.\right.\\ &\left.\left.+\sin(i_1)\sin(i_2)\right]\right\}\sin(g_1)\left(-\sin(i_1)\cos(i_2)\cos(\Delta h) + \cos(i_1)\sin(i_2)\right) \Rightarrow\\ \left.\frac{\partial\left(Z_a^2+Z_c^2\right)}{\partial i_1}\right|_{\Delta h=\pi} &= 2\sin(g_1)\left(-\cos(i_1)\cos(i_2) + \sin(i_1)\sin(i_2)\right)\sin(g_1)\left(\sin(i_1)\cos(i_2) + \cos(i_1)\sin(i_2)\right)\\ &= -2\sin^2(g_1)\cos(i_{\rm tot})\sin(i_{\rm tot}).\end{aligned}$$

Similarly, it may be shown that:

$$\left.\frac{\partial\left(Z_b^2+Z_d^2\right)}{\partial i_1}\right|_{\Delta h=\pi} = -2\cos^2(g_1)\cos(i_{\rm tot})\sin(i_{\rm tot}).$$

With these results it follows from Eq. 2.27 that:

$$\begin{aligned}\left.\frac{\partial\langle\langle R_{\rm quad}\rangle_2\rangle_1}{\partial i_1}\right|_{\Delta h=\pi} &= 6\,C_{\rm quad}\left[-2\sin^2(g_1)\cos(i_{\rm tot})\sin(i_{\rm tot})\left(1+4e_1^2\right)-2\cos^2(g_1)\cos(i_{\rm tot})\sin(i_{\rm tot})\left(1-e_1^2\right)\right]\\ &= 6\,C_{\rm quad}\cos(i_{\rm tot})\sin(i_{\rm tot})\left[-2-8e_1^2\sin^2(g_1)+2e_1^2\cos^2(g_1)\right]\\ &= 6\,C_{\rm quad}\cos(i_{\rm tot})\sin(\rm tot)\left[-2-4e_1^2+4e_1^2\cos(2g_1)+e_1^2+e_1^2\cos(2g_1)\right]\\ &= -6\,C_{\rm quad}\cos(i_{\rm tot})\sin(i_{\rm tot})\left[2+e_1^2(3-5\cos(2g_1))\right]. \end{aligned} \tag{A.1.37}$$

Furthermore, differentiating $G_{\rm tot}^2 = G_1^2 + G_2^2 + 2G_1G_2\cos(i_{\rm tot})$ with G_2 and i_2 (and $G_{\rm tot}$) constant gives:

$$\begin{aligned}0 &= 2G_1\,{\rm d}G_1 + 2G_2\cos(i_{\rm tot})\,{\rm d}G_1 - 2G_1G_2\sin(i_{\rm tot})\,{\rm d}i_1 = 2(G_1+G_2\cos(i_{\rm tot}))\,{\rm d}G_1 - 2G_1G_2\sin(i_{\rm tot})\,{\rm d}i_1\\ \Rightarrow \frac{\partial i_1}{\partial G_1} &= \frac{1}{\sin(i_{\rm tot})}\left[\frac{\cos(i_{\rm tot})}{G_1}+\frac{1}{G_2}\right]. \end{aligned} \tag{A.1.38}$$

Combining Eqs. A.1.34, A.1.35, A.1.36, A.1.37 and A.1.38 yields:

$$\begin{aligned}\dot g_{1,\rm quad} &= \frac{1-e_1^2}{e_1G_1}\,6\,C_{\rm quad}\,e_1\left[5\cos(2g_1)+3\cos^2(i_{\rm tot})-5\cos(2g_1)\cos^2(i_{\rm tot})-1\right]\\ &\quad+\frac{6\,C_{\rm quad}}{\sin(i_{\rm tot})}\left[\frac{\cos(i_{\rm tot})}{G_1}+\frac{1}{G_2}\right]\cos(i_{\rm tot})\sin(i_{\rm tot})\left[2+e_1^2(3-5\cos(2g_1))\right]\\ &= 6\,C_{\rm quad}\left\{\frac{1}{G_1}\left[5\cos(2g_1)+3\cos^2(i_{\rm tot})-5\cos(2g_1)\cos^2(i_{\rm tot})-1-5e_1^2\cos(2g_1)-3e_1^2\cos^2(i_{\rm tot})\right.\right.\\ &\quad\left.+5e_1^2\cos(2g_1)\cos^2(i_{\rm tot})+e_1^2+2\cos^2(i_{\rm tot})+3e_1^2\cos^2(i_{\rm tot})-5e_1^2\cos^2(i_{\rm tot})\cos(2g_1)\right]\\ &\quad\left.+\frac{\cos(i_{\rm tot})}{G_2}\left[2+e_1^2(3-5\cos(2g_1))\right]\right\}\\ &= \boxed{6\,C_{\rm quad}\left\{\frac{1}{G_1}\left[4\cos^2(i_{\rm tot})+(5\cos(2g_1)-1)\left(1-e_1^2-\cos^2(i_{\rm tot})\right)\right]+\frac{\cos(i_{\rm tot})}{G_2}\left[2+e_1^2(3-5\cos(2g_1))\right]\right\}}. \end{aligned} \tag{A.1.39}$$

To compute $\dot g_{2,\rm quad}$ note that $\langle\langle R_{\rm quad}\rangle_2\rangle_1$ has the form $\langle\langle R_{\rm quad}\rangle_2\rangle_1 = C_{\rm quad}(G_2)\cdot f_{\rm quad}(i_2(G_2))$, where the function $f_{\rm quad}$ is defined by Eq. 2.27, i.e. $f_{\rm quad} = 6\left(Z_a^2+Z_c^2\right)\left(1+4e_1^2\right)+6\left(Z_b^2+Z_d^2\right)\left(1-e_1^2\right)-4\left(2+3e_1^2\right)$. Therefore:

$$\dot g_{2,\rm quad} = -\left.\frac{\partial\langle\langle R_{\rm quad}\rangle_2\rangle_1}{\partial G_2}\right|_{\Delta h=\pi} = -\left.\frac{\partial C_{\rm quad}}{\partial G_2}f_{\rm quad}\right|_{\Delta h=\pi} - C_{\rm quad}\left.\frac{\partial f}{\partial i_2}\frac{\partial i_2}{\partial G_2}\right|_{\Delta h=\pi}. \tag{A.1.40}$$

From Eq. A.1.32 it follows that $\partial C_{\rm quad}/\partial G_2 = -3\,C_{\rm quad}/G_2$. Furthermore, with similar calculations as above the following relations follow from Eq. 2.30:

$$\left.\frac{\partial\left(Z_a^2+Z_c^2\right)}{\partial i_2}\right|_{\Delta h=\pi} = -2\sin^2(g_1)\cos(i_{\rm tot})\sin(i_{\rm tot});\qquad \left.\frac{\partial\left(Z_b^2+Z_d^2\right)}{\partial i_2}\right|_{\Delta h=\pi} = -2\cos^2(g_1)\cos(i_{\rm tot})\sin(i_{\rm tot}),$$

from which it follows that (analogously to the derivation in Eq. A.1.37):

$$\begin{aligned}\left.\frac{\partial f_{\rm quad}}{\partial i_2}\right|_{\Delta h=\pi} &= 6\left.\frac{\partial\left(Z_a^2+Z_c^2\right)}{\partial i_2}\right|_{\Delta h=\pi}\cdot\left(1+4e_1^2\right)+6\left.\frac{\partial\left(Z_b^2+Z_d^2\right)}{\partial i_2}\right|_{\Delta h=\pi}\cdot\left(1-e_1^2\right)\\ &= -6\cos(i_{\rm tot}\sin(i_{\rm tot})\left[2+e_1^2(3-5\cos(2g_1))\right]. \end{aligned} \tag{A.1.41}$$

Similarly to Eq. A.1.38, but now with G_2 and i_2 varying and G_1 and i_1 (and $G_{\rm tot}$) constant one finds:

$$\frac{\partial i_2}{\partial G_2} = \frac{1}{\sin(i_{\rm tot})}\left[\frac{\cos(i_{\rm tot})}{G_2}+\frac{1}{G_1}\right]. \tag{A.1.42}$$

Combining Eqs. A.1.40, A.1.41 and A.1.42 and using Eq. A.1.25 for $f_{\rm quad}\big|_{\Delta h=\pi}$ gives:

$$\begin{aligned}
\dot{g}_2 &= \frac{3\,C_{\rm quad}}{G_2}\left[\left(2+3e_1^2\right)\left(3\cos^2(i_{\rm tot})-1\right)+15e_1^2\left(1-\cos^2(i_{\rm tot})\right)\cos(2g_1)\right] \\
&\quad+\frac{6\,C_{\rm quad}}{\sin(i_{\rm tot})}\left[\frac{\cos(i_{\rm tot})}{G_2}+\frac{1}{G_1}\right]\sin(i_{\rm tot})\cos(i_{\rm tot})\left[2+e_1^2(3-5\cos(2g_1))\right] \\
&= \frac{6\,C_{\rm quad}}{G_1}\cos(i_{\rm tot})\left[2+e_1^2(3-5\cos(2g_1))\right]+\frac{3\,C_{\rm quad}}{G_2}\left[6\cos^2(i_{\rm tot})-2+9e_1^2\cos^2(i_{\rm tot})-3e_1^2+15e_1^2\cos(2g_1)\right. \\
&\quad\left.-15e_1^2\cos^2(i_{\rm tot})\cos(2g_1)+4\cos^2(i_{\rm tot})+6e_1^2\cos^2(i_{\rm tot})-10e_1^2\cos(2g_1)\cos^2(i_{\rm tot})\right] \\
&= \boxed{3\,C_{\rm quad}\left\{\frac{2\cos(i_{\rm tot})}{G_1}\left[2+e_1^2(3-5\cos(2g_1))\right]+\frac{1}{G_2}\left[4+6e_1^2+\left(5\cos^2(i_{\rm tot})-3\right)\left(2+e_1^2(3-5\cos(2g_1))\right)\right]\right\}}. \qquad \text{(A.1.43)}
\end{aligned}$$

Lastly, the change of the inner orbit eccentricity with time valid in the quadrupole order follows from Eq. 2.35 as follows:

$$\dot{e}_{1,\rm quad} = \frac{\partial e_1}{\partial G_1}\dot{G}_1\Big|_{\Delta h=\pi} = \frac{\partial e_1}{\partial G_1}\frac{\partial\langle\langle R_{\rm quad}\rangle_2\rangle_1}{\partial g_1}\bigg|_{\Delta h=\pi}. \qquad \text{(A.1.44)}$$

The derivative $\partial e_1/\partial G_1$ is given by Eq. A.1.35 whereas $\partial\langle\langle R_{\rm quad}\rangle_2\rangle_1/\partial g_1$ follows from Eqs. 2.27 and 2.30:

$$\begin{aligned}
\frac{\partial\left(Z_a^2+Z_c^2\right)}{\partial g_1} &= 2\left(D_a\cos(g_1)-D_b\sin(g_1)\right)\left(-D_a\sin(g_1)-D_b\cos(g_1)\right)+2\left(D_c\cos(g_1)+D_d\sin(g_1)\right) \\
&\quad\times\left(-D_c\sin(g_1)+D_d\cos(g_1)\right)\Rightarrow\ \frac{\partial\left(Z_a^2+Z_c^2\right)}{\partial g_1}\bigg|_{\Delta h=\pi} = -2\cos(g_1)\sin(g_1)+2\sin(g_1)\cos(g_1)\cos^2(i_{\rm tot}) \\
&= -\sin(2g_1)\sin^2(i_{\rm tot}); \\
\frac{\partial\left(Z_b^2+Z_d^2\right)}{\partial g_1} &= 2\left(D_a\sin(g_1)+D_b\cos(g_1)\right)\left(D_a\cos(g_1)-D_b\sin(g_1)\right)+2\left(D_c\sin(g_1)-D_d\cos(g_1)\right) \\
&\quad\times\left(D_c\cos(g_1)+D_d\sin(g_1)\right)\Rightarrow\ \frac{\partial\left(Z_b^2+Z_d^2\right)}{\partial g_1}\bigg|_{\Delta h=\pi} = 2\sin(g_1)\cos(g_1)-2\sin(g_1)\cos(g_1)\cos^2(i_{\rm tot}) \\
&= \sin(2g_1)\sin^2(i_{\rm tot}),
\end{aligned}$$

such that:

$$\begin{aligned}
\frac{\partial\langle\langle R_{\rm quad}\rangle_2\rangle_1}{\partial g_1}\bigg|_{\Delta h=\pi} &= 6\,C_{\rm quad}\left[\frac{\partial\left(Z_a^2+Z_c^2\right)}{\partial g_1}\bigg|_{\Delta h=\pi}\cdot\left(1+4e_1^2\right)+\frac{\partial\left(Z_b^2+Z_d^2\right)}{\partial g_1}\bigg|_{\Delta h=\pi}\cdot\left(1-e_1^2\right)\right] \\
&= 6\,C_{\rm quad}\sin(2g_1)\sin^2(i_{\rm tot})\left[-\left(1+4e_1^2\right)+\left(1-e_1^2\right)\right] = -30\,C_{\rm quad}e_1^2\sin(2g_1)\sin^2(i_{\rm tot}). \qquad \text{(A.1.45)}
\end{aligned}$$

Combining Eqs. A.1.44, A.1.35 and A.1.45 gives:

$$\boxed{\dot{e}_{1,\rm quad} = C_{\rm quad}\frac{1-e_1^2}{G_1}30\,e_1\sin^2(i_{\rm tot})\sin(2g_1)}. \qquad \text{(A.1.46)}$$

Octupole order

In contrast to the quadrupole order, the secular octupole order perturbation term $\langle\langle R_{\rm oct}\rangle_2\rangle_1$ does depend on g_2 such that e_2 is no longer constant in this limit. As mentioned above, it is allowed to substitute $\Delta h=\pi$ in the perturbing term without affecting the equations for $\dot{g}_j$ and $\dot{e}_j$ thus Eq. 2.32 is used below. The equations for $\dot{g}_{j,\rm oct}$ follow from:

$$\dot{g}_{j,\rm oct} = -\frac{\partial\left(\langle\langle R_{\rm oct}\rangle_2\rangle_1|_{\Delta h=\pi}\right)}{\partial G_j} = -\frac{\partial\left(\langle\langle R_{\rm oct}\rangle_2\rangle_1|_{\Delta h=\pi}\right)}{\partial e_j}\frac{\partial e_j}{\partial G_j}-\frac{\partial\left(\langle\langle R_{\rm oct}\rangle_2\rangle_1|_{\Delta h=\pi}\right)}{\partial i_j}\frac{\partial i_j}{\partial G_j}. \qquad \text{(A.1.47)}$$

The quantities $\partial e_j/G_j$ and i_j/G_j were computed in the above derivation for the quadrupole order (cf. Eqs. A.1.35, A.1.38 and A.1.42):

$$\frac{\partial e_j}{\partial G_j} = -\frac{1-e_j^2}{e_j G_j}; \quad \frac{\partial i_j}{G_j} = \frac{1}{\sin(i_{\rm tot})}\left[\frac{\cos(i_{\rm tot})}{G_j} + \frac{1}{G_{3-j}}\right]. \tag{A.1.48}$$

The other required quantities are obtained from Eqs. 2.32 and 2.33:

$$\begin{aligned}
\frac{\partial\left(\langle\langle R_{\rm oct}\rangle_2\rangle_1|_{\Delta h=\pi}\right)}{\partial e_1} &= C_{\rm oct} e_2\left[A\cos(\phi) + 10\cos(i_{\rm tot})\sin^2(i_{\rm tot})\left(1-e_1^2\right)\sin(g_1)\sin(g_2)\right] + C_{\rm oct} e_2\left[e_1\frac{\partial A}{\partial e_1}\cos(\phi)\right.\\
&\quad \left. -20e_1^2\cos(i_{\rm tot})\sin^2(i_{\rm tot})\sin(g_1)\sin(g_2)\right];\\
e_1\frac{\partial A}{\partial e_1} &= 2\left[3e_1^2 - \frac{5}{2}\sin^2(i_{\rm tot})\left(5e_1^2 - 7e_1^2\cos(2g_1)\right)\right] = 2\left[4 + 3e_1^2 - \frac{5}{2}\sin^2(i_{\rm tot})\left(2 + 5e_1^2 - 7e_1^2\cos(2g_1)\right)\right]\\
&\quad -8 + 10\sin^2(i_{\rm tot}) = 2A - 10\cos^2(i_{\rm tot}) + 2 \Rightarrow\\
\frac{\partial\left(\langle\langle R_{\rm oct}\rangle_2\rangle_1|_{\Delta h=\pi}\right)}{\partial e_1} &= C_{\rm oct} e_2\left[\left(3A - 10\cos^2(i_{\rm tot}) + 2\right)\cos(\phi) + 10\cos(i_{\rm tot})\sin^2(i_{\rm tot})\left(1-3e_1^2\right)\sin(g_1)\sin(g_2)\right];
\end{aligned} \tag{A.1.49}$$

$$\begin{aligned}
\frac{\partial\left(\langle\langle R_{\rm oct}\rangle_2\rangle_1|_{\Delta h=\pi}\right)}{\partial i_1} &= C_{\rm oct} e_1 e_2\left[\frac{\partial A}{\partial i_1}\cos(\phi) + A\frac{\partial\cos(\phi)}{\partial i_1} + 10\frac{\partial}{\partial i_1}\left\{\cos(i_{\rm tot})\left(1-\cos^2(i_{\rm tot})\right)\right\}\left(1-e_1^2\right)\sin(g_1)\sin(g_2)\right]\\
&= C_{\rm oct} e_1 e_2\left[-5B\sin(i_{\rm tot})\cos(i_{\rm tot})\cos(\phi) + A\sin(i_{\rm tot})\sin(g_1)\sin(g_2) + 10\sin(i_{\rm tot})\right.\\
&\quad \left.\times\left(3\cos^2(i_{\rm tot}) - 1\right)\left(1-e_1^2\right)\sin(g_1)\sin(g_2)\right]\\
&= C_{\rm oct} e_1 e_2\sin(i_{\rm tot})\left[\sin(g_1)\sin(g_2)\left\{A + 10\left(3\cos^2(i_{\rm tot}) - 1\right)\left(1-e_1^2\right)\right\} - 5B\cos(i_{\rm tot})\cos(\phi)\right].
\end{aligned} \tag{A.1.50}$$

Combining Eqs. A.1.47, A.1.48, A.1.49 and A.1.50 gives:

$$\begin{aligned}
\dot{g}_{1,\rm oct} &= \frac{1-e_1^2}{e_1 G_1} C_{\rm oct} e_2\left[\cos(\phi)\left(3A - 10\cos^2(i_{\rm tot}) + 2\right) + 10\cos(i_{\rm tot})\sin^2(i_{\rm tot})\left(1-3e_1^2\right)\sin(g_1)\sin(g_2)\right]\\
&\quad - C_{\rm oct} e_1 e_2\left(\frac{1}{G_2} + \frac{\cos(i_{\rm tot})}{G_1}\right)\left\{\sin(g_1)\sin(g_2)\left[A + 10\left(3\cos^2(i_{\rm tot}) - 1\right)\left(1-e_1^2\right)\right] - 5B\cos(i_{\rm tot})\cos(\phi)\right\}.
\end{aligned}$$

For $\dot{g}_{2,\rm oct}$ note that $\langle\langle R_{\rm oct}\rangle_2\rangle_1|_{\Delta h=\pi} = C_{\rm oct}(G_2)\, e_1 e_2\, f_{\rm oct}(e_1, i_1, i_2, g_1, g_2)$, where the function $f_{\rm oct}$ is defined in Eq. 2.32. Therefore:

$$\dot{g}_{2,\rm oct} = -\frac{\partial\left(\langle\langle R_{\rm oct}\rangle_2\rangle_1|_{\Delta h=\pi}\right)}{\partial G_2} = -\frac{\partial C_{\rm oct}}{\partial G_2} e_1 e_2 f_{\rm oct} - C_{\rm oct} e_1\frac{\partial e_2}{\partial G_2} f_{\rm oct} - C_{\rm oct} e_1 e_2\frac{\partial f_{\rm oct}}{\partial i_2}\frac{\partial i_2}{\partial G_2}. \tag{A.1.51}$$

From Eq. A.1.33 it follows that $\partial C_{\rm oct}/\partial G_2 = -5\, C_{\rm oct}/G_2$. Furthermore, $\partial f_{\rm oct}/\partial i_2 = \partial f_{\rm oct}/\partial i_1$ and the latter quantity is given by Eq. A.1.50. Therefore Eq. A.1.51 gives:

$$\begin{aligned}
\dot{g}_{2,\rm oct} &= 5\, C_{\rm oct}\frac{e_1 e_2}{G_2}\left[A\cos(\phi) + 10\cos(i_{\rm tot})\sin^2(i_{\rm tot})\left(1-e_1^2\right)\sin(g_1)\sin(g_2)\right] + C_{\rm oct} e_1\frac{1-e_2^2}{e_2 G_2}\left[A\cos(\phi) + 10\cos(i_{\rm tot})\right.\\
&\quad \left.\times\sin^2(i_{\rm tot})\left(1-e_1^2\right)\sin(g_1)\sin(g_2)\right] - C_{\rm oct} e_1 e_2\frac{1}{\sin(i_{\rm tot})}\left(\frac{1}{G_1} + \frac{\cos(i_{\rm tot})}{G_2}\right)\sin(i_{\rm tot})\left\{\sin(g_1)\sin(g_2)\left[A + 10\right.\right.\\
&\quad \left.\left.\times\left(3\cos^2(i_{\rm tot}) - 1\right)\left(1-e_1^2\right)\right] - 5B\cos(i_{\rm tot})\cos(\phi)\right\}
\end{aligned}$$

$$\begin{aligned}
&= C_{\rm oct} e_1\left\{\sin(g_1)\sin(g_2)\left[\frac{4e_2^2+1}{e_2 G_2} 10\cos(i_{\rm tot})\sin^2(i_{\rm tot})\left(1-e_1^2\right) - e_2\left(\frac{1}{G_1} + \frac{\cos(i_{\rm tot})}{G_2}\right)\left(A + 10\left(3\cos^2(i_{\rm tot}) - 1\right)\right.\right.\right.\\
&\quad \left.\left.\left.\times\left(1-e_1^2\right)\right)\right] + \cos(\phi)\left[5B\cos(i_{\rm tot}) e_2\left(\frac{1}{G_1} + \frac{\cos(i_{\rm tot})}{G_2}\right) + \frac{4e_2^2+1}{e_2 G_2} A\right]\right\}.
\end{aligned}$$

Lastly, $\dot{e}_{j,\mathrm{oct}}$ follow from:

$$\dot{e}_{j,\mathrm{oct}} = \left.\frac{\partial e_j}{\partial G_j}\dot{G}_j\right|_{\Delta h=\pi} = \frac{\partial e_j}{\partial G_j}\frac{\partial\left(\langle\langle R_{\mathrm{oct}}\rangle_2\rangle_1|_{\Delta h=\pi}\right)}{\partial g_j}. \tag{A.1.52}$$

The required quantities follow from Eqs. 2.32 and 2.33:

$$\begin{aligned}
\frac{\partial\left(\langle\langle R_{\mathrm{oct}}\rangle_2\rangle_1|_{\Delta h=\pi}\right)}{\partial g_1} &= C_{\mathrm{oct}}e_1e_2\left[\frac{\partial A}{\partial g_1}\cos(\phi) + A\frac{\partial\cos(\phi)}{\partial g_1} + 10\cos(i_{\mathrm{tot}})\sin^2(i_{\mathrm{tot}})\left(1-e_1^2\right)\cos(g_1)\sin(g_2)\right];\\
\frac{\partial\left(\langle\langle R_{\mathrm{oct}}\rangle_2\rangle_1|_{\Delta h=\pi}\right)}{\partial g_2} &= C_{\mathrm{oct}}e_1e_2\left[A\frac{\partial\cos(\phi)}{\partial g_2} + 10\cos(i_{\mathrm{tot}})\sin^2(i_{\mathrm{tot}})\left(1-e_1^2\right)\sin(g_1)\cos(g_2)\right];\\
\frac{\partial A}{\partial g_1} &= -35\sin^2(i_{\mathrm{tot}})e_1^2\sin(2g_1); \quad \frac{\partial\cos(\phi)}{\partial g_1} = \sin(g_1)\cos(g_2) - \cos(i_{\mathrm{tot}})\cos(g_1)\sin(g_2);\\
\frac{\partial\cos(\phi)}{\partial g_2} &= \cos(g_1)\sin(g_2) - \cos(i_{\mathrm{tot}})\sin(g_1)\cos(g_2),
\end{aligned}$$

hence:

$$\begin{aligned}
\dot{e}_{1,\mathrm{oct}} &= C_{\mathrm{oct}}e_2\frac{1-e_1^2}{G_1}\Big[35\cos(\phi)\sin^2(i_{\mathrm{tot}})e_1^2\sin(2g_1) - 10\cos(i_{\mathrm{tot}})\sin^2(i_{\mathrm{tot}})\cos(g_1)\sin(g_2)\left(1-e_1^2\right) - A\left\{\sin(g_1)\cos(g_2)\right.\\
&\quad\left.-\cos(i_{\mathrm{tot}})\cos(g_1)\sin(g_2)\right\}\Big];\\
\dot{e}_{2,\mathrm{oct}} &= -C_{\mathrm{oct}}e_1\frac{1-e_2^2}{G_2}\left[10\cos(i_{\mathrm{tot}})\sin^2(i_{\mathrm{tot}})\left(1-e_1^2\right)\sin(g_1)\cos(g_2) + A\left(\cos(g_1)\sin(g_2) - \cos(i_{\mathrm{tot}})\sin(g_1)\cos(g_2)\right)\right].
\end{aligned}$$

A.1.5 Analytic solutions in the test particle quadrupole order limit

Differential equation for the inner orbit eccentricity

From Eq. 2.44, substituting $\theta^2 = (x_0/x)\,\theta_0^2$ with $x = 1-e_1^2$ and $x_0 = 1-e_{1,0}^2$, $\cos(2g_1)$ follows as:

$$\cos(2g_1) = \frac{r_0 - (5-3x)\left(3\theta_0^2\frac{x_0}{x} - 1\right)}{15(1-x)\left(1-\theta_0^2\frac{x_0}{x}\right)} = \frac{r_0x - (5-3x)\left(3\theta_0^2x_0 - x\right)}{15(1-x)\left(x-\theta_0^2x_0\right)}. \tag{A.1.53}$$

As Eq. A.1.45 shows the quantity $\sin(2g_1) = 2\sin(g_1)\cos(g_1)$ is required for $\dot{e}_{1,\mathrm{quad}}$. To this end we compute:

$$\begin{aligned}
\cos^2(g_1) &= \frac{1}{2}(1+\cos(2g_1)) = \frac{1}{2}\frac{1}{15(1-x)\left(x-\theta_0^2x_0\right)}\left[15(1-x)\left(x-\theta_0^2x_0\right) + r_0x - 15\theta_0^2x_0 + 5x + 9\theta_0^2x_0x - 3x^2\right]\\
&= \frac{1}{30(1-x)\left(x-\theta_0^2x_0\right)}\left[-18x^2 + x\left(20 + r_0 + 24\theta_0^2x_0\right) - 30\theta_0^2x_0\right];\\
\sin^2(g_1) &= \frac{1}{2}(1-\cos(2g_1)) = \frac{1}{2}\frac{1}{15(1-x)\left(x-\theta_0^2x_0\right)}\left[15(1-x)\left(x-\theta_0^2x_0\right) - r_0x + 15\theta_0^2x_0 - 5x - 9\theta_0^2x_0x + 3x^2\right]\\
&= \frac{x}{30(1-x)\left(x-\theta_0^2x_0\right)}\left[-12x + 6\theta_0^2x_0 + 10 - r_0\right].
\end{aligned}$$

Eq. A.1.45 is thus formulated in terms of x as:

$$\begin{aligned}\frac{\mathrm{d}x}{\mathrm{d}t} &= -2e_1\frac{\mathrm{d}e_1}{\mathrm{d}t} = -2e_1 C_{\mathrm{quad}}\frac{1-e_1^2}{L_1\sqrt{1-e_1^2}}\,30\,e_1\underbrace{\frac{x-\theta_0^2 x_0}{x}}_{=\sin^2(i_{\mathrm{tot}})}\frac{2}{30(1-x)\left(x-\theta_0^2 x_0\right)}\sqrt{x\left(-12x+6\theta_0^2x_0+10-r_0\right)}\\ &\times\sqrt{-18x^2+x\left(20+r_0+24\theta_0^2x_0\right)-30\theta_0^2x_0} = -4\,\frac{C_{\mathrm{quad}}}{L_1}(1-x)\frac{\sqrt{x}}{x}\left(x-\theta_0^2x_0\right)\frac{1}{(1-x)\left(x-\theta_0^2x_0\right)}\sqrt{x}\\ &\times\sqrt{12\left[x-\left(\frac{1}{2}\theta_0^2x_0+\frac{5}{6}-\frac{1}{12}r_0\right)\right]}\sqrt{18\left[x^2-x\left(\frac{10}{9}+\frac{1}{18}r_0+\frac{4}{3}\theta_0^2x_0\right)+\frac{5}{3}\theta_0^2x_0\right]}\\ &= \boxed{-\frac{24\sqrt{6}}{\tau}\sqrt{(x-x_A)(x-x_B)(x-x_C)}},\end{aligned} \tag{A.1.54}$$

where $\tau \equiv L_1/C_{\mathrm{quad}}$ is a quantity with dimensions of time and sets a characteristic time scale; with Kepler's equation to convert a_j to P_j and with Eqs. 2.24 and 2.34 it can be can written as:

$$\begin{aligned}\tau \equiv \frac{L_1}{C_{\mathrm{quad}}} &= \frac{m_1m_2\sqrt{G_Na_1}}{\sqrt{m_1+m_2}}\,16\,\frac{(m_1+m_2)\,a_2}{G_Nm_1m_2m_3}\left(\frac{a_2}{a_1}\right)^2\left(1-e_2^2\right)^{3/2} = \sqrt{\frac{G_N}{m_1+m_2}}\left(\frac{2\pi}{P_1}\right)\frac{1}{\sqrt{G_N(m_1+m_2)}}\,\frac{16}{G_N}\,\frac{m_1+m_2}{m_3}\\ &\times\left(\frac{P_2}{2\pi}\right)^2 G_N(m_1+m_2+m_3)\left(1-e_2^2\right)^{3/2} = \frac{8}{\pi}\left(\frac{P_2}{P_1}\right)P_2\frac{m_1+m_2+m_3}{m_3}\left(1-e_2^2\right)^{3/2}.\end{aligned} \tag{A.1.55}$$

Furthermore, $x_A \equiv \frac{1}{2}\theta_0^2x_0 + \frac{5}{6} - \frac{1}{12}r_0$ may be written explicitly in terms of x_0, θ_0 and $g_{1,0}$ with Eq. 2.44 as:

$$\begin{aligned}x_A &= \frac{1}{2}\theta_0^2x_0+\frac{5}{6}-\frac{1}{2}\theta_0^2+\frac{1}{6}-\frac{3}{4}(1-x_0)\theta_0^2+\frac{1}{4}(1-x_0)-\frac{5}{4}(1-x_0)\left(1-\theta_0^2\right)\cos(2g_{1,0})\\ &= x_0+\frac{5}{4}\left[\left(1-\theta_0^2\right)-x_0\left(1-\theta_0^2\right)-(1-x_0)\left(1-\theta_0^2\right)\cos(2g_{1,0})\right] = x_0+\frac{5}{2}(1-x_0)\left(1-\theta_0^2\right)\sin^2(g_{1,0}),\end{aligned} \tag{A.1.56}$$

whereas x_B and x_C are defined via $x^2 - x\left(\frac{10}{9}+\frac{1}{18}r_0+\frac{4}{3}\theta_0^2x_0\right)+\frac{5}{3}\theta_0^2x_0 \equiv (x-x_B)(x-x_C)$ such that $x_B = b/2 - (1/2)\sqrt{b^2-4c}$ and $x_C = b/2 + (1/2)\sqrt{b^2-4c}$, where $c \equiv \frac{5}{3}\theta_0^2x_0$ and b may be written with in terms of x_0, θ_0 and $g_{1,0}$ with Eq. 2.44 as:

$$\begin{aligned}b \equiv \frac{10}{9}+\frac{1}{18}r_0+\frac{4}{3}\theta_0^2x_0 &= x_0+\frac{5}{6}+\frac{5}{6}\theta_0^2+\frac{5}{6}\theta_0^2x_0-\frac{5}{6}x_0+\frac{5}{6}(1-x_0)\left(1-\theta_0^2\right)\underbrace{\cos(2g_{1,0})}_{=2\cos^2(g_{1,0})-1}\\ &= x_0+\frac{5}{3}\left[\theta_0^2+(1-x_0)\left(1-\theta_0^2\right)\cos^2(g_{1,0})\right].\end{aligned} \tag{A.1.57}$$

Solving the equation for $\dot{x}$

To solve Eq. 2.45, let $\tilde{x} = x - x_B$. As will be clear from the solution, x_B corresponds to the maximum inner orbit eccentricity therefore $x_B < x$, or $\tilde{x} > 0$. Eq. 2.45 in terms of $\tilde{x}$ reads:

$$\frac{\mathrm{d}\tilde{x}}{\mathrm{d}t} = -\frac{24\sqrt{6}}{\tau}\sqrt{\tilde{x}\,(x_A-x_B-\tilde{x})\,(x_C-x_B-\tilde{x})}. \tag{A.1.58}$$

From Eq. 2.47 it follows that $x_C - x_B > 0$ and that $x_A - x_B > 0$ thus the quantity in the square root in Eq. A.1.58 is always positive. With the substitution $y^2 = \tilde{x}$, Eq. A.1.58 is transformed to:

$$\begin{aligned}2y\frac{\mathrm{d}y}{\mathrm{d}t} &= -\frac{24\sqrt{6}}{\tau}y\sqrt{(x_A-x_B-y^2)\,(x_C-x_B-y^2)}\\ \Rightarrow\left(\frac{\mathrm{d}y}{\mathrm{d}t}\right)^2 &= \left(\frac{12\sqrt{6}}{\tau}\right)^2(x_A-x_B)\left(1-\frac{y^2}{x_A-x_B}\right)(x_C-x_B)\left(1-\frac{y^2}{x_C-x_B}\right).\end{aligned}$$

With $\tilde{y} = y/\sqrt{x_A-x_B}$ this becomes:

$$\left(\frac{\mathrm{d}\tilde{y}}{\mathrm{d}t}\right)^2(x_A-x_B) = \left(\frac{12\sqrt{6}}{\tau}\right)^2(x_A-x_B)\left(1-\tilde{y}^2\right)(x_C-x_B)\left(1-\tilde{y}^2\frac{x_A-x_B}{x_C-x_B}\right),$$

or, in terms of a dimensionless time $\tilde{t} = 12\sqrt{6}\,(t/\tau)\sqrt{x_C - x_B}$:

$$\left(\frac{\mathrm{d}\tilde{y}}{\mathrm{d}\tilde{t}}\right)^2 = \left(1-\tilde{y}^2\right)\left(1-k^2\tilde{y}^2\right); \quad k^2 \equiv \frac{x_A - x_B}{x_C - x_B}. \tag{A.1.59}$$

A solution of Eq. A.1.59 is found by noting that the Jacobian elliptic function $\mathrm{sn}(t|k)$ satisfies (Gradshteyn & Ryzhik 2007, 8.158):

$$\frac{\mathrm{d}\,\mathrm{sn}(t|k)}{\mathrm{d}t} = \mathrm{cn}(t|k)\,\mathrm{dn}(t|k) \Rightarrow \left(\frac{\mathrm{d}\,\mathrm{sn}(t|k)}{\mathrm{d}t}\right)^2 = \mathrm{cn}^2(t|k)\,\mathrm{dn}^2(t|k) = \left[1-\mathrm{sn}^2(t|k)\right]\left[1-k^2\mathrm{sn}^2(t|k)\right], \tag{A.1.60}$$

where the properties $\mathrm{sn}^2(t|k) + \mathrm{cn}^2(t|k) = 1$ and $k^2\,\mathrm{sn}^2(t|k) + \mathrm{dn}^2(t|k) = 1$ were used (Gradshteyn & Ryzhik 2007, 8.154). Comparison between Eqs. A.1.59 and A.1.60 shows:

$$\tilde{y}\,(\tilde{t}) = \mathrm{sn}\left(\tilde{t}-\tilde{t}_0\,\middle|\,k\right) \Longleftrightarrow \frac{1}{x_A - x_B}(x - x_B) = 1 - \mathrm{cn}^2\left(\tilde{t}-\tilde{t}_0\,\middle|\,k\right) \Longleftrightarrow \boxed{x\,(\tilde{t}) = x_A + (x_B - x_A)\,\mathrm{cn}^2\left(\tilde{t}-\tilde{t}_0\,\middle|\,k\right)}, \tag{A.1.61}$$

where $\tilde{t}_0$ is such that $x(0) = x_0$, i.e. $\tilde{t}_0$ is given by Eq. 2.50.

Appendix B

General relativistic apsidal motion

In the following we investigate the validity of the canonical expression Eq. 2.53 which describes apsidal motion due to general relativity. Specifically, we shall investigate this validity in the most extreme conditions which we find in the population synthesis study. In particular, for inner binary orbits of $a_1 \sim 1$ AU we find eccentricities of at most $e_1 \sim 1 - 10^{-5}$ and for $a_1 \sim 10^3$ AU we find at most $e_1 \sim 1 - 10^{-8}$ (see also Sect. 5). First we derive the equation of motion which is exact[1], Eq. B.1.7. Subsequently we compute the frequency of apsidal motion with the assumption that the orbits are still instantaneously described in terms of Keplerian orbits and in the above limits.

B.1 Equation of motion

Firstly, we employ canonical spherical coordinates (r, θ, ϕ) in which the Schwarzschild line element reads (with $c = 1$):

$$\mathrm{d}s^2 = g_{\mu\nu}\mathrm{d}x^\mu\,\mathrm{d}x^\nu = -\left(1 - \frac{2G_N M}{r}\right)\mathrm{d}t^2 + \left(1 - \frac{2G_N M}{r}\right)\mathrm{d}r^2 + r^2\mathrm{d}\Omega^2, \tag{B.1.1}$$

where t denotes coordinate time, $M \equiv m_1 + m_2$ and $\mathrm{d}\Omega^2 \equiv \mathrm{d}\theta^2 + r^2\sin^2(\theta)\,\mathrm{d}\phi^2$. The metric is independent on t and ϕ giving rise to two Killing vectors associated with conservation of energy E and angular momentum L. Application of the Killing equations then leads to the following two relations:

$$\left(1 - \frac{2G_N M}{r}\right)\frac{\mathrm{d}t}{\mathrm{d}\lambda} = E; \quad r^2\frac{\mathrm{d}\phi}{\mathrm{d}\lambda} = L, \tag{B.1.2}$$

where λ denotes proper time. Conservation of angular momentum implies that the motion takes place within a plane, thus justifying the constraint $\theta = \pi/2$ such that $\mathrm{d}\Omega^2 = r^2\mathrm{d}\phi^2$. For timelike massive particles the four-velocity $U^\mu = \mathrm{d}x^\mu/\mathrm{d}\lambda$ has a norm of -1. Therefore, from Eq. B.1.1:

$$-1 = g_{\mu\nu}U^\mu U^\nu = -\left(1 - \frac{2G_N M}{r}\right)\left(\frac{\mathrm{d}t}{\mathrm{d}\lambda}\right)^2 + \left(1 - \frac{2G_N M}{r}\right)^{-1}\left(\frac{\mathrm{d}r}{\mathrm{d}\lambda}\right)^2 + r^2\left(\frac{\mathrm{d}\phi}{\mathrm{d}\lambda}\right)^2. \tag{B.1.3}$$

Eliminating $\mathrm{d}t/\mathrm{d}\lambda$ and $\mathrm{d}\phi/\mathrm{d}\lambda$ from Eq. B.1.3 with Eq. B.1.2 and rewriting the subsequent equation for $\mathrm{d}r/\mathrm{d}\lambda$ gives:

$$\left(\frac{\mathrm{d}r}{\mathrm{d}\lambda}\right)^2 + \left(1 - \frac{2G_N M}{r}\right)\left(\frac{L^2}{r^2} + 1\right) = E^2. \tag{B.1.4}$$

Since $\mathrm{d}r/\mathrm{d}\phi = (\mathrm{d}r/\mathrm{d}\lambda)/(\mathrm{d}\phi/\mathrm{d}\lambda)$ the latter can be rewritten to a differential equation for $\mathrm{d}r/\mathrm{d}\phi$ by once again using Eq. B.1.2:

$$\left(\frac{\mathrm{d}r}{\mathrm{d}\phi}\right)^2 + \left(1 - \frac{2G_N M}{r}\right)\left(\frac{L^2}{r^2} + 1\right)\frac{r^4}{L^2} = E^2\frac{r^4}{L^2}. \tag{B.1.5}$$

Eq. B.1.5 can be written in a more manageable form by introducing the dimensionless quantity $x \equiv L^2/(G_N M r)$:

$$\left(\frac{\mathrm{d}x}{\mathrm{d}\phi}\right)^2 + x^2 + \left(\frac{L}{G_N M}\right)^2 - 2\left(\frac{G_N M}{L}\right)^2 x^3 - 2x = \left(\frac{EL}{G_N M}\right)^2. \tag{B.1.6}$$

[1] The derivation of this equation is adapted from a lecture on general relativity given in 2011-2012 by Tomislav Prokopec at Utrecht University.

By differentiating Eq. B.1.6 we find the following second-order non-linear differential equation, which is the equation of motion:

$$\frac{\mathrm{d}^2 x}{\mathrm{d}\phi^2} + x - 1 - 3x^2\left(\frac{G_N M}{L}\right)^2 = 0. \tag{B.1.7}$$

Note that in the Newtonian limit the term $\propto x^2$ in Eq. B.1.7 vanishes, in which case Eq. B.1.7 reduces to the equation of a harmonic oscillator. The solution of this equation is the familiar Kepler orbit $x = 1+e_1\cos(\phi)$ or $r = \left[L^2/(G_N M)\right] / \left[1 + e_1\cos(\phi)\right]$ (here the eccentricity e_1 is an integration constant).

B.2 Apsidal motion

If the orbit is instantaneously described in terms of a Kepler orbit then we may write $r = a_1\left(1-e_1^2\right)/(1+e_1\cos(\alpha\phi))$, where α is a constant on the order of unity which describes the asynchrony between a complete cycle of r and a complete cycle of ϕ. For $\alpha = 1$, there is no apsidal motion; in general, $\dot{g}_{1,\mathrm{GR}} = (1/\alpha - 1)\left(G_N M/a_1^3\right)^{1/2}$ (i.e. dividing the relative change of g_1 by the orbital period). The angular momentum L is given by $L^2 = G_N M a_1\left(1-e_1^2\right)$ hence the above assumption implies $x = 1 + e_1\cos(\alpha\phi)$. Inserting this relation into Eq. B.1.7 and isolating e_1 we find the following relation which is valid for all $\phi \in [0, 2\pi]$:

$$3\left(\frac{G_N M}{L}\right)^2 + \left[\cos(\alpha\phi)\left(\alpha^2 - 1 + 6\left(\frac{G_N M}{L}\right)^2\right)\right] e_1 + 3\left(\frac{G_N M}{L}\right)^2 \cos^2(\alpha\phi)\, e_1^2 = 0 \tag{B.2.1}$$

In particular, Eq. B.2.1 should be valid for $\phi = 0$:

$$3\left(\frac{G_N M}{L}\right)^2 + \left(\alpha^2 - 1 + 6\left(\frac{G_N M}{L}\right)^2\right) e_1 + 3\left(\frac{G_N M}{L}\right)^2 e_1^2 = 0. \tag{B.2.2}$$

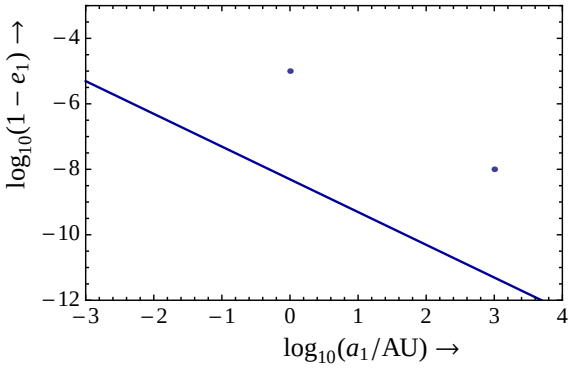

Figure B.1: The critical relation between e_1 and a_1 given by Eq. B.2.4 for $M = 1\,M_\odot$. The canonical expression Eq. 2.53 is valid to good approximation in regions above this curve. In addition the two extreme limits found in the population synthesis study are indicated.

Consider the limit $(G_N M)^2 \ll L^2$. For the two extreme limits stated above, $e_1 \sim 1 - 10^{-5}$ for $a_1 \sim 1$ AU and $e_1 \sim 1 - 10^{-8}$ for $a_1 \sim 10^3$ AU and assuming $M = m_1 + m_2 = 1\,M_\odot$, this limit is certainly satisfied since $(G_N M/L)^2 = G_N M/\left[c^2 a_1\left(1-e_1^2\right)\right] \sim 5\cdot 10^{-4}$ for these two cases. In the limit $(G_N M)^2 \ll L^2$ the first and third terms in Eq. B.2.2 are negligible and thus the second term must be equal to zero. This condition is straightforwardly solved for α and the associated degree of apsidal motion thus follows as:

$$\begin{aligned}\dot{g}_{1,\mathrm{GR}} &\approx \left(\left[1 - 6\left(\frac{G_N M}{L}\right)^2\right]^{-1/2} - 1\right)\left(\frac{G_N M}{a_1^3}\right)^{1/2} = \left\{1 + 3\left(\frac{G_N M}{L}\right)^2 + \frac{27}{2}\left(\frac{G_N M}{L}\right)^4 + O\left[\left(\frac{G_N M}{L}\right)^6\right] - 1\right\}\left(\frac{G_N M}{a_1^3}\right)^{1/2} \\ &= \frac{3}{c^2 a_1\left(1-e_1^2\right)}\left(\frac{G_N M}{a_1^3}\right)^{3/2}\left\{1 + \frac{9}{2}\frac{G_N M}{c^2 a_1\left(1-e_1^2\right)} + O\left[\left(\frac{G_N M}{c^2 a_1\left(1-e_1^2\right)}\right)^2\right]\right\},\end{aligned} \tag{B.2.3}$$

where we used a Taylor expansion. The largest contributing term in Eq. B.2.3 is immediately identified as the canonical expression Eq. 2.53, whereas the additional terms describe corrections to this term. The ratio of the first of these additional terms to the canonical expression is proportional to $(G_N M/L)^2 = G_N M/\left[c^2 a_1\left(1-e_1^2\right)\right]$. If the canonical expression Eq. 2.53 is to be a good approximation, then this latter ratio must be small. This is satisfied if $(G_N M/L)^2 \ll 1$, which for $M = 1\,M_\odot$ is equivalent to:

$$\log_{10}\left(1-e_1^2\right) \gg \log_{10}\left(\frac{G_N M}{c^2 a_1}\right) \approx -8.0 - \log_{10}\left(\frac{a_1}{\mathrm{AU}}\right). \tag{B.2.4}$$

Note that to good approximation Eq. B.2.4 can be written as:

$$\log_{10}(1-e_1) \gg \log_{10}\left(1 - \left[1 - \frac{G_N M}{c^2 a_1}\right]^{1/2}\right) \approx \log_{10}\left(\frac{G_N M}{2c^2 a_1}\right) \approx -8.3 - \log_{10}\left(\frac{a_1}{\mathrm{AU}}\right). \tag{B.2.5}$$

Fig. B.1 shows the critical relation between e_1 and a_1 given by Eq. B.2.4 for $M = 1\,M_\odot$. The canonical expression Eq. 2.53 is valid to good approximation in regions above this curve. In addition the two extreme limits found in the population synthesis study are indicated. The corresponding points lie well within the region for which the canonical expression is valid. We thus conclude that it is justified to use Eq. 2.53 for the systems computed in the population synthesis study.

Appendix C

DTD normalization calculations

The predicted delay time distribution (DTD) must be normalized to the part of the mass represented by the sampled triple systems. Note that in Sect. 5.4.2 a comparison is made to the binary population synthesis DTD of Claeys et al. (2012), in which case one must restrict to the TSM1 population where the same (inner) binary distributions are used (we briefly mention the normalization quantities for TSM2 below for completeness). In this work the triple populations are split into two parts with $1.0 < m_1/M_\odot < 2.0$ (TSM[1/2]A) and $2.0 < m_1/M_\odot < 6.5$ (TSM[1/2]B) (cf. Sect. 5.3). Therefore we perform the calculations separately for these separate mass ranges. First we illustrate the method in general in Sect. C.1, i.e. without specifying to the A and B populations. Subsequently, we state the explicit numbers which we find in Sect. C.2.

C.1 General procedure

We decompose the galactic population of $N_{\rm tot}$ gravitationally bound stellar systems into $N_{\rm bin} = \alpha_{\rm bin} N_{\rm tot}$ binary star systems, $N_{\rm tr} = \alpha_{\rm tr} N_{\rm tot}$ triple star systems and $N_{\rm s} = (1 - \alpha_{\rm bin} - \alpha_{\rm tr}) N_{\rm tot}$ single star systems (i.e. we neglect higher-order multiplicities). We disregard from the calculated triple systems the MS mergers and MS destabilizations as these are not expected to be part of the observed population. The remaining triple systems constitute a fraction $f_{\rm calc}$ of all $N_{\rm tr}$ triple systems. Assuming that the initial stellar mass m_1 is uncorrelated with a_1 and e_1, $f_{\rm calc} = f_{{\rm calc},m_1} \times f_{{\rm calc},e_1,a_1,a_2}$, where $f_{{\rm calc},m_1}$ is the fraction of calculated systems to all systems with respect to the mass distribution and $f_{{\rm calc},e_1,e_2,a_1,a_2}$ is this fraction with respect to the eccentricity and semi-major axes distributions of the inner and outer orbits. For a Kroupa et al. (1993) initial mass distribution as is assumed in TSM1,

$$\frac{{\rm d}N}{{\rm d}m} \propto \begin{cases} m^{\alpha_1}, & m_{\rm Kr,1} < m < m_{\rm Kr,2}; \\ m^{\alpha_2}, & m_{\rm Kr,2} < m < m_{\rm Kr,3}; \\ m^{\alpha_3}, & m_{\rm Kr,3} < m < m_{\rm Kr,4}, \end{cases} \tag{C.1.1}$$

where $\alpha_j = \{-1.3, -2.2, -2.7\}$ and $m_{{\rm Kr},j}/M_\odot = \{0.1, 0.5, 1, 80\}$, the fraction of systems with $m_{1,l} < m_1 < m_{1,u}$, is given by:

$$f_{{\rm calc},m_1} = \frac{1}{\alpha_3 + 1} C_{\rm Kr} C_{\rm Kr,3} \left(m_{1,u}^{\alpha_3+1} - m_{1,l}^{\alpha_3+1} \right), \tag{C.1.2}$$

where

$$C_{\rm Kr} = \left\{ \sum_{j=1}^{3} \frac{C_{{\rm Kr},j}}{\alpha_j + 1} \left(m_{{\rm Kr},j+1}^{\alpha_j+1} - m_{{\rm Kr},j}^{\alpha_j+1} \right) \right\}^{-1} \tag{C.1.3}$$

and $C_{{\rm Kr},j} = \{1, m_{\rm Kr,2}^{\alpha_1-\alpha_2}, m_{\rm Kr,2}^{\alpha_1-\alpha_2} m_{\rm Kr,3}^{\alpha_2-\alpha_3}\}$. Here $m_{1,l} = 1.0\,M_\odot$ and $m_{1,u} = 2.0\,M_\odot$ for TSM[1/2]A and $m_{1,l} = 2.0\,M_\odot$ and $m_{1,u} = 6.5\,M_\odot$ for TSM[1/2]B. Furthermore, the determination of $f_{{\rm calc},e_1,e_2,a_1,a_2}$ is complicated by the fact that a_1 and a_2 are correlated because the stability criterion of Eq. 3.6 is used and because the selection $a_1 > \left(1 - e_1^2\right) > 12$ AU is made. In an analytic treatment one would therefore have to integrate the probability density function associated with $f_{{\rm calc},e_1,e_2,a_1,a_2}$, ${\rm d}^4N/\left({\rm d}e_1{\rm d}e_2{\rm d}a_1{\rm d}a_2\right) \propto e_1 e_2/(a_1 a_2)$, with respect to e_1, e_2, a_1 and a_2, where $a_1\beta_{\rm crit} < a_2 < a_u$, $a_l/\left(1 - e_1^2\right) < a_1 < a_u$, $0 < e_1 < (1 - l_{1,l}/a_u)^{1/2}$ and $0 < e_2 < 1$. Here $a_l = 5\,R_\odot$ and $a_u = 5 \cdot 10^6\,R_\odot$ are the lower and upper limits respectively for the semi-major axis distribution (Kouwenhoven et al., 2007); the upper limit of e_1 is a consequence of the requirement that $a_u\left(1 - e_1^2\right) > l_{1,l}$ or equivalently

$e_1 < e_{1,u} \equiv (1 - l_{1,l}/a_u)^{1/2}$. The required integration is complicated to do analytically, in particular because of the dependence of $\beta_{\rm crit}$ on e_2 (cf. Eq. 3.6).

Instead we determine the fraction $f_{{\rm calc},e_1,e_2,a_1,a_2}$ by the following method: we generate a large sample of systems according to the method appropriate for TSM1A and TSM1B without making the selection $l_1 \equiv a_1\left(1-e_1^2\right) > l_{1,l} = 12\,{\rm AU}$. From these systems we subsequently select the systems which satisfy $l_1 > 12\,{\rm AU}$. The number of these systems normalized to the number of sampled systems represents an estimate of $f_{{\rm calc},e_1,e_2,a_1,a_2}$ if a sufficiently large number of systems is sampled. We perform this procedure with sizes varying between 10^4 and 10^6 and thus find $f_{{\rm calc},e_1,e_2,a_1,a_2} \approx 0.130$ for both TSM1A and TSM1B (i.e. this fraction is independent of primary mass).

The last step is to add the mass contributions from the single, binary and triple systems. In general, for a Kroupa IMF the total mass M in a population of size N is given by:

$$\begin{aligned} M &= \int_{m_{\rm Kr,1}}^{m_{\rm Kr,4}} m\frac{{\rm d}N}{{\rm d}m}\,{\rm d}m \\ &= N \times C_{\rm Kr}\sum_{j=1}^{3}\frac{C_{{\rm Kr},j}}{\alpha_j+2}\left(m_{{\rm Kr},j+1}^{\alpha_j+2} - m_{{\rm Kr},j}^{\alpha_j+2}\right) \\ &\equiv N M_{\rm Kr}, \end{aligned} \tag{C.1.4}$$

where we have defined the "Kroupa mass" $M_{\rm Kr} \approx 0.5006\,M_\odot$ which represents the average mass of a single star in the population. Hence the total mass of the single star population is given approximately by $M_{\rm s} \approx M_{\rm Kr}N_{\rm s}$. For the binary population, we assume a flat mass ratio distribution such that the secondary is on average half as massive as the primary. Therefore the total mass contained in the binary population $M_{\rm bin}$ is given approximately by $M_{\rm bin} \approx \left(1+\frac{1}{2}\right)M_{\rm Kr}N_{\rm bin} = \frac{3}{2}M_{\rm Kr}N_{\rm bin}$. Similarly, assuming that in triple systems the distribution of the outer orbit mass ratio $q_2 = m_3/(m_1+m_2)$ is flat, the total mass contained in the triple population is $M_{\rm tr} \approx \left(\frac{3}{2}+\frac{1}{2}\cdot\frac{3}{2}\right)M_{\rm Kr}N_{\rm tr} = \frac{9}{4}M_{\rm Kr}N_{\rm tr}$. Hence the total mass $M_{\rm tot} = M_{\rm s} + M_{\rm bin} + M_{\rm tr}$ represented by the number of triple systems we have calculated ($N_{\rm calc}$) is given by:

$$\begin{aligned} M_{\rm tot} &\approx M_{\rm Kr}\left(N_{\rm s} + \frac{3}{2}N_{\rm bin} + \frac{9}{4}N_{\rm tr}\right) \\ &= M_{\rm Kr}\frac{N_{\rm calc}}{f_{\rm calc}}\frac{1}{\alpha_{\rm tr}}\left(1 + \frac{1}{2}\alpha_{\rm bin} + \frac{5}{4}\alpha_{\rm tr}\right). \end{aligned} \tag{C.1.5}$$

C.2 Explicit numbers

TSM1 We state the explicit numbers of the quantities mentioned in Sect. C.1 for TSM1. Firstly, for a Kroupa IMF with $0.1 < m_1/M_\odot < 80$ we find that the calculated mass fractions are given by $f_{{\rm calc},m_1,A} \approx 0.0634$ and $f_{{\rm calc},m_1,B} \approx 0.0244$ for the A and B populations respectively (hence the mass fraction with respect to the total TSM1 population is $f_{{\rm calc},m_1} \approx 0.0878$). With the value of $f_{{\rm calc},e_1,e_2,a_1,a_2} \approx 0.130$ as determined above this implies that $f_{{\rm calc},A} \approx 0.00824$ and $f_{{\rm calc},B} \approx 0.00317$. Furthermore, after rejecting the MS mergers and MS destabilizations we find that there remain $N_{{\rm calc},A} = 915,395$ and $N_{{\rm calc},B} = 923,660$ computed systems for the TSM1A and TSM1B subpopulations respectively. With a binary fraction of $\alpha_{\rm bin} = 0.60$ and a triple fraction of $\alpha_{\rm tr} = 0.25$ we thus find that the parts of the masses represented by TSM1A and TSM1B are given by $M_{{\rm tot},A} \approx 3.59\cdot10^8\,M_\odot$ and $M_{{\rm tot},B} \approx 9.41\cdot10^8\,M_\odot$. These masses are used to normalize the DTDs in Sect. 5.4.2.

TSM2 For completeness we also include these numbers for TSM2 for which different mass and period distributions apply (cf. Sect. 5.2). For both fractions $f_{{\rm calc},m_1}$ and $f_{{\rm calc},e_1,e_2,a_1,a_2}$ we use a Monte Carlo method similar to the above procedure. With the distributions of TSM2 we generate systems with $0.1 < m_1/M_\odot < 80$. In TSM2, without the restriction $l_1 > 12\,{\rm AU}$ systems with very small a_1, i.e. significantly smaller than $5\,R_\odot$, are present. Such systems are expected to merge early during the MS, however, hence from the generated systems we reject those with $a_1 < 5\,R_\odot$ (this lower limit is also consistent with TSM1). From the systems that remain we select systems within the A and B mass ranges and find $f_{{\rm calc},m_1,A} \approx 0.0880$ and $f_{{\rm calc},m_1,B} \approx 0.0580$. Subsequently, making the selection $l_1 > 12\,{\rm AU}$ we find $f_{{\rm calc},e_1,e_2,a_1,a_2} \approx 0.0863$. Therefore $f_{{\rm calc},A} \approx 0.00759$ and $f_{{\rm calc},B} \approx 0.00500$. Rejecting MS mergers and destabilizations we find that there remain $N_{{\rm calc},A} = 920,137$ and $N_{{\rm calc},B} = 927,061$ computed systems. With the same binary and triple fractions as above we then find $M_{{\rm tot},A} \approx 3.92\cdot10^8\,M_\odot$ and $M_{{\rm tot},B} \approx 5.98\cdot10^8\,M_\odot$. Note, however, that the latter two mass calculations are only approximate because the mass distribution of TSM2 is different from that in TSM1.